

SURFACE STUDIES OF SOME METALLIC THIN FILMS BY OPTICAL METHODS

K. P. VIJAYAKUMAR

THESIS SUBMITTED
TO THE UNIVERSITY OF COCHIN
IN PARTIAL FULFILMENT OF THE REQUIREMENTS
FOR THE DEGREE OF
DOCTOR OF PHILOSOPHY

DEPARTMENT OF PHYSICS
UNIVERSITY OF COCHIN
1984

DECLARATION

Certified that the work presented in this thesis is based on the original work done by me under the guidance of Dr.C.Purushothaman, Professor, Department of Physics, University of Cochin and has not been included in any other thesis submitted previously for the award of any degree.

Cochin 682022

May 28, 1984




K.P.VIJAYAKUMAR.

CERTIFICATE

Certified that the work presented in the present thesis is based on bona fide work done by Mr.K.P.Vijayakumar, Research Scholar, under my guidance in the Department of Physics, University of Cochin and has not been included in any other thesis submitted previously for the award of any degree.

Cochin 682022

May 28, 1984


Dr.C.PURUSHOTHAMAN
Professor of Physics
(Supervising Teacher)

PREFACE

Optical properties of thin films are well-known due to the practical applications of thin films in different fields. The main limitation in experimental as well as theoretical aspects of the same was the difficult calculations involved and this has been removed by the introduction of high speed computers. But the factors affecting the surface and structure of films, causing variations in their optical properties, are enormous in number. In this work, the effects of some among them are studied in detail.

The thesis aims to present the results of experimental investigations on the changes of optical properties of metallic thin films due to heating. The parameters which are measured are reflectivity, refractive indices and the ellipsometric quantities Ψ and Δ . The materials used in the studies are metals like Silver, Aluminium and Copper. By applying the optical method the interdiffusion taking place in multilayer films of Aluminium and Silver has also been studied. Special interest has been taken to reveal the mechanisms of the hillock growth and surface roughness caused by heating and their relation with the stress in the film.

The thesis contains nine chapters which are generally self-contained with separate abstracts; however there exist many cross references among chapters. Chapter I is of an introductory nature. It contains some general considerations regarding the scope and importance of the present work. It also gives a brief description of the different features affecting the optical properties of films and a summary of different methods for its analysis. A brief survey of the earlier works is also included in this chapter. The present status and some aspects of the application of the optical studies are presented in the second half of this chapter.

The next chapter gives the details of the experimental procedure. It contains the description of method of preparation of the samples and the thickness measuring technique. The experimental set up for annealing and optical measurements are also included in the chapter.

The changes in the reflectivity of Silver films due to annealing in the temperature range 30°C to 300°C are discussed in chapter III. Here the results of annealing in air and vacuum are considered separately. The explanation of these changes is given on the basis

of the relationship between the internal stress and the surface energy of the film.

In the chapter IV, the study of interdiffusion in multilayer films by using reflectivity measurements is presented. Here the materials are Aluminium and Silver with the former always forming the lower layer. The changes of reflectivity of both surfaces of the film are studied as a function of temperature. The effect of different thickness ratios of the two layers is also considered.

The chapter V contains the results of the studies on Copper films. Here the temperature variation is from 50°C to 200°C and the thickness of the samples varies from 500\AA to 3000\AA . From these results an attempt is made to calculate the intrinsic stress values of Copper films of different thickness.

A brief description of ellipsometry, including the basic theory, is presented in the next chapter. It also contains the details of the ellipsometric set up used for the investigation. In the second half of this chapter, the different uses of ellipsometry are included.

In chapter VII, the results of ellipsometric measurements of thermally induced surface roughness (hillock growth) of silver films are presented along with the required theory for the measurement of surface roughness by using ellipsometry. The variation of the hillock growth with thickness of the film is also brought under discussion. This chapter also contains the calculated values of intrinsic stress in Silver films of different thicknesses.

The light scattering measurements can give a lot of information regarding the roughness of film surfaces. Hence the surfaces of the samples analysed by using the ellipsometric method have been again examined by using light scattering technique and this is presented in the next chapter. These confirm the results of ellipsometric measurements mentioned in earlier chapter.

All these observations are summarised in chapter IX. This also points out the importance of the low temperature annealing.

A theoretical study of the lattice dynamics of ZnS crystal is also included as an appendix in the thesis. In this, the phonon frequencies for [100],[110]

and [111] wave vector directions are calculated for both normal crystal and the isotope substituted one (Zn^{34}S). From these two values the eigenvector magnitude is computed for the three wavevector directions.

Part of the investigations presented in the thesis has been published/communicated in the form of following papers:

1. Effect of annealing on the reflectivity of Silver film
K.P.Vijayakumar and C.Purushothaman
Thin Solid Films 82, 225 (1981).
2. Temperature variations of reflectivity of Al-Ag double layer films
K.P.Vijayakumar and C.Purushothaman
Proceedings of Nuclear Physics and Solid State Physics Symposium held at Banaras Hindu University, Varanasi, Vol.25C, p.8JB5 (1982).
3. An optical study of the thermal effects on Cu films
K.P.Vijayakumar and C.Purushothaman
Thin Solid Films, 112, 71 (1984).

4. Optical study of surface diffusion in Silver films
K.P.Vijayakumar and C.Purushothaman
Proceedings of Nuclear Physics and Solid State
Physics Symposium held at University of Mysore,
Mysore, Vol.26c, p.SAB8 (1983).
5. Lattice vibrations and eigenvector magnitudes in ZnS
K.P.Vijayakumar and C.Purushothaman
Indian Journal of Pure and Applied Physics,
19, 749 (1981).
6. Ellipsometric study of thermal effects on Silver films
K.P.Vijayakumar and C.Purushothaman
(Communicated to Surface Science).
7. Hillock growth measurement by light scattering
technique
(Communicated to Applied Optics).

ACKNOWLEDGEMENTS

--

I wish to express my deep sense of gratitude to Dr.C.Purushothaman for introducing me to the field of optics and suggesting the problem. His able guidance, profound interest and constant encouragement enabled me to complete this work.

I am also thankful to Dr.K.Sathianandan, Professor and Head of the Department of Physics, for his keen interest in the progress of my research work especially in the field of Ellipsometry. Let me also take this opportunity to express my gratitude to all the faculty members of this Department.

I express my sincere gratitude to Rev.Fr.Antony J.Panackal, Principal, St.Albert's College, Ernakulam and also to Prof.P.V.Vareed, Head of the Department of Physics, St.Albert's College, Ernakulam who helped me a lot to spend maximum amount of time for the completion of this work. I am also thankful to all the faculty members of the Department of Physics, St.Albert's College, Ernakulam, for their interest in my research work.

I owe much to all my colleagues in the Department of Physics, Cochin University especially to those in Thin film division, Laser division and Solid state ionics division for their timely and invaluable help in the preparation and measurement of samples during this work. A special note of gratitude goes to Mr.M.K.Satheesh Kumar, Mr.T.Ramachandran and Mr.A.T.Raghunath, for their assistance in preparing diagrams and photographs.

I am grateful to Mr.K.Madhusoodanan, Scientific Officer, University Service and Instrumentation Centre for his great help in running the computer programmes of the Ellipsometric and Lattice dynamics problems. I am also thankful to Mr.Peter Koshy, Scientist, Regional Research Laboratory, Trivandrum for his help in taking the Scanning Electron Micrographs. Thanks are also due to Mr.K.P.Sasidharan for neatly typing the manuscript.

Finally, I would like to add that I am ever indebted to my parents and in-laws whose love and blessings are always with me. I do not know how to express my gratitude to my wife Sudha whose patience and endurance were the forces behind this work.

CONTENTS

--

Page

PREFACE	i
CHAPTER I	OPTICAL PROPERTIES OF SINGLE AND MULTILAYER FILMS:GENERAL INTRODUCTION	..	1
1.1	Introduction	..	1
1.2	Theory of thin film optics	..	3
1.2a	Single layer film	..	4
1.2b	Multilayer films	..	18
1.3	Recent developments in optical studies of thin films	..	29
1.4	Factors affecting the optical properties of thin films	..	32
1.5	Investigations in the present work		38
CHAPTER II	DESCRIPTION OF THE EXPERIMENTAL SET UP FOR THE DIFFERENT INVESTI- GATIONS	..	45
2.1	Introduction	..	45
2.2	Film preparation and thickness measurement	..	45
2.3	Annealing	..	47
2.4	Optical measurements	..	50
2.4a	Reflectivity measurements	..	52
2.4b	Ellipsometric set up	..	53
2.4c	Light scattering measurements	..	54
2.5	The Scanning Electron Micrographs..		55
CHAPTER III	OPTICAL STUDY OF THE EFFECTS OF ANNEALING ON SILVER FILMS	..	58
3.1	Introduction	..	58
3.2	Theory of hillock growth	..	59
3.2a	Stress in thin films (metallic)	..	63
3.3	Experimental details	..	65
3.4	Results	..	67
3.4a	Annealing in vacuum	..	67
3.4b	Annealing in air	..	67
3.5	Discussion	..	68
3.6	Conclusion	..	70

		<u>Page</u>
CHAPTER IV	STUDY OF SURFACE CHANGES ON COPPER FILMS DUE TO THERMAL TREATMENT	.. 75
4.1	Introduction	.. 75
4.2	Experimental set up	.. 78
4.3	Results	.. 79
4.4	Discussion	.. 81
4.4a	Calculation of the intrinsic stress	83
4.5	Conclusion	.. 84
CHAPTER V	OPTICAL STUDY OF INTERDIFFUSION IN Al/Ag BILAYER FILMS	.. 88
5.1	Introduction	.. 88
5.1a	Brief review of earlier works	.. 90
5.2	Experimental	.. 93
5.3	Results	.. 95
5.4	Discussion	.. 96
5.4a	The silver side	.. 96
5.4b	Aluminium side	.. 99
5.5	Conclusion	.. 101
CHAPTER VI	ELLIPSOMETRY	.. 108
6.1	Introduction	.. 108
6.1a	Brief review of earlier works	.. 110
6.2	Theory	.. 114
6.2a	Ellipsometric evaluation of	.. 121
6.3a	Null ellipsometry	.. 132
6.3b	Photometric ellipsometers	.. 133
6.3b.1	Dynamic photometric ellipsometers..	134
6.3b.2	Static photometric ellipsometers ..	136
CHAPTER VII	ELLIPSOMETRIC STUDY OF THERMAL EFFECTS ON SILVER THIN FILM SURFACES	.. 143
7.1	Introduction	.. 143
7.1a	Brief review of earlier works	.. 144
7.2	Theory of roughness measurement	.. 148
7.3	Experimental	.. 150
7.4	Results	.. 152
7.4a	For films with thickness 1500Å	.. 152

		<u>Page</u>
7.4b	For films with thickness 3000\AA ^o	.. 153
7.5	Discussion	.. 155
7.5a	Annealing in vacuum	.. 156
7.5b	Calculation of intrinsic stress	.. 158
7.5c	Annealing in air	.. 160
7.6	Conclusion	.. 161
CHAPTER VIII	LIGHT SCATTERING MEASUREMENTS ON SILVER FILM SURFACE	.. 166
8.1	Introduction	.. 166
8.2	Theory	.. 167
8.2a	Random rough surfaces	.. 172
8.3	Experimental	.. 176
8.4	Results	.. 177
8.5	Discussion	.. 178
8.6	Conclusion	.. 179
CHAPTER IX	SUMMARY OF CONCLUSION	.. 183
APPENDIX-I	LATTICE DYNAMICS AND EIGENVECTOR MAGNITUDES IN ZnS CRYSTAL	.. 187
A.1	Introduction	.. 187
A.1a	Brief review of earlier works	.. 188
A.2	Theory	.. 190
A.2a	Approximations in the theory	.. 191

CHAPTER I

OPTICAL PROPERTIES OF SINGLE AND MULTILAYER FILMS : GENERAL INTRODUCTION

1.1 Introduction

Thin films are used in a wide variety of scientific, engineering and industrial appliances. For example, their use is pervasive in integrated circuits; metal films are used for electrical connections and on the gate regions of the field-effect transistors; oxide or nitride films form insulating barriers between films; and layers of semiconductors are unavoidable parts of all structures. The latest application of thin film technology is in circuits based on films made from superconductors forming Josephson junctions. Similarly, thin films are familiar in optics as antireflection coatings on video screens, camera lenses etc. The ingenious exploitation of the interference phenomena in thin films has led to the development of sophisticated multilayer systems with nearly ideal reflection, antireflection polarisation, narrow and wide band

reflection transmission and filtering, absorptance and emittance properties. These optical coatings are indispensable for several optical instruments.

Thin films also play an important role in the field of material studies when optical methods are employed. This is because they provide clean and smooth surfaces which can be used for the optical experiments like the determination of the optical constants of materials. Again studies on absorption in infrared and ultraviolet and photoemission have yielded valuable information on the basic electronic parameters of materials. The surface modes in an ionic lattice can be excited in thin films and this affects the plasma radiation emission and absorption in metals. Studies of these absorption phenomena give information about the lattice dynamics of the materials.

The phenomenal growth of thin film research and development owes much to the stimulus provided by the early utilitarian interest in the application of optical films in mirrors and interferometers. The theoretical and experimental investigations on the optical behaviour of thin films mainly deals with

optical reflection, transmission and absorption properties and their relation to the optical constants of the films. These elaborate studies have led to the development of complex multilayer optical systems with remarkable reflection, antireflection, interference and polarisation properties for both industrial and laboratory applications. Moreover, using the reflection, transmission and interference properties of thin films new methods have been developed to determine the optical constants conveniently which will be discussed later.

1.2 Theory of thin film optics

In order to understand different optical experiments one has to see the theoretical aspects regarding the interaction of electromagnetic waves with a multilayered system. In many of the optical experiments on thin films, one is mainly concerned with reflection and transmission and hence the theory is also oriented in that direction. For convenience, this section is divided into two parts; the first part deals with ambient-film-substrate system and the second part gives the more complicated case of ambient-multilayer film-substrate system. A very

much simplified version of the first part is included in chapter VI to show the relation of ellipsometric parameters with reflectivity and transmission coefficients.

1.2a Single layer film

The system consists of ambient (medium-0), the film (medium-1) and the substrate (medium-2) as in fig.1.1. All these layers are considered to be homogeneous optically isotropic with their surfaces smooth and flat. They are having indices of refraction N_0 , N_1 and N_2 respectively of which most probably, N_0 is real (since ambient may be air) and the rest may be complex. In this section, the complex index of refraction is denoted as

$$N = n - ik \quad (1.1)$$

where n is the index of refraction and k is the extinction coefficient (n and k may also be called as real and imaginary parts of the complex index of refraction N). The film is having a thickness ' d '. A plane wave is incident on the interface between the medium-0 and medium-1 (the 0-1 interface) at an

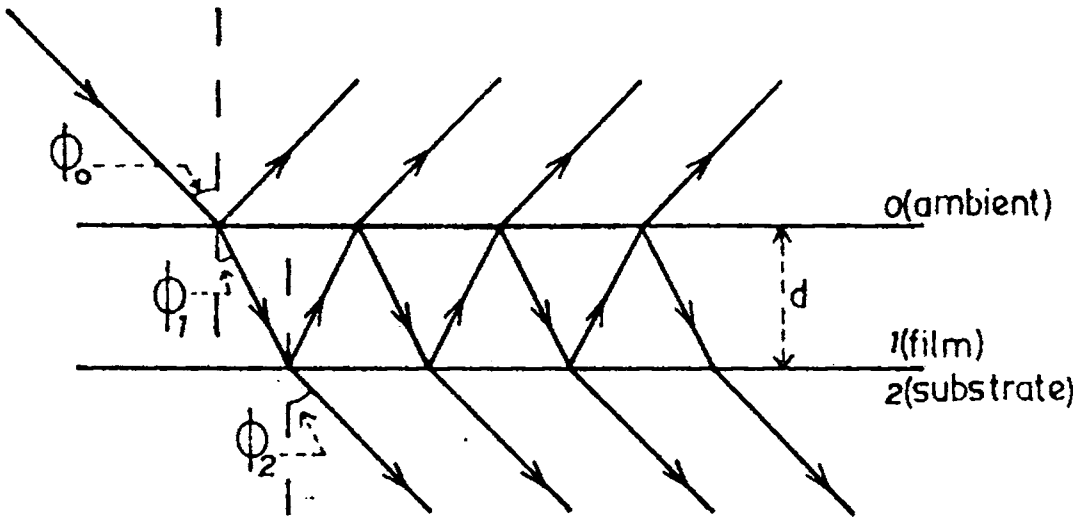


Fig.1.1 Oblique reflection and transmission of a plane wave by an ambient (0)-film(1)-substrate(2) system with parallel plane boundaries.

an angle of incidence ϕ_0 . This wave gives rise to a 'resultant reflected wave' in the same medium and a 'resultant transmitted wave' in the medium-2 at an angle ϕ_2 . Here the aim is to relate the complex amplitudes of the resultant reflected and transmitted waves to the amplitude of the incident wave when the latter is linearly polarised parallel (p) and perpendicular (s) to the plane of incidence. Fresnel reflection and transmission coefficients are necessary for this part and the derivation of the coefficients are given in all text books on optics¹. As an example, if one has E_{ip} and E_{rp} to be the complex amplitudes of components of electric vectors (parallel to the plane of incidence) of incident and reflected waves respectively then r_{oip} the Fresnel reflection coefficient at O-1 interface can be obtained from the expression,

$$E_{rp}/E_{ip} = r_{olp} = \frac{N_1 \cos \phi_0 - N_0 \cos \phi_1}{N_1 \cos \phi_0 + N_0 \cos \phi_1} \quad (1.2)$$

Similarly one can get coefficients for other component (s-component) and for other interfaces also.

$$r_{ols} = \frac{N_0 \cos \phi_0 - N_1 \cos \phi_1}{N_0 \cos \phi_0 + N_1 \cos \phi_1} \quad (1.3)$$

$$r_{12p} = \frac{N_2 \cos \phi_1 - N_1 \cos \phi_2}{N_2 \cos \phi_1 + N_1 \cos \phi_2} \quad (1.4)$$

$$r_{12s} = \frac{N_1 \cos \phi_1 - N_2 \cos \phi_2}{N_1 \cos \phi_1 + N_2 \cos \phi_2} \quad (1.5)$$

$$t_{01s} = \frac{2N_0 \cos \phi_0}{N_0 \cos \phi_0 + N_1 \cos \phi_1} \quad (1.6)$$

$$t_{01p} = \frac{2N_0 \cos \phi_0}{N_1 \cos \phi_0 + N_0 \cos \phi_1} \quad (1.7)$$

$$t_{12s} = \frac{2N_1 \cos \phi_1}{N_1 \cos \phi_1 + N_2 \cos \phi_2} \quad (1.8)$$

$$t_{12p} = \frac{2N_1 \cos \phi_1}{N_2 \cos \phi_1 + N_1 \cos \phi_2} \quad (1.9)$$

To determine the relation between the reflected, transmitted and incident amplitudes here, the procedure originally due to Drude² is followed. (For simplicity the suffix p or s is omitted in following steps. When the coefficient of a particular component alone is

required, the specified suffix is to be added and this will be shown at the end of the derivation). According to this theory, as the incident wave first meets the 0-1 interface, a part of it is reflected into the medium-0 and another part is refracted in the film (medium-1) strictly following the Fresnel reflection and transmission coefficients in eqns (1.2)-(1.9). The refracted wave inside the film subsequently undergoes multiple internal reflections at 1-2 and 1-0 film bounding interfaces which are in general, not perfectly reflecting. Hence each time the multiply reflected wave strikes the 1-0 or 1-2 interface a component (partial) wave is leaked (refracted) into the ambient or substrate medium respectively. If the Fresnel reflection and transmission coefficients at 0-1 (1-0) and 1-2 interfaces are denoted by r_{01} , t_{01} (r_{10} , t_{10}) and r_{12} , t_{12} respectively the complex amplitudes of successive partial plane waves that make up the 'resultant reflected wave' in the medium-0 are given by r_{01} , $t_{01}r_{12}t_{10}e^{-i2\beta}$, $t_{01}r_{10}r_{12}^2t_{10}e^{-i4\beta}$, $t_{01}r_{10}^2r_{12}^3t_{10}e^{-i6\beta}$where β is the phase change that the multiply reflected wave inside the film experiences as it traverses the film once from one boundary to the

other. The expression for β can be obtained in terms of the free space wave length of the light wave λ , film thickness d , the complex index of refraction of the film material N_1 and the (complex) angle of refraction ϕ_1 (ie., the angle between the direction of propagation of the wave in the film and the normal to the film boundaries) as,

$$\beta = 2\pi N_1 d \cos \phi_1 / \lambda \quad (1.10)$$

Similarly one can write the expressions for the complex amplitudes of successive partial plane waves that make up the resultant transmitted wave in medium-2 as,

$$t_{01}t_{12}e^{-i\beta}, t_{01}r_{12}r_{10}t_{12}e^{-i3\beta}, t_{01}r_{12}^2r_{10}^2t_{12}e^{-i5\beta} \dots\dots$$

Addition of partial reflected waves leads to an infinite geometric series for the total reflected amplitude, (R)

$$\begin{aligned} R &= r_{01} + t_{01}r_{12}t_{10}e^{-i2\beta} + t_{01}r_{12}^2r_{10}^2t_{10}e^{-i4\beta} \\ &\quad + t_{01}r_{12}^3r_{10}^2t_{10}e^{-i6\beta} + \dots\dots \end{aligned}$$

$$= r_{01} + \frac{t_{01}t_{10}r_{12}e^{-i2\beta}}{1-r_{10}r_{12}e^{-i2\beta}} \quad (1.11)$$

The expression for R in eqn(1.11) can be further simplified using two relations

$$r_{10} = -r_{01} \quad \text{and} \quad (1.12a)$$

$$t_{01}t_{10} = 1 - r_{01}^2 \quad (1.12b)$$

which can be proved very easily using the expressions for Fresnel coefficients given in eqns (1.2)-(1.9). After simplification the expression for R becomes,

$$R = \frac{r_{01} + r_{12}e^{-i2\beta}}{1 + r_{01}r_{12}e^{-i2\beta}} \quad (1.13)$$

If one requires the reflected amplitude of p- or s-component alone it can be obtained as

$$R_p = \frac{r_{01p} + r_{12p}e^{-i2\beta}}{1 + r_{01p}r_{12p}e^{-i2\beta}} \quad (1.13a)$$

and

$$R_s = \frac{r_{01s} + r_{12s}e^{-i2\beta}}{1 + r_{01s}r_{12s}e^{-i2\beta}} \quad (1.13b)$$

Similarly total transmitted amplitude (T) is given by another infinite geometric series,

$$\begin{aligned}
 T &= t_{01}t_{12}e^{-i\beta} + t_{01}r_{12}r_{10}t_{12}e^{-i3\beta} + \\
 &\quad t_{01}r_{12}^2r_{10}^2t_{12}e^{-i5\beta} \\
 &= \frac{t_{01}t_{12}e^{-i\beta}}{1 + r_{01}r_{12}e^{-i2\beta}} \quad (1.14)
 \end{aligned}$$

which is obtained after simplification using eqn (1.12a). Here also the transmitted amplitude for the two components can be obtained as

$$T_p = \frac{t_{01p}t_{12p}e^{-i\beta}}{1 + r_{01p}r_{12p}e^{-i2\beta}} \quad (1.14a)$$

$$T_s = \frac{t_{01s}t_{12s}e^{-i\beta}}{1 + r_{01s}r_{12s}e^{-i2\beta}} \quad (1.14b)$$

The reflectivity (I_R) is the ratio of intensity of reflected light to that of the incident light. From

eqn (1.13) one can obtain the expression for the reflectivity as,

$$I_R = \frac{r_{01}^2 + r_{12}^2 + 2r_{01}r_{12} \cos(2\beta)}{1 + r_{01}^2 r_{12}^2 + 2r_{01}r_{12} \cos(2\beta)} \quad (1.15)$$

Similarly the expression for the transmissivity (I_T), which is the ratio of intensity of transmitted light to that of the incident light can be written as,

$$I_T = \frac{N_0}{N_2} \frac{t_{01}^2 t_{12}^2}{1 + 2r_{01}r_{12} \cos(2\beta) + r_{01}^2 r_{12}^2} \quad (1.16)$$

It should be noted that eqns (1.15) and (1.16) are common for both p- and s-polarisations. The general expressions can be obtained by substituting the values of Fresnel coefficients in eqns (1.15) and (1.16) and the expressions are too long to write. A much simplified version is obtained for the case of normal incidence and then the expressions for reflectivity and transmissivity become,

$$I_R = \frac{(N_0^2 + N_1^2)(N_1^2 + N_2^2) - 4N_0N_1N_2 + (N_0^2 - N_1^2)(N_1^2 - N_2^2)\cos(2\beta)}{(N_0^2 + N_1^2)(N_1^2 + N_2^2) + 4N_0N_1N_2 + (N_0^2 - N_1^2)(N_1^2 - N_2^2)\cos(2\beta)} \quad (1.17)$$

$$I_T = \frac{8N_0N_1^2N_2}{(N_0^2 + N_1^2)(N_1^2 + N_2^2) + 4N_0N_1N_2 + (N_0^2 - N_1^2)(N_1^2 - N_2^2)\cos(2\beta)} \quad (1.18)$$

The normal reflectance exhibits oscillatory variations as shown in fig.1.2 which gives the variations of R with film thickness normalised by the wavelength of light³. The reflectivity at the positions of maxima and minima are as follows.

For $N_0 \leq N_1 \leq N_2$,

$$I_R(\max) = \left(\frac{N_2 - N_0}{N_2 + N_0} \right)^2 \text{ at } \lambda_{\max} = \frac{2N_1d}{m} \quad (1.19)$$

and

$$I_R(\min) = \left(\frac{N_1^2 - N_0N_2}{N_1^2 + N_0N_2} \right)^2 \text{ at } \lambda_{\min} = \frac{4N_1d}{2m+1} \quad (1.20)$$

For $N_0 \leq N_1 \geq N_2$,

$$I_R(\max) = \left(\frac{N_1^2 - N_0 N_2}{N_1^2 + N_0 N_2} \right)^2 \text{ at } \lambda_{\max} = \frac{4N_1 d}{2m+1} \quad (1.21)$$

$$I_R(\min) = \left(\frac{N_2 - N_0}{N_2 + N_0} \right)^2 \text{ at } \lambda_{\min} = \frac{2N_1 d}{m} \quad (1.22)$$

where m is an integer.

In order to study the change of amplitude and phase separately, as the plane wave is obliquely reflected from or transmitted by a film covered substrate, the overall complex amplitude reflection (R_p, R_s) and transmission (T_p, T_s) coefficients are written in terms of their absolute values and angles.

$$R_p = |R_p| e^{i \Delta r_p} \quad (1.23a)$$

$$R_s = |R_s| e^{i \Delta r_s} \quad (1.23b)$$

$$T_p = |T_p| e^{i \Delta t_p} \quad (1.24a)$$

$$T_s = |T_s| e^{i \Delta t_s} \quad (1.24b)$$

From eqns (1.13a & b) and (1.14a & b) it is clear that, because the interface Fresnel reflection and transmission coefficients for the p- and s-polarisations are different, the overall reflection and transmission coefficients of an ambient-film-substrate system for these two polarisations are also different. This is the basis of reflection and transmission ellipsometry measurements on the ambient-film-substrate system where a change of polarisation takes place due to reflection and transmission as a result of the difference in amplitude attenuation and phase shift experienced by p- and s-components. From the above expressions one can calculate the ratio

$$\rho = R_p/R_s = \frac{|R_p|}{|R_s|} e^{i(\Delta_{rp} - \Delta_{rs})} \quad (1.25)$$

of overall complex amplitude reflection coefficients of ambient-film-substrate system for p- and s-polarisations. In terms of ellipsometric parameters⁴ ψ and Δ this can be expressed as

$$\rho = \tan \psi e^{i\Delta} \quad (1.26)$$

$$\tan \psi = |R_p|/|R_s| \quad (1.27a)$$

$$\Delta = \Delta_{rp} - \Delta_{rs} \quad (1.27b)$$

This is the case of 'reflection ellipsometry'. If the ratio for the transmission amplitudes is calculated it becomes 'transmission ellipsometry'.

Heavens⁵ pointed out that for the application of the above theory to the practical film-substrate system, one must have (i) the lateral dimensions of the film to be many times its thickness so that the multiply reflected and transmitted partial waves can be summed to infinity (ii) the source band width, beam diameter, degree of collimation and film thickness to be such that the multiply reflected and transmitted waves combine coherently and (iii) the film material to be not amplifying. These conditions are readily met in most of the practical applications.

With the help of the above theory almost all the optical experiments performed on thin films can be explained. In the case of reflectometry one measures the reflectivity of the film at different wavelengths. This can be theoretically calculated using eqn (1.15). From the deviation of the experimental value, due to the absorption of the film, the electronic structure of the material of the film and such other important factors can be obtained. If the material of the film is

dielectric or semiconductor the band gap can be determined in this way.

Eqn (1.17) shows that the reflectivity exhibits an oscillatory variation. This is illustrated in fig.1.2 also. Hence it is clear from eqns (1.19)-(1.22) that one can either enhance or diminish the reflectivity of a substrate at a specified wavelength (most probably in a range of wavelength) by a suitable choice of the film index. This is the principle of reflection and antireflection coatings. The functioning of such selective mirrors is improved by using multilayer coatings. Another practical application of this principle is that this can be used as a spectrophotometric method for monitoring the thickness of single or multilayer films. The film thickness can be determined from maxima or minima of reflectivity using the expression⁶

$$2m\lambda/4 = n_f t \quad (1.28)$$

where n_f is the refractive index of the film t is the film thickness, λ is the wavelength of light and m is the order of maximum or minimum. For example if $\lambda = 1\mu$ and SiO film ($n_f=2$) is deposited, a thickness of 1μ is obtained after four maxima or minima.

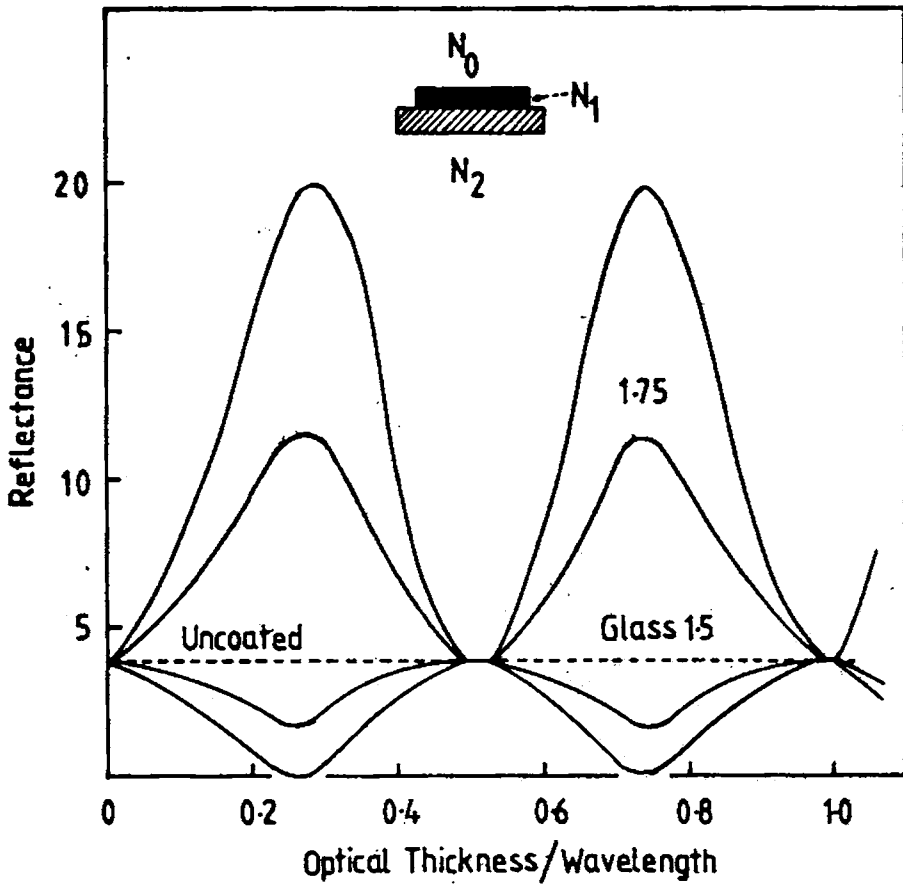


Fig.1.2 Theoretical variation of reflectivity (at air side) with normalised thickness for films of various refractive indices on glass substrates.

Now considering the ellipsometric measurements, one has to calculate ρ from ψ and Δ values. But ρ is defined as the ratio of R_p to R_s (eqn 1.25). Substituting the value of R_p and R_s in terms of refractive indices and angles from eqns (1.13a & b) the expression

$$= \tan \psi e^{i\Delta} = \frac{r_{01p} + r_{12p} e^{-i2\beta}}{1 + r_{01p} r_{12p} e^{-i2\beta}} \times \frac{1 + r_{01s} r_{12s} e^{-i2\beta}}{r_{01s} + r_{12s} e^{-i2\beta}} \quad (1.29)$$

Now it can be easily seen that eqn (1.29) relates the measured values of ψ and Δ to the optical properties of the three phase system namely the (complex) refractive indices of the ambient (N_0), film (N_1) substrate (N_2) and film thickness (d) for given values of the vacuum wavelength (λ) of the ellipsometer light beam and its angle of incidence (ϕ_0) in the ambient. This dependence of ψ and Δ on the parameters can be written as

$$\tan \psi e^{i\Delta} = \rho(N_0, N_1, N_2, d, \phi_0, \lambda) \quad (1.30)$$

Here anyone of the parameters can be determined if the values of others are known. If the film thickness (d) is the unknown quantity, β in eqn (1.29) is to be evaluated since it is the only factor involving d . The

function ϵ in eqn (1.30) is quite complicated and can be handled satisfactorily only by a computer. But this is a very sensitive technique and can give information about layers formed on the surface having thickness as little as 0.1\AA to as much as 5000\AA and this has been proved to be superior to other surface analysis techniques like photoelectron emission, water contact angle measurement, surface potential difference etc.⁴ The detailed theory of this method and its measuring techniques are given in chapter VI.

1.2b Multilayer films

The case of multilayer films is also to be considered here since it is more important when compared to the case of single layer films. This is more complicated in comparison with the earlier case and hence the method of addition of multiple reflection is not possible here. A more elegant approach employing 2×2 matrices is applied, which is based on the fact that the equations that govern the propagation of light are linear and that the continuity of the tangential fields across an interface between two isotropic media can be regarded as a 2×2 linear matrix transformation^{7,8}.

Let the stratified structure consists of a stack of $1, 2, 3, \dots, j \dots, m$ parallel layers sandwiched between two semi-infinite ambient (0) and substrate ($m+1$) media as in fig.1.3. Here also the media are considered to be linear homogeneous isotropic and having their interfaces to be parallel and ideally flat. Let the complex index of refraction of the j^{th} layer be N_j and its thickness be ' d_j '. N_0 and N_{m+1} are the complex indices of the ambient and the substrate media respectively. When a plane monochromatic wave is incident on the first layer at an angle of incidence ϕ_0 , it generates a resultant reflected wave in the medium-0 and a resultant transmitted wave in medium ($m+1$). The total field in the j^{th} layer, which is excited by the incident plane wave, consists of two plane waves: a forward travelling plane wave denoted by (+) and a backward travelling wave denoted by (-). The wave vectors of all plane waves lie in the same plane (ie., in the plane of incidence) and the wave vectors of the two plane waves in the j^{th} layer make equal angles with the z-axis (The z-axis is perpendicular to the plane boundaries directed towards the substrate). When the incident wave in the ambient is linearly polarised

Fig.1.3

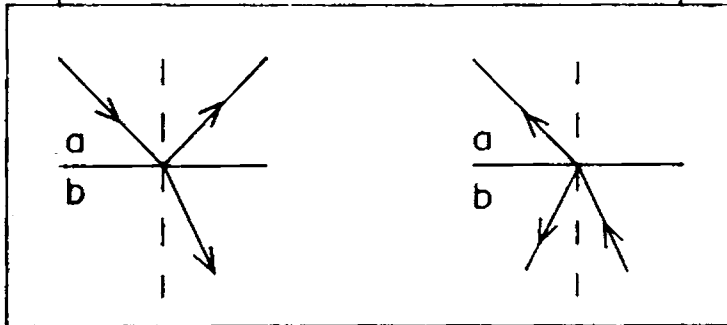
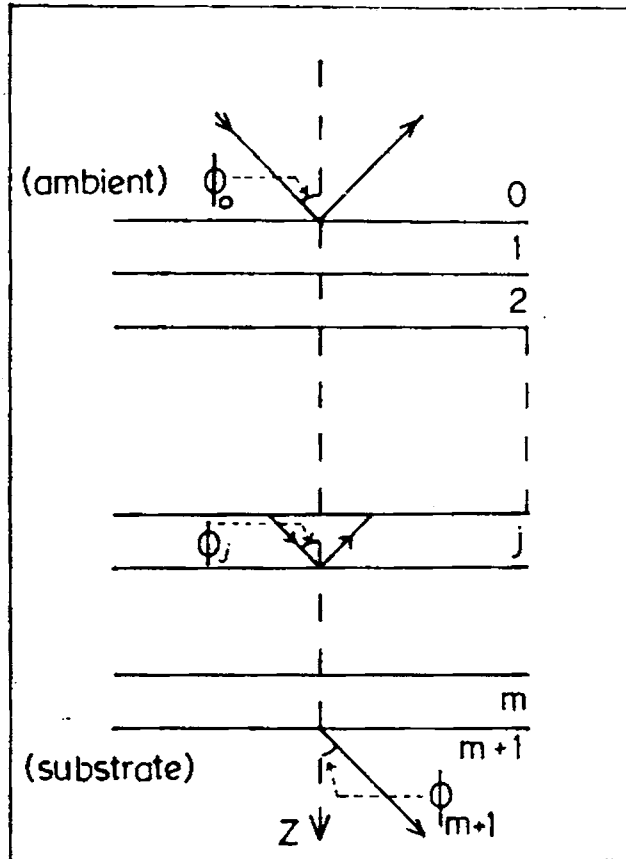


Fig.1.4A

Fig.1.4B

Fig.1.3 Reflection and transmission of a plane wave by a multi-film structure (films 1,2,...m) sandwiched between the semi-infinite ambient (0) and substrate (m+1) media.

Fig.1.4A Reflection and transmission of a plane wave at a two-media (ab) interface.

Fig.1.4B The direction of propagation of the transmitted wave is assumed to be reversed.

with its electric vector vibrating parallel (p) or perpendicular (s) to the plane of incidence all plane waves excited by that incident wave in various layers of the stratified structure will be similarly polarised. In the following discussion it is assumed that all waves are either p- or s-polarised.

Let $E_{(z)}^+$ and $E_{(z)}^-$ represent the complex amplitudes of forward and backward travelling plane waves at an arbitrary plane z . The total field at z can be described by a 2x1 column vector,

$$E_{(z)} = \begin{bmatrix} E_{(z)}^+ \\ E_{(z)}^- \end{bmatrix} \quad (1.31)$$

If one considers z' and z'' as two planes parallel to the layer boundaries then due to the linearity of the system $E_{(z'')}^+$ and $E_{(z')}^-$ are related as

$$\begin{bmatrix} E_{(z')}^+ \\ E_{(z')}^- \end{bmatrix} = \begin{bmatrix} S_{11} & S_{12} \\ S_{21} & S_{22} \end{bmatrix} \begin{bmatrix} E_{(z'')}^+ \\ E_{(z'')}^- \end{bmatrix} \quad (1.32)$$

$$\text{Or } E_{(z')} = S E_{(z'')} \quad (1.33)$$

$$\text{where } S = \begin{bmatrix} S_{11} & S_{12} \\ S_{21} & S_{22} \end{bmatrix} \quad (1.34)$$

Here S characterises that part of the stratified structure confined between the two parallel planes at z' and z'' . Only the reflected wave in the ambient medium and the transmitted wave in the substrate are accessible for measurement and hence it is necessary to relate their fields to those of the incident wave. By considering the planes z' and z'' to be lying in the ambient and substrate media, immediately adjacent to the $0-1$ and $m-(m+1)$ interfaces respectively eqn (1.33) becomes,

$$E_{(z_1)} = S E_{(z_{m+1})} \quad (1.35)$$

S is a scattering matrix which can be written as a product of the interface and layer matrices I and L which describe the effect of individual interfaces and layers of the entire stratified structure taken

in order and can be expressed as,

$$S = I_{01}L_1I_{12}L_2\cdots I_{(j-1)j}L_j\cdots L_mI_{m(m+1)} \quad (1.36)$$

Now one has to calculate the individual interface and layer matrices I and L. The matrix I of an interface between two media 'a' and 'b' relates the fields on both sides as

$$\begin{bmatrix} E_a^+ \\ E_a^- \end{bmatrix} = \begin{bmatrix} I_{11} & I_{12} \\ I_{21} & I_{22} \end{bmatrix} \begin{bmatrix} E_b^+ \\ E_b^- \end{bmatrix} \quad (1.37)$$

Consider fig.1.4A in which a plane wave is incident on the ab interface. The complex amplitude of the transmitted wave in medium b and that of the reflected wave in medium a can be expressed in terms of the complex amplitude of the incident wave in the medium a as,

$$E_b^+ = t_{ab} E_a^+ \quad (1.38a)$$

$$E_a^- = r_{ab} E_a^+ \quad (1.38b)$$

It is quite evident that $E_b^- = 0$ and r_{ab} and t_{ab} are

Fresnel reflection and transmission coefficients of the ab interface. But using the matrix notation in this case eqn (1.37) can be rewritten as

$$\begin{bmatrix} E_a^+ \\ E_a^- \end{bmatrix} = \begin{bmatrix} I_{11} & I_{12} \\ I_{21} & I_{22} \end{bmatrix} \begin{bmatrix} E_b^+ \\ 0 \end{bmatrix} \quad (1.39)$$

which can be expanded as

$$E_a^+ = I_{11} E_b^+ \quad (1.40a)$$

$$E_a^- = I_{21} E_b^+ \quad (1.40b)$$

Comparing eqns (1.40a & b) with eqns (1.38a & b),

$$I_{11} = 1/t_{ab} \quad (1.41)$$

$$I_{21} = r_{ab}/t_{ab} \quad (1.42)$$

Considering the fig.1.4B in which a plane wave is incident on the ba interface from the medium b at an angle of incidence equal to the angle of refraction in the medium b in the case represented in fig.1.4A,

one can write the expressions for the fields immediately adjacent to the ba interface as,

$$E_b^+ = r_{ba} E_b^- \quad (1.43a)$$

$$E_a^- = t_{ba} E_b^- \quad (1.43b)$$

Here $E_a^+ = 0$ and r_{ba} and t_{ba} are Fresnel reflection and transmission coefficients of ba interface respectively.

Using the matrix notation from eqn (1.37)

$$\begin{bmatrix} 0 \\ E_a^- \end{bmatrix} = \begin{bmatrix} I_{11} & I_{12} \\ I_{21} & I_{22} \end{bmatrix} \begin{bmatrix} E_b^+ \\ E_b^- \end{bmatrix} \quad (1.44)$$

$$\text{Or } 0 = I_{11} E_b^+ + I_{12} E_b^- \quad (1.45a)$$

$$E_a^- = I_{21} E_b^+ + I_{22} E_b^- \quad (1.45b)$$

Substituting for I_{11} and I_{21} ,

$$E_b^+ = t_{ab} I_{12} E_b^- \quad (1.46a)$$

$$E_a^- = \left[\frac{r_{ab} r_{ba}}{t_{ab}} + I_{22} \right] E_b^- \quad (1.46b)$$

Comparing eqns (1.46a & b) with eqns (1.43a & b) one gets,

$$I_{12} = -r_{ba}/t_{ab} \quad (1.47)$$

$$I_{22} = (t_{ab} t_{ba} - r_{ab} r_{ba})/t_{ab} \quad (1.48)$$

Using the relations in eqns (1.12a & b) these expressions of I_{12} and I_{22} can be further simplified and then the interface matrix becomes,

$$\begin{aligned}
 I_{ab} &= \begin{bmatrix} 1/t_{ab} & r_{ab}/t_{ab} \\ r_{ab}/t_{ab} & 1/t_{ab} \end{bmatrix} \\
 &= 1/t_{ab} \begin{bmatrix} 1 & r_{ab} \\ r_{ab} & 1 \end{bmatrix} \quad (1.49)
 \end{aligned}$$

These Fresnel reflection and transmission coefficients occurring in eqn (1.49) must be evaluated using the complex indices of refraction of the two media that define the interface and the local angle of incidence. The latter can be obtained by the repeated application of Snell's law

$$N_0 \sin \phi_0 = N_1 \sin \phi_1 \dots = N_j \sin \phi_j \dots = N_{m+1} \sin \phi_{m+1} \quad (1.50)$$

The effect of propagation through a homogeneous layer of index of refraction N and thickness d can be found out by getting the relationship between the fields inside

the layer at both ends. This can be written as

$$\begin{bmatrix} E_o^+ \\ E_o^- \end{bmatrix} = \begin{bmatrix} e^{i\beta} & 0 \\ 0 & e^{-i\beta} \end{bmatrix} \begin{bmatrix} E_d^+ \\ E_d^- \end{bmatrix} \quad (1.51)$$

where the subscripts 'O' and 'd' denote the beginning and end of the layer (along the direction of the forward travelling wave) and the phase shift (layer phase thickness) β is given by,

$$\beta = \frac{2\pi d N}{\lambda} \cos \phi \quad (1.52)$$

Here ϕ is the angle between the direction of propagation in the layer and the perpendicular to its boundaries (the z-axis). Therefore the layer matrix L can be written as,

$$L = \begin{bmatrix} e^{i\beta} & 0 \\ 0 & e^{-i\beta} \end{bmatrix} \quad (1.53)$$

Thus from the interface and layer matrices I and L ie, from eqns (1.49) and (1.53), one can get the overall scattering matrix S of the stratified structure. It is

determined by direct matrix multiplication. Hence eqn (1.35) can be written as,

$$\begin{bmatrix} E_a^+ \\ E_a^- \end{bmatrix} = \begin{bmatrix} S_{11} & S_{12} \\ S_{21} & S_{22} \end{bmatrix} \begin{bmatrix} E_s^+ \\ 0 \end{bmatrix} \quad (1.54)$$

where the subscripts a and s denote the ambient and the substrate and it is quite clear that $E_s^- = 0$. From eqn (1.54) the overall reflection and transmission coefficients of the stratified structure is obtained as

$$R = \frac{E_a^-}{E_a^+} = \frac{S_{21}}{S_{11}} \quad (1.55)$$

$$T = \frac{E_s^+}{E_a^+} = \frac{1}{S_{11}} \quad (1.56)$$

Here also, for ellipsometry the stratified structure scattering matrix S has to be calculated for both linear polarisations, parallel (p-) and perpendicular (s-) to the plane of incidence. If S_p and S_s represent the scattering matrices for p- and s-polarisations, then,

$$R_p = \frac{S_{21p}}{S_{11p}} \quad (1.57a)$$

$$R_s = \frac{S_{21s}}{S_{11s}} \quad (1.57b)$$

$$T_p = \frac{1}{S_{11p}} \quad (1.58a)$$

$$T_s = \frac{1}{S_{11s}} \quad (1.58b)$$

Considering the case of reflection ellipsometer one can write

$$e = R_p/R_s = \frac{S_{21p}}{S_{11p}} \times \frac{S_{11s}}{S_{21s}} \quad (1.59)$$

For determining the optical constants alone, one can use either reflectivity measurements or ellipsometry using a monochromatic source of light. By these methods the surface nature of the film can also be studied. But for the study of the interior of the multilayer films one has to use reflectometry (spectrophotometry) or spectroscopic ellipsometry. Employing spectroscopic ellipsometry one can study the variation of index of refraction⁹ or the complex dielectric constant^{10,11} and these experimental values can furnish a lot more information^{12,13}. For example, Meyer¹⁴ has calculated

the surface state densities on clean semiconductor surfaces from ellipsometric measurements.

1.3 Recent developments in optical studies of thin films

The reflectivity measurements, which is just the ratio of reflected intensity of light to that of the incident light, gives information about the surface and optical constants of the film. But the variation of reflectivity with wavelength (reflectometry or spectrophotometry) can furnish information regarding the electronic structure of the material, absorption, variation of optical constants etc. This method has been used by several workers to study thin films and their optical properties¹⁵⁻¹⁸. In this itself, the method of differential reflectometry is gaining much importance recently¹⁹⁻²². This technique involves alternate scanning of two samples with a monochromatic light beam and this is achieved by means of an oscillating mirror. Another recent technique evolved in this field is the time-resolved optical reflectivity. This has been used to study the properties of amorphous

and crystalline silicon prepared by using the chemical vapour deposition technique²³. Attenuated total reflection (ATR) is another branch which is gaining more importance recently. This has been used by Lopez-Rios et al²⁴ for the study of the silver film surface. The theoretical aspects of ATR and its recent trend in experimental side are described in detail by Otto²⁵. As the latest developments in thin film optics, one can see the use of Photo acoustic spectroscopy (PAS—which involves the conversion of light waves into sound or pressure waves) and Photo thermal deflection spectroscopy (PDS) for the surface study,^{26,27} thickness measurement,²⁸ and optical constants measurement²⁹.

In ellipsometry the main developments are in the instrumentation and in the different types of uses. Regarding the latter part description is given in chapter VI. Considering the case of developments in the field of instrumentation, the automatic ellipsometers have been of great help in the study of some fast surface reactions whose analysis require a large set of data. In null as well as photometric ellipsometers automation has taken place. In the case of null

ellipsometers the work of Takasaki³⁰, Ord et al³¹ and Roberts et al³² are to be mentioned. There are two types of automatic photometric ellipsometers; one is rotating analyser ellipsometer (RAE) and the other is polarisation modulated ellipsometer (PME). The RAE systems employ both analog³³ and digital^{34,35} signal detection. The importance of this development (ie., automation) in the field of ellipsometry lies in the fact that this made the technique suitable for modern investigations. For example, due to the work of Hauge et al³⁵ the ellipsometric set up could be used for measuring the thickness of dielectric films on silicon wafers in a manufacturing environment. The speciality of the set up is that it requires just five seconds for sample alignment, data acquisition, analysis and recording of film thickness with an accuracy of about 1Å. Another new branch in the field of ellipsometry is the spectroscopic ellipsometry. Its theory experimental aspects and uses are described by Aspnes³⁶. The Muller Matrix Ellipsometer (MME)^{37,38} is a recently evolved set up, in this field. The speciality of this set up is that it can determine the Muller matrix³⁹ of the measured optical system completely. Pulsed ellipsometry is a new technique used for high temporal resolution studies and uses pulsed lasers as

the light source. In this, the multichannel technique^{40,41} is to be noted here due to its speciality that the portions of the measured beam are individually routed to separate detectors having different polarisation sensitivities. This is achieved by using four separate beam splitters which provide four incident beams (nearly parallel) linearly polarised at 45° . These rays after reflection (or transmission) at the optical system are detected by four separate detectors from which the four Stokes parameters³⁹ are obtained. A fifth detector is also provided to monitor the incident intensity and to measure absolute reflectance.

1.4 Factors affecting the optical properties of thin films

The theory discussed above (in section 1.2) for a single layer film and stratified structure touches almost all the aspects of their optical properties. But there are several factors affecting the film (especially its surface) and thereby causing variations in its optical properties. This can be represented in a simple way⁴² as in fig.1.5. In that a single crystal film at OK, ∇ having no dislocations and vacancies and

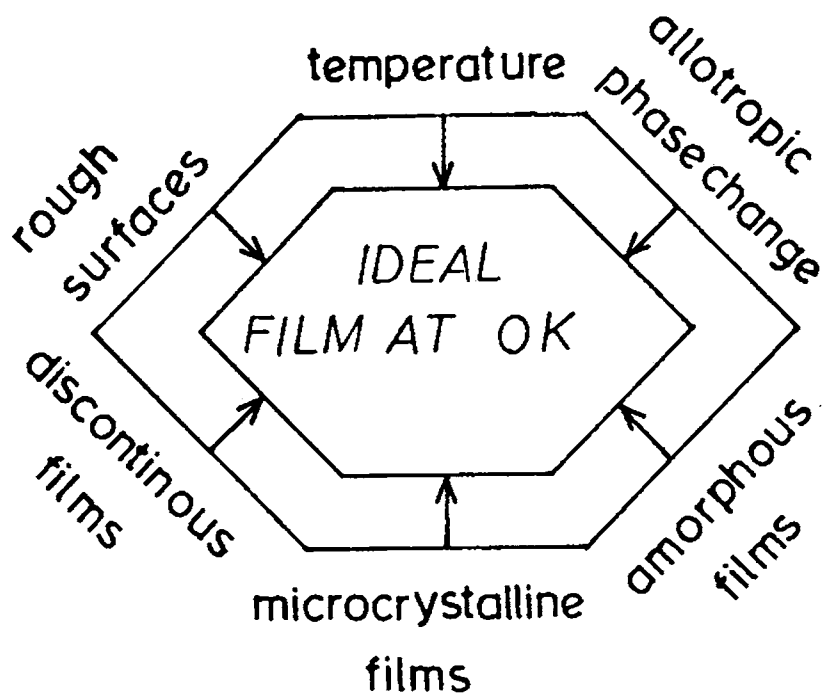


Fig.1.5 Factors affecting the optical properties of 'ideal film'.

having perfectly smooth and flat surfaces, is considered to be an 'ideal film'. Any deviation from this state represents a change in its structure and hence influences the optical property. The variation in temperature is an important factor affecting the optical property considerably. Due to the increase in temperature, the number of phonons increase and this will affect both interband and intraband parts of the absorption. The variation in intraband part of the absorption has been reported by Fäldt et al⁴² by measuring the optical conductivity in caesium. The effect on interband absorption has been elucidated through the optical conductivity measurements in aluminium⁴³. The same effect has been verified in the case of gold and copper by Pells et al⁴⁴ and studies in the same direction was carried out on gold and silver by Winsemius⁴⁵. Phase transitions in materials is another factor affecting their optical properties. The difference between graphite and diamond is a good practical example. Gallium is another example for this. The conventional α -phase of gallium which is stable at room temperature is

orthorhombic. But at temperatures below 70K one can get monoclinic β -phase by quench condensation. These two phases have entirely different optical absorption. The α -phase has a group of parallel bands in the region 1.3-2.3eV while the β -phase has a broad peak at 1.5eV^{46,47}. The transition from amorphous to crystalline state can affect the optical properties of films very much. For example amorphous films of germanium has a broad absorption band centred at 3eV while the optical absorption of its crystalline film has two prominent peaks, one at 2.5eV and the other at 4.5eV⁴⁸. Similarly in the case of gallium also, the strong parallel band absorption peaks in the visible and IR are completely absent in the amorphous state^{46,47}. The 'amorphous spectrum' is quite similar to the spectrum of liquid gallium. The same phenomenon is taking place in the case of amorphous and crystalline bismuth also⁴⁹. Another factor to be considered here is the micro-crystalline character of thin films. Evaporated films consist of small crystallites whose radius is (approximately) of the order of $1\mu\text{m}$ and these crystallites are separated by a region of highly disordered material along the grain boundaries. There is little or no

periodicity along the grain boundary whose thickness is of the order of $10-15\text{\AA}$ and this is independent of the grain size. As the deposition temperature is lowered there is considerable decrease in grain size⁵⁰ and at liquid helium temperatures the grain diameter of a large number of materials is of the order of $50-100\text{\AA}$. About 30% of the material is in a highly disordered state in this type of (micro-crystalline) samples and hence this can produce drastic effects on their optical properties. This effect has been observed by Welkowsky et al⁵¹ in the wavelength modulation spectrum of silver. Similarly Hunderi et al⁵² have obtained two peaks at 140K, one at 2.4eV and the other at 3.2eV. These peaks are attributed to modes excited by light polarised perpendicular and parallel to the grain boundary. Also these are absent when the films are annealed at 300 K. The film formation starts with the formation of islands and if the mass thickness is below a critical value the film is discontinuous. These islands cause anomalous absorption due to the excitation of a charge density oscillation in them. A theoretical model was set up by Maxwell-Garnett^{53,54} (the detailed discussion of which is given in chapter VIII)

in which the discontinuous film was treated as a collection of small metallic spheres. This has been verified experimentally and qualitative agreement has been obtained⁵⁵. Theoretical investigations with an aim to extend and modify the idea of Maxwell-Garnett are also carried out⁵⁶. Another important factor affecting the optical properties of thin films is the surface roughness and this has been an area of interest and several works have been published (both theoretical and experimental) regarding its effect on the optical properties of thin films⁵⁷⁻⁶². In the theories of optical properties of thin films the main assumption is that the surface (or interface between two media) of the medium is ideally smooth and flat. Also the variation in refractive index (as light enters into one medium from another) is considered to be sharp which will be true only if there is no 'mixing' between the media at the interface. These assumptions are hard to achieve in practical case, the main difficulty being in the nature of the surface itself. When the film surface comes into contact with the atmosphere several factors contribute to roughness. For example, the variation

in temperature is an important factor as far as metallic films are considered. The interaction with different impurities in the atmosphere (corrosion) is another cause of surface roughness. Again, layer formation (mainly oxide) over the film surface is a factor affecting the smoothness of the same. These factors causing surface roughness affect the optical properties in a three fold way⁴². First of all a part of the incident light is diffusely scattered into various directions. Secondly, on a rough metal surface, the incident wave may excite surface plasmons and this may alter the reflection and transmission coefficients very much. Finally a rough surface is having a larger effective surface area and this can increase, to some extent, the interband and intraband absorptions.

Thus it can be easily seen that the type of ideal film conceived in the theory is practically very difficult to obtain and the experimental results will be affected by many of the factors described earlier. But some of them can be avoided. For example, the variations due to thermal effects can be minimised

by using low temperature ambient for the film. However the factors like surface roughness or defects cannot be avoided and hence they must be taken into account while analysing the results.

1.5 Investigations in the present work

In the present work, the surface roughness due to thermal variation has been investigated optically. For this, reflectivity studies are done on silver and copper films. In the case of copper films electron micrographs are also taken. The variation of surface nature due to interdiffusion in Al-Ag films have been investigated by using reflectivity. Ellipsometric studies are performed to study the surface variation of silver films due to annealing (in low temperature range) and these results are again verified by using light scattering measurements. The apparatus and devices for these optical measurements were fabricated. The details of experimentation are provided at appropriate places in the following chapters.

A theoretical study, though on a different topic, carried out during the time of the investigation

is included in the appendix. It is a calculation of the eigenvector magnitudes in ZnS crystal by using the method of isotopic substitution.

REFERENCES

1. Max Born and Emil Wolf, Principles of optics, Pergamon, Oxford (1964) p.38.
2. P.Drude, Ann.Phys.Chem., 39 481 (1890).
3. O.S.Heavens, Optical properties of thin films, Dover Publications, New York (1965).
4. Tennyson Smith and G.Lundberg, Surf.Tech., 9, 1 (1979).
5. O.S.Heavens in G.Hass and R.E.Thun (eds), Physics of thin films, Vol.2, Academic Press, New York (1964).
6. K.L.Chopra, Thin film phenomena, McGraw-Hill, New York (1969) p.99.
7. Max Born and Emil Wolf, Principles of optics, Pergamon Press, Oxford (1970) p.57.
8. P.C.S.Hayfield and G.W.T.White in E.Passaglia, R.R.Stromberg and J.Kruger (eds.), Ellipsometry in the measurement of surfaces and thin films, Natl.Bur. Std.Misc.Publ. 256, U.S.Govt. Printing Office, Washington.
9. N.M.Bashara and D.W.Peterson, J.Opt.Soc.Am., 56,1320 (1966).

10. A.B.Buckman and N.M.Bashara, Phys.Rev., 174,719 (1968).
11. T.E.Faber and N.V.Smith, J.Opt.Soc.Am., 58, 102 (1968).
12. M.Erman, J.B.Theeten, N.Fodjdani and Y.Demay, J.Vac. Sci. & Tech. 131 328 (1983).
13. M.Erman and P.M.Frijilink, Appl.Phys.Lett., 43,285 (1983).
14. F.Meyer, Phys.Rev., B9, 3622 (1974).
15. C.L.Nagendra and R.L.Thutupalli, Appl.Opt., 20 2747 (1981).
16. C.L.Nagendra and R.L.Thutupalli, J.Phys.D 15 1153 (1982).
17. R.Dimmich and F.Warkusz, Phys.Status Solidi, A72 117 (1982).
18. E.Santamato, G.Abbate and P.Maddalena, Optics Commun. 46,284 (1983).
19. R.E.Hummel, D.B.Dove and J.Alfaro Holbrook, Phys. Rev.Lett., 25, 290 (1970).
20. J.Alfaro Holbrook and R.E.Hummel, Rev.Sci.Instr., 44,463 (1973).
21. R.E.Hummel, Optics Commun., 39, 55 (1981).
22. F.K.Urban III, R.E.Hummel and E.D.Vernik Jr., Corros.Sci., 22, 647 (1982).

23. A.M.Beers, H.T.J.M.Hintzen and J.Bloem, J.Elect. Chem.Soc., 130,1426 (1983).
24. T.Lopez-Rios, F.Abelés and G.Vuye, Le Journal de Physique, 40, L343 (1979).
25. Andreas Otto in B.O.Seraphin (ed.) Optical properties of solids : New developments, North Holland, Amsterdam (1976) p.677.
26. Zhang Shu-Yi, Yu Chao, Meao Yong-Zhi, Tang Zhing-yan and Gao Dun-tang, Accoustical imaging Vol.12, Proceedings of XII International Symp. on Accoustical imaging, London (1982)
27. J.Inagaki and Y.Nakagawa, Phys.Rev., B26, 6421 (1982).
28. A.Rosencwaig, J.Opsal and D.L.Willenberg, Appl. Phys.Lett., 43, 166 (1983).
29. Andreas Mandelles, J.Appl.Phys., 54, 3404 (1983).
30. H.Takasaki, Appl. Opt., 5, 759 (1966).
31. L.Ord and B.L.Wills, Appl.Opt., 6, 1673 (1967).
32. E.F.Roberts and A.Meadows, J.Phys.E, 7,379 (1974).
33. B.D.Cahan and R.F.Spanier, Surf.Sci., 16, 166 (1969).
34. D.E.Aspnes, Optics Commun., 8, 222 (1973).

35. P.S.Hauge and F.H.Dill, IBM J.Res.Devel., 17, 472 (1973).
36. D.E.Aspnes in B.O.Seraphin (ed.) Optical properties of solids : New developments, North Holland, Amsterdam (1976) p.799.
37. P.S.Hauge, J.Opt.Soc.Am., 69, 1519 (1979).
38. R.M.A.Azzam, Optics Commun., 25, 137 (1978).
39. P.S.Hauge, R.H.Muller and C.G.Smith, Surf.Sci., 96, 81 (1980).
40. F.H.Dill, E.P.Harris and P.S.Hauge, IBM Tech. Disclosure Bull., 19, 1487 (1976).
41. E.Collett, Surf.Sci., 96, 156 (1980).
42. O.Hunderi, Thin solid films, 57, 15 (1979).
43. A.G.Methewson and H.P.Meyers, J.Phys.F, 2, 403 (1972).
44. G.P.Pells and M.Shiga, J.Phys.C, 2, 1835 (1969).
45. P.Winsemius, Thesis, University of Leiden (1973).
46. O.Hunderi and R.Ryberg, J.Phys.F, 4, 2084 (1974).
47. O.Hunderi and R.Ryberg, J.Phys.F, 4, 2096 (1974).
48. M.Gandais, J.Rivory and M.L.Théye, Thin solid films, 12, 201 (1972).

49. O.Hunderi, J.Phys.F, 5, 2214 (1975).
50. H.Bulow and W.Buckel, Z.Phys., 145, 141 (1956).
51. M.Welkowsky and R.Braunstein, Solid State Commun., 9, 2139 (1971).
52. O.Hunderi and H.P.Myers, J.Phys.F., 3, 683 (1973).
53. J.C.Maxwell-Garnett, Philos.Trans.R.Soc.London, 203, 385 (1904).
54. J.C.Maxwell-Garnett, Philos.Trans.R.Soc.London, 205, 237 (1906).
55. S.Norrman, T.Anderson, C.G.Granqvist and O.Hunderi, Phys.Rev., B18, 674 (1978).
56. D.Bedaux and J.Vlieger, Physica, 73, 287 (1974).
57. P.Beckmann in E.Wolf (ed.) Progress in Optics, Vol.6, North Holland, Amsterdam (1967) p.53.
58. Carl A.Fenstermaker and Frank L.Mc Crackin, Surf.Sci., 16, 85 (1969).
59. I.Ohlidal and F.Lukes, Opt.Acta, 19, 817 (1972).
60. F.U.Hillebrecht, J.Phys.D, 13, 1625 (1980).
61. O.Hunderi, Surf.Sci., 96, 1 (1980).
62. G.Rasigni, F.Varnier, M.Rasigni, J.P.Palmari and A.Llebaria, Phys.Rev., B27, 819 (1983).

CHAPTER II

DESCRIPTION OF THE EXPERIMENTAL SET UP FOR THE DIFFERENT INVESTIGATIONS

2.1 Introduction

This chapter deals with the description of the experimental set up for the different experiments and also the method of preparation of the films in brief. This is divided into three parts. First part deals with the film preparation and its thickness measurement while the second one describes the method of annealing. The third part includes the optical measurements under three sub divisions dealing with reflectivity, ellipsometry and light scattering measurements.

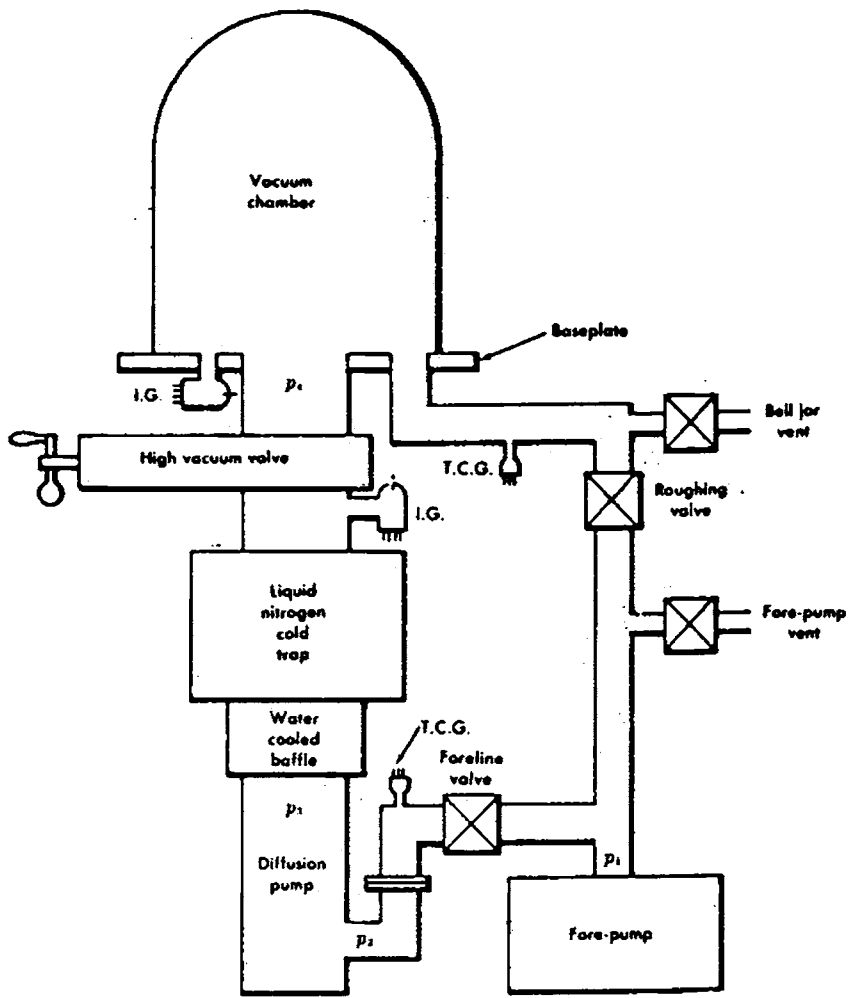
2.2 Film preparation and thickness measurement

All the films were prepared on glass substrates of size 7.5cms x 2.5cm x .14cm. This was first cleaned by using a detergent like Teepole and then using Acetone. After rinsing in distilled water these substrates were then subjected to ultrasonic vibrations to remove all traces of dust particles.

These were used for the film preparation after drying in an enclosed chamber.

The vacuum evaporation technique had been used for the preparation of films for all the experiments. During the time of coating, the pressure was always maintained at 10^{-5} torr. As usual in the vacuum evaporation technique, this low pressure was achieved in two stages. The pressure was lowered to 10^{-2} torr by using a Rotary pump and later for still lower pressure, the Diffusion pump was used. The block diagram of a typical vacuum evaporation unit is shown in fig.2.1. When the pressure was brought down ($< 10^{-5}$ torr) the required material was evaporated by heating it suitably. For aluminium, the heater was a coil made of tungsten wire while for silver and copper it was molybdenum boats. When two materials were evaporated one after the other (as in the case of Al-Ag bilayer films) two heating sources were used which were well separated using mica sheets. Always the distance between the heating source and the substrate was 15cms, their relative positions also being kept constant.

The required thickness for the films was



I.G. indicates positions of ionization gauges.
 T.C.G. indicates positions of thermocouple or Pirani gauges.

Fig.2.1 Typical vacuum coating unit.

obtained by evaporating the calculated quantity of the material and for this the expression used was

$$m = 4\pi\ell d^2t \quad (\text{for point source}) \quad (2.1)$$

and

$$m = \pi\ell d^2t \quad (\text{for small plane source}) \quad (2.2)$$

where m is the mass, ℓ is the density of the material, d is the distance between source and substrate and t is the required thickness. Among the films prepared, one would be made with a sharp edge (obtained by keeping the edge of a blade on the substrate). Later this film was overcoated with silver or aluminium and the thickness of the step thus formed was measured by the method of multiple beam interferometry². This is illustrated in fig.2.2. the details of which is given in a large number of text books dealing with thin films and other related properties. Here it was found that the thickness variation from the calculated value was always within $\pm 50\overset{\circ}{\text{A}}$.

2.3 Annealing

Annealing of the thin films was done in vacuum and also air. The pressure was maintained at

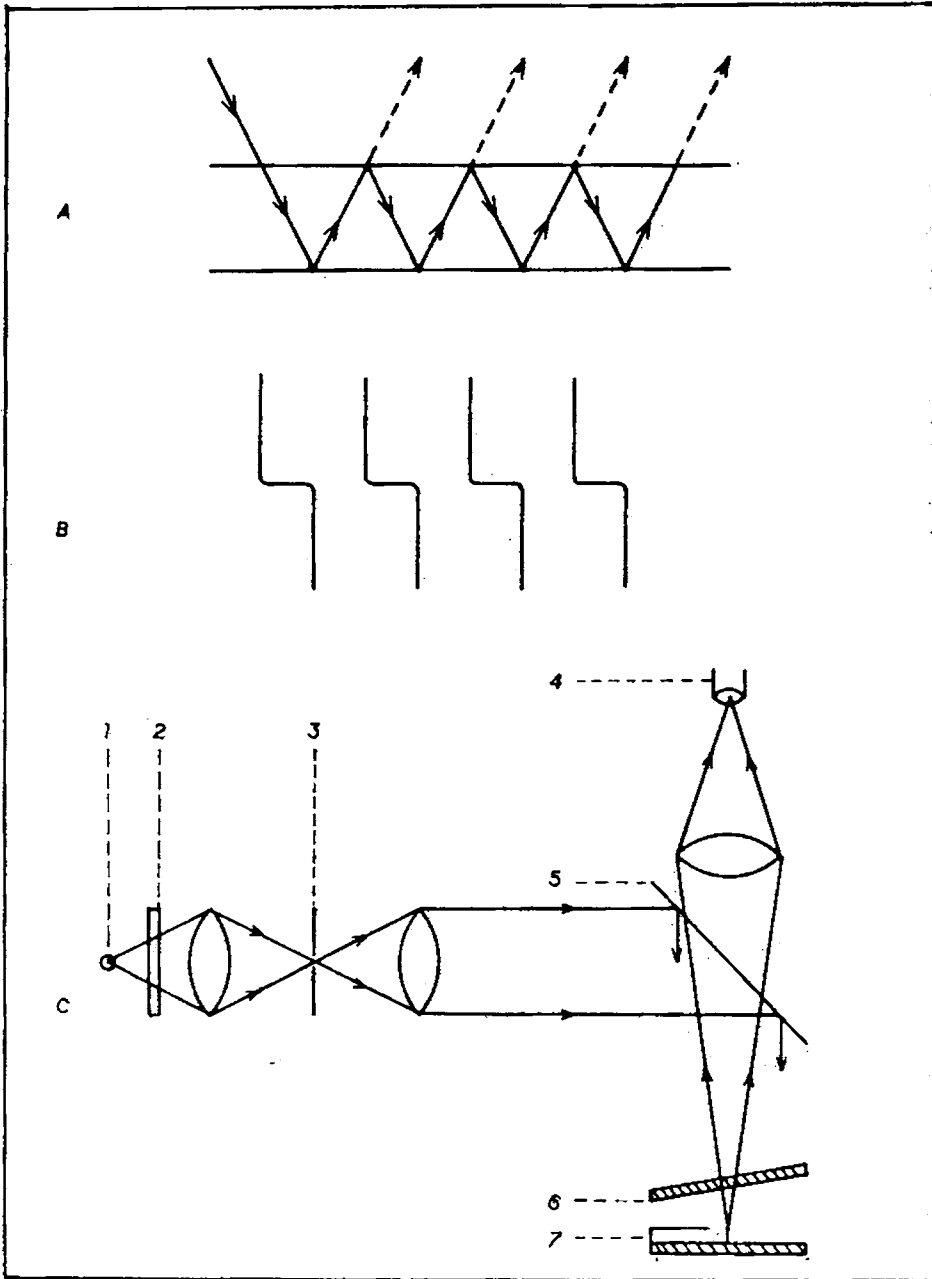


Fig.2.2 Optical method (multiple beam interferometry) for the film thickness measurement.
 A. Path of the light beam B. Shape of the fringes C. Experimental arrangement.
 1. Light source, 2. Filter, 3. Pin hole, 4. Microscope, 5. Beam splitter 6. Reference plate, 7. Film.

10^{-2} torr for the annealing in vacuum. This was achieved by using a rotary pump. Depending upon the type of the optical measurement, the annealing was performed in two different types of glass cells.

When the optical measurement was done after the annealing of the film at a particular temperature, it was done in an ordinary glass cell. It had a length of 30cms and diameter 10cms. The film to be annealed was kept at the centre of the cell. The junction of an Iron-Constantan thermocouple was kept in contact with the surface of the film. If the annealing was to be done in vacuum, the pressure was first reduced to 10^{-2} torr before heating started. The heating was applied radially by using a heating tape which was wound round the glass cell. The heating rate was controlled by regulating the voltage applied to the tape using a variac. Generally, the films were kept at the annealing temperature for 20 minutes and during this time the temperature was kept constant by adjusting the voltage (If the annealing time is different from this in any of the experiment that is noted in the concerned chapter). The heating

rate for the films with larger thickness value (ie., those having thickness $>2000\text{\AA}$) was usually $1^{\circ}\text{C}/\text{minute}$ and for the films with low thickness value (ie., thickness $<2000\text{\AA}$) it was $0.5^{\circ}\text{C}/\text{minute}$. The temperature was measured by noting the voltage developed across the thermocouple junction. This was done by using a microvoltmeter.

For in situ optical measurements during heating a special type of glass cell was designed (fig.2.3). This also had arrangements for evacuation. Its front side was made flat and it served as a glass window and hence the optical measurements could be done during heating itself. Here the heater coil was kept inside an aluminium block (electrically isolated from it by using mica sheets) and the film was kept in contact with the aluminium block. Generally, the films had their glass-side (back side) touching the aluminium block. The gradient drop of temperature across the thin substrate is negligible. In some cases, (especially for the Al-Ag bilayer films) heating was performed by keeping the front side of the film touching the aluminium block (see chapter IV). The temperature was measured by

using Iron-Constantan thermocouple. Its junction was kept in contact with the front side of the film without obstructing the light beam (see fig.2.3). Here also the heating rate was controlled with the help of a variac. The values of the heating rate were the same as before. But the optical measurement (most probably, the intensity of the reflected light) at a particular temperature was taken only after keeping the film at that temperature for five minutes.

The whole set up was fixed on a stand so that the film was always at a fixed position at the centre of the spectrometer (fig.2.4). The light from the collimator was made to fall on the film and the reflected light was collected by the telescope and subsequently by the PMT. When this cell was used, the angle of incidence was not varied, which was always 45° . This cell was very much useful for the diffusion studies of the Al-Ag bilayer films described in chapter V.

2.4 Optical measurements

This section deals with the description of the experimental set up for different optical

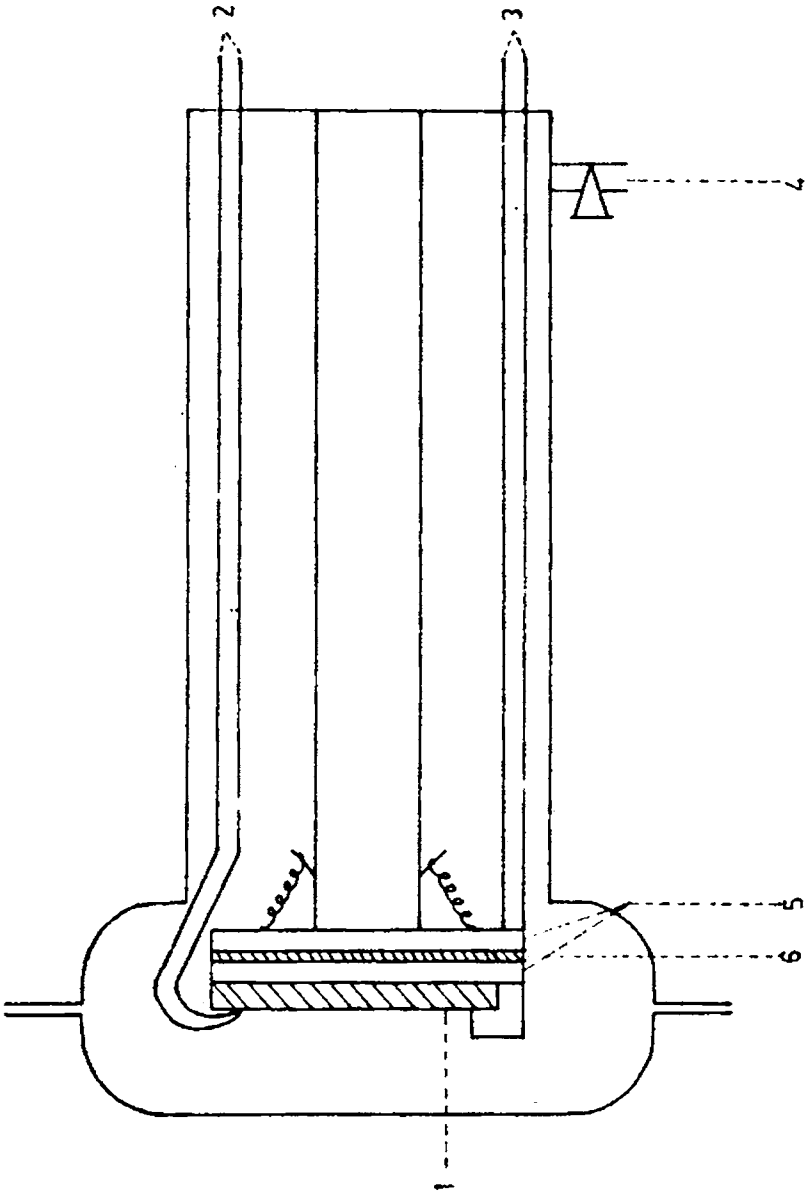


Fig.2.3 Glass cell for reflectivity measurements along with heating.
 1. Film, 2. Thermocouple, 3. Current leads (for heater),
 4. Connection to pump, 5. Aluminium blocks, 6. Heater.

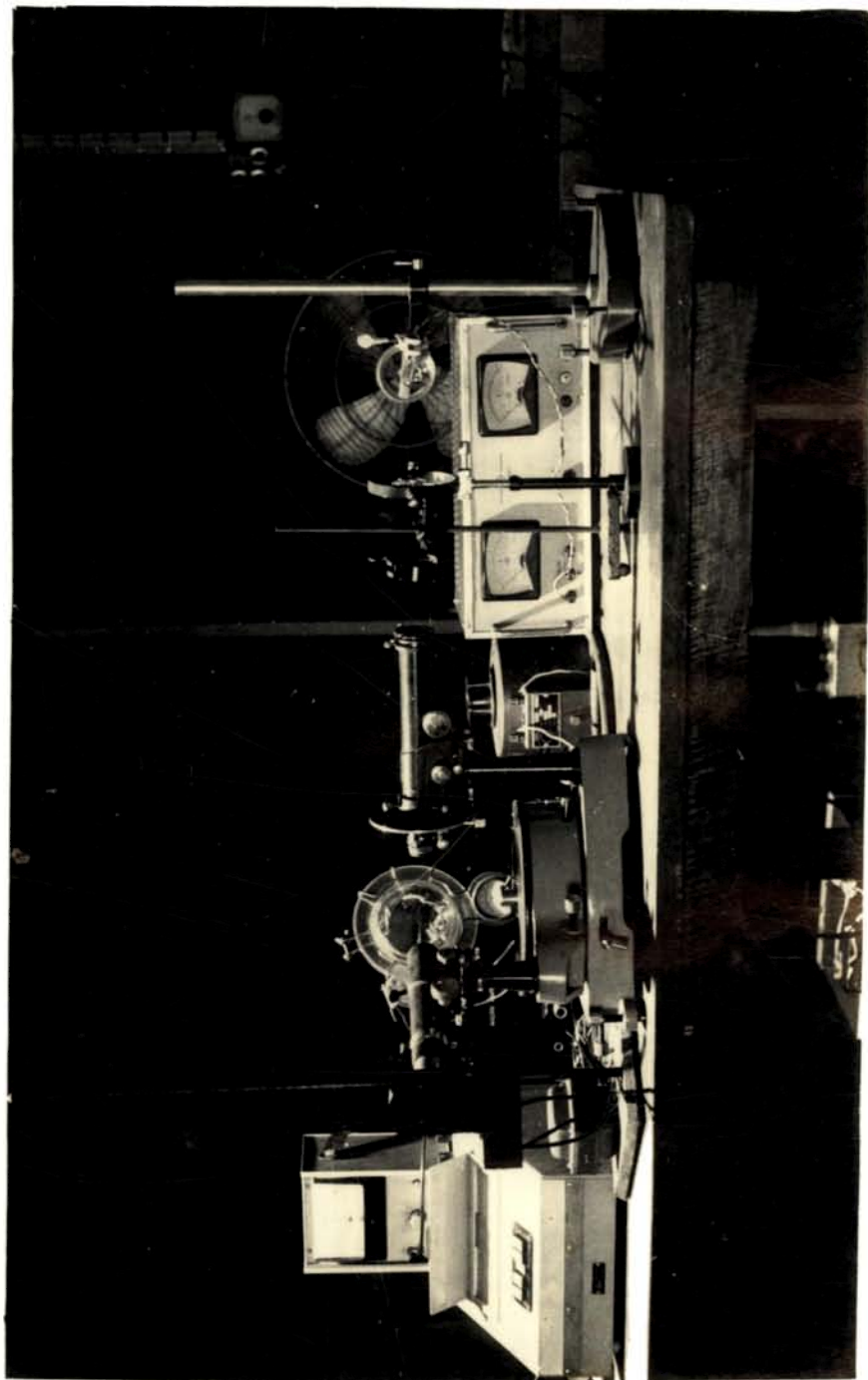


Fig-2-4 Exptl.set up for reflectivity measurement

experiments divided into three sub-headings. First one is the reflectivity measurements used for the study of silver films (chapter III), copper films (chapter V) and the interdiffusion in Al-Ag bilayer films (chapter IV). The second part describes the ellipsometric set up with which the hillock growth on silver films is studied (chapter VII) and the third part deals with the light scattering measurements on silver films (chapter VIII).

In all these experiments the light signal reflected from the surface is detected by a photomultiplier tube (PMT) 931-A RCA. Its maximum sensitivity is in the region $4000\overset{\circ}{\text{A}}-4500\overset{\circ}{\text{A}}$. Hence in all the experiments (unless specified otherwise) the wavelength of light used was $4400\overset{\circ}{\text{A}}$ and for this a filter was used. The output of the PMT was given to a Multiflex galvanometer and the deflection was noted. The D.C.voltage required for the PMT was in the range 750-1000V. The power supply for this was fabricated in the Laboratory and always 750V was given to the PMT.

The light source for the experiments was a tungsten filament lamp (36W). The power supplied to it was stabilised using a stabilised D.C.power supply.

The collimeter of a spectrometer was adjusted to give a parallel beam of light, which was used as the incident beam. The size of the beam was 1mm diameter. The reflected light was collected by the telescope. At the place of its eye-piece, the PMT was fixed and thus the intensity of the reflected light was measured. The film was fixed on the circular prism table using a clamp. But when the special type of heating cell (described in section 2.3) was in use, the prism table was removed and the cell was placed there (see fig.2.4).

2.4a Reflectivity measurements

When the reflectivity is measured along with heating the angle of incidence was kept constant and the film was kept inside the cell described in section 2.3. The well collimated light beam was adjusted to be incident on the film. The intensity of the reflected beam was measured using the PMT Galvanometer arrangement described earlier. After taking the initial reading the heating could be started and reflectivity was measured at different values of temperature. This arrangement is shown in fig.2.4.

But when the reflectivity is measured after annealing, the experiment is performed in a different way. Here the film was annealed in a simple cell described in section 2.3. After this, it was cooled to room temperature (at the same rate as the heating was done) and was fixed on to the prism table using the clamp. The intensity of the reflected beam was measured as explained earlier, at different angles of incidence. The whole procedure was repeated after annealing the film at a different temperature. In the reflectivity measurements care was taken to have the incident beam falling on the same portion of the film always. In all the cases the experiments were repeated a number of times.

2.4b Ellipsometric set up

The experimental set up consisted of polariser-system-analyser (PSA) arrangement. Its detailed theory and the method of measurement are given in chapter VI while the experimental results obtained using this is included in chapter VII. The polariser was introduced after the collimator and the analyser was fixed on the telescope (see fig.2.5). Both polariser and analyser could be



Fig. 2.5 Ellipsometric set up

used to measure a change in the polarisation as low as $1'$. The plane of incidence was fixed on the polariser by keeping a plane glass plate in the position of the film at an angle of incidence, equal to the polarising angle. Keeping the polariser at a fixed azimuth with respect to the plane of incidence (at $+45^\circ$, 0 and -45°). This was repeated for different angles of incidence (The range of angle of incidence was between 50° and 80°). During these measurements the film was kept fixed on the prism table by means of a clamp. The whole process was performed after each annealing.

2.4c Light scattering measurements

The experimental arrangement for this was almost similar to that of the ellipsometric set up with the only difference that here no analyser was used (see fig.2.6). The polariser was having its azimuth such that the plane of polarisation was always parallel to the plane of incidence (ie., the incident light beam is p-polarised). This was merely to make the theoretical calculation of the reflected intensity of light from the ideally smooth

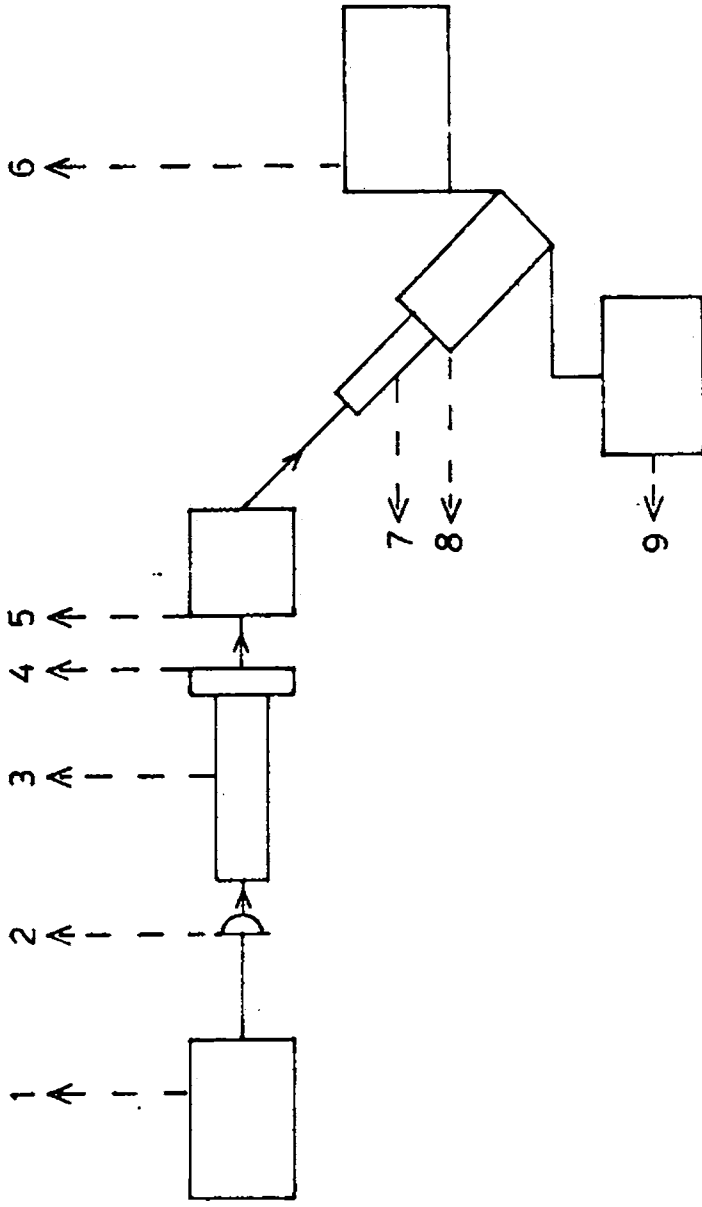


Fig.2.6 Block diagram of the experimental set up for the light scattering measurements.

1. Stabilised low voltage power supply
2. light source
3. Collimator
4. Polariser
5. Optical system (film)
6. PMT Power supply
7. Telescope
8. PMT
9. Galvanometer.

surface (I_{s0}) much easier. Theoretical aspects regarding the scattering of light waves from a rough surface and the calculation of the rms value of roughness are given in chapter VIII. It also contains the results of the measurements done on silver films.

Here also, the film was kept fixed on the prism table and the intensity of reflected light was measured at different angles of incidence (θ). The graph was plotted with $\cos^2 \theta$ on X-axis and $\ln R_s$ on Y-axis (R_s is the ratio of the intensity of reflected light from the rough surface (I_s) to that from an ideally smooth surface (I_{s0})). The size of the roughness is obtained from the slope of the curve.

2.5 The scanning electron micrographs

The pictures of the surface of copper films (before and after heating) given in chapter IV were obtained by using the scanning electron microscope at the Regional Research Laboratory, Trivandrum. The magnification was 5000X. The analysis using the electron microscope showed that the smoothing of the surface

due to annealing is taking place on all the films and the micrograph given in chapter V is that of the film with lowest thickness (ie., $500\overset{\circ}{\text{Å}}$).

REFERENCES

1. Robert W.Berry, Peter M.Hall, and Murray T.Harris, Thin film technology, D.Van Nostrand Company, New Jersey (1968) p.160.
2. S.Tolansky, Surface Microtopography, John Wiley and Sons, New York (1960).

CHAPTER III

OPTICAL STUDY OF THE EFFECTS OF ANNEALING ON SILVER FILMS

3.1 Introduction

Silver films have been extensively studied by many workers mainly due to two reasons. One is that it has got very high reflectivity in the visible region^{1,2}. The second reason is that it is highly inert under different ambient conditions. It is not oxidised even in the presence of oxygen at a pressure of 90.7 kP and in the temperature range -78°C to 400°C ³. Hence these films find extensive use in solar reflectors and also in other branches of physics, like lasers, holography etc., where very high reflectivity is essential.

However even for the inert films there can be considerable variations in their optical properties, due to heating⁴. This happens as a result of the changes occurring in their structure and in the nature of their surface. This is much pronounced in the case of silver thin films. Hence several investigations

have been carried out to study the thermal effects on these films and most of them are centred around their optical properties. Of these Richard Zito⁵, has studied the variations in reflectivity and resistance due to heating and he explained these on the basis of hillock growth. A.E.B.Presland et al^{6,7} has given a theoretical approach for the changes produced by heating. Sharma and Spitz, through a series of publications, have gone much deeper into the problem and their study was mainly by using electron microscope⁸⁻¹². A lot of other workers have also studied different aspects of heating on silver and other thin films¹³⁻¹⁹. In almost all the publications, it is shown that heating results in hillock growth on the surface of films. This has a strong dependence of factors like ambient conditions in which films are heated, thickness of the film, its structure etc. In order to understand these factors, the theory behind hillock growth may be considered in detail.

3.2 Theory of hillock growth

When thin metal films are bonded to rigid substrates, thermal stress arises upon heating it above the deposition temperature. This is due to the difference

in coefficients of thermal expansion between the substrate and the film. If the coefficient of thermal expansion of the substrate is smaller than that of the film (which is the case when film is metallic and substrate is a material like glass) the thermal stress in the film plane is compressive upon heating and tensile on cooling. Sufficiently large thermal stress can cause slip in epitaxial films and both slip and hillock formation in polycrystalline films²⁰⁻²³.

Through a rigorous mathematical analysis, Presland^{6,7} has shown that the hillock growth occurs due to surface diffusion and this is closely linked with surface energy and the stress in the film. He has given the equation for the diffusion flux, as

$$j = \frac{D_s}{kTr_c} \left(\sigma - \frac{2\gamma}{r} \right) \quad (3.1)$$

where D_s is the surface diffusion coefficient, k is Boltzmann's Constant, T is the absolute temperature σ is the stress in the film, γ is the surface energy, r_c is half the interhillock distance and r is the

radius of the circle from which the diffusion takes place for the hillock growth. From the above equation it is easily seen that if hillock growth is to occur,

$$\gamma \leq \frac{\sigma r_0}{2} \quad (3.2)$$

where r_0 , is the (average) size of initial surface irregularities. Thus in hillock growth as in the case of void growth (where the applied stress must be sufficient to overcome the increase in surface energy caused by creating a void) the applied stress is only sufficient to create hillocks if it outbalances the surface energy.

But the surface energy (γ) strongly depends upon the partial pressure of oxygen (P_{O_2}) and is independent of temperature. Its relation with pressure of oxygen is governed by the equation²⁴

$$\gamma = 228 - 188 \log_{10} P_{O_2} \quad (3.3)$$

The second factor to be considered (in eqn.3.1) is r . Its variations can be studied by noting the variations in 'catchment area' (ie., the area from where the

material for the hillock growth comes by diffusion). This also is not affected by the variations in temperature. But a strong relationship with oxygen pressure has been noted²⁵ similar to that in the case of surface energy as

$$A_c = 0.67 - 0.16 \log P_{O_2} \quad (3.4)$$

This relation between P_{O_2} and A_c is illustrated in fig.3.1. The diffusion coefficient (D_s) is also found to be free from temperature effects. But here also, the presence of oxygen can produce a slight increase in the value of D_s which is not a significant change⁶. From eqns.3.3 and 3.4 it is clear that the diffusion flux (j) has a much higher value when heating is done in presence of oxygen (ie., in air). Or in other words heating in air results in larger hillocks.

The only factor in eqn.3.1 to be considered is the stress in the film (σ). It is found that heating directly affects its value. Hence to understand the thermal effects deeply, one has to consider the stress in the film in a more detailed manner.

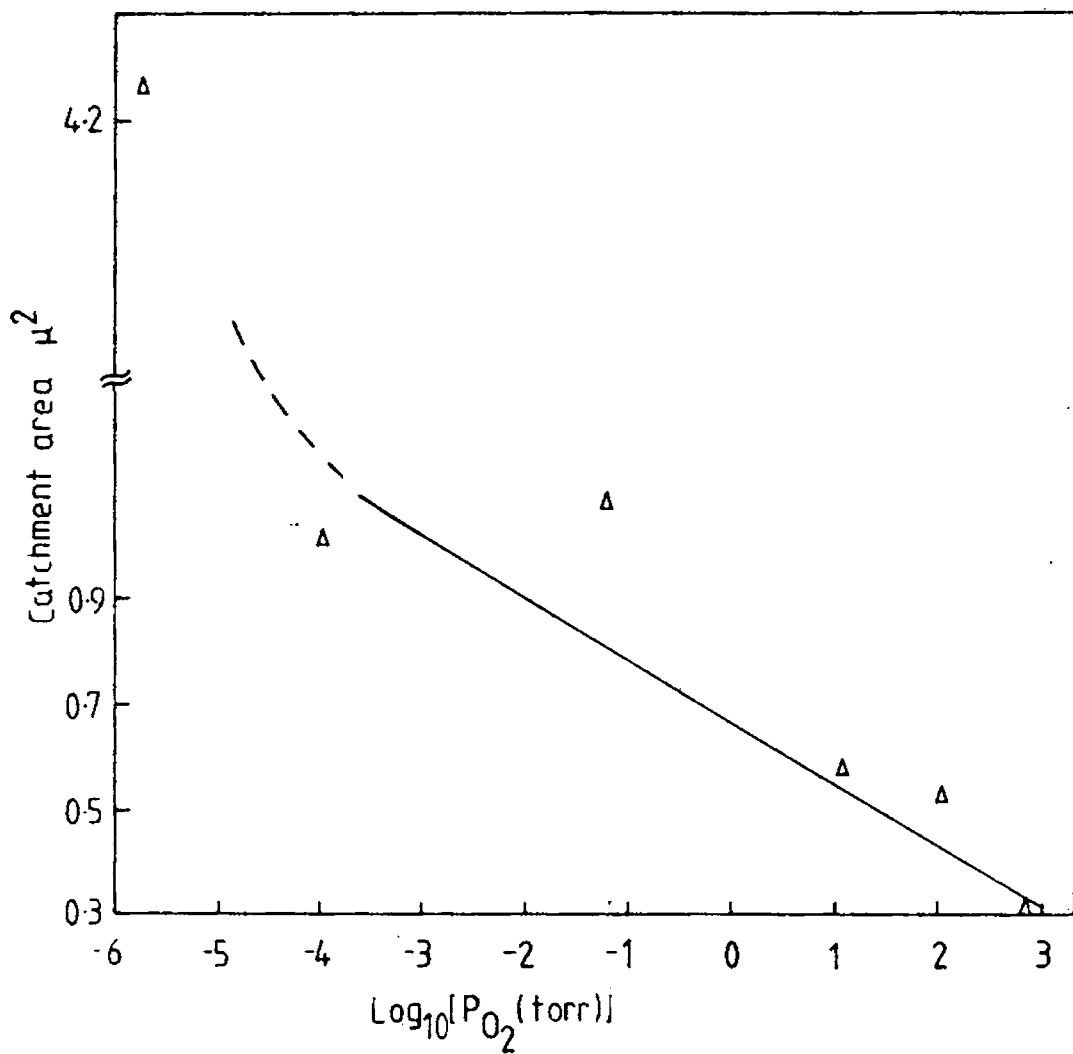


Fig.3.1 Variation of catchment area (A_c) with pressure of oxygen (P_{O_2}) for silver films.

3.2a Stress in thin films (metallic)

Nearly all films irrespective of their method of preparation, have internal stress. This may be compressive (in which case the film would 'like' to expand parallel to the surface) or tensile (in which case the film would 'like' to contract) as explained in section 3.2. This internal stress will be normally of the order of 10^8 to 10^{10} dynes cm^{-2} for metallic films when the deposition temperature is between 50°C and a few hundred $^\circ\text{C}$.

In general, the stress in a film can be written as a sum of three components as

$$\sigma = \sigma_{\text{intrinsic}} + \sigma_{\text{thermal}} + \sigma_{\text{external}} \quad (3.5)$$

In this eqn. the first term on RHS ($\sigma_{\text{intrinsic}}$) arises from different factors. One is that there can be a temperature gradient across the substrate due to the radiant heat from the source and the latent heat of evaporant²⁶. The second factor causing the intrinsic stress is the difference in thermal expansion of the film and substrate and the third factor behind

this is the nonuniformity in the expansion of the substrate itself²⁷. This stress is found to be tensile in nature^{23,27} for metallic films.

The second term on RHS of eqn.3.5 arises only when the film is heated such that its temperature increases above its deposition temperature. The nature of this stress is compressive for metallic films deposited on glass substrates (as explained in the section 3.2). The third term (ie., σ_{external}) represents any stress applied externally on the film.

Thus it becomes clear that the intrinsic stress and thermal stress are mutually opposite. Or in other words, if one is taken to be positive the other is to be taken as negative. Also, if the film is heated to a temperature above its deposition-temperature the component σ_{thermal} alone increases. Hence the resultant stress in the film (σ) which is the algebraic sum of these, is reduced and becomes a minimum at a particular temperature whose value depends on the value of $\sigma_{\text{intrinsic}}$. As the value of stress in the film is reduced, the condition for

hillock growth given in eqn.3.2 is not satisfied whereby the hillock growth is stopped. To get a film of minimum stress, is of great importance since it has applications in different applied fields. The present work on silver films was done to investigate this aspect in detail and also to study variations of the surface energy of silver films in different ambient conditions.

3.3 Experimental details

The films were prepared by vacuum evaporation technique which is described in detail in chapter II. The pressure during the deposition was 10^{-5} torr and the substrates were maintained at room temperature itself. To ensure uniform coating, substrates were kept at a large distance (ie., 15cm) from the heating source. The thickness of the films was approximately 1000^oÅ. For this the mass of the evaporant was calculated using the expression²⁸,

$$m = \pi \rho d^2 t \quad (3.6)$$

where ρ is the density of the material, d is the

distance between heating source and the substrate and t is the thickness of the film. Later the thickness was verified by using the multiple beam interferometry²⁹.

Annealing was done both in air and vacuum, maintaining a pressure of 10^{-2} torr in the latter case. The details of the cell used for this purpose are given in chapter 2. The heating rate was always kept fixed at $1^{\circ}\text{C}/\text{minute}$ since fast heating was found damage the film surface appreciably. The annealing time, ie., time for which the film is kept at the annealing temperature, was 30 minutes in all the cases. Cooling was also done at a slow rate ie., $1^{\circ}\text{C}/\text{minute}$ to avoid damage due to sudden cooling. All the films were heated on the glass-side (ie., substrate side).

The reflectivity measurement was performed by using a PMT and galvanometer arrangement (as described in the earlier chapter). The wavelength of the light used for the investigation was $4400\overset{\circ}{\text{A}}$ since the PMT has a maximum sensibility in this region.

3.4 Results

Results can be considered separately for films annealed in air and vacuum. Fig.3.2 gives the variations in reflectivity with angle of incidence due to annealing in vacuum while fig.3.3 gives those for films annealed in air. One thing to be noted in common for both cases is that before annealing they are having similar reflectivities for all angles of incidence.

3.4a Annealing in vacuum

Due to vacuum annealing the reflectivity is found to be increasing upto a temperature of $\sim 200^{\circ}\text{C}$. Beyond that the increase is almost stopped, which is clear from the fig.3.2. A steep increase is occurring as a result of annealing at 105°C . But afterwards the increase is reduced and finally it is almost stopped at 286°C . About 20 percent increase in reflectivity is obtained when films are annealed at 105°C .

3.4b Annealing in air

From the fig.3.3 it can be seen that annealing at 104°C does not produce much effect. Only

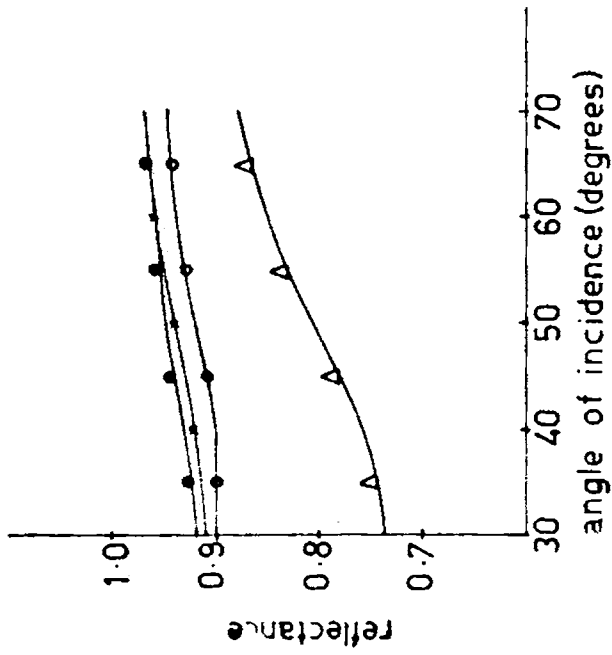


Fig. 3.2 Reflectivity of silver films annealed in vacuum (wavelength - 4400Å):
 Δ—Δ before annealing;
 ○—○ after annealing at 105°C
 x—x after annealing at 210°C
 ●—● after annealing at 286°C

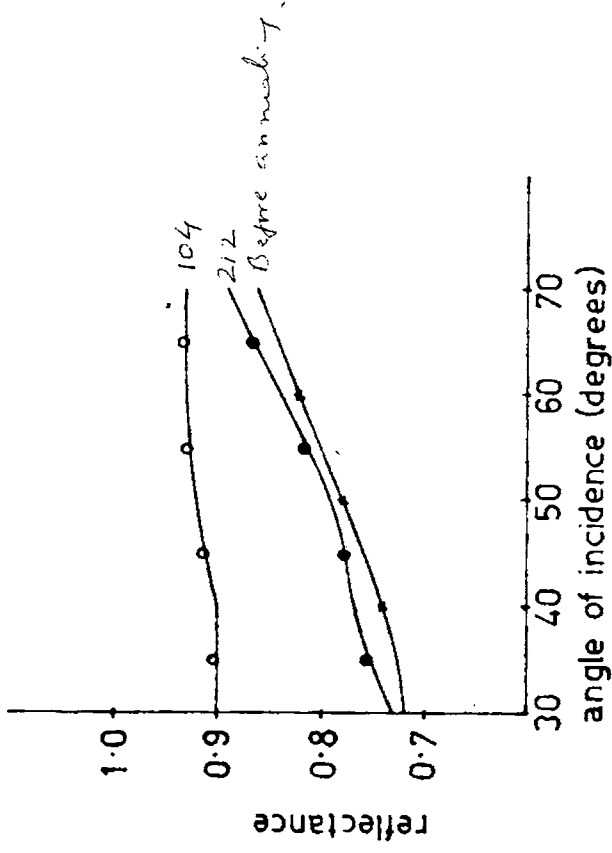


Fig. 3.3 Reflectivity of silver films annealed in air (wavelength - 4400Å): x—x before annealing;
 ○—○ after annealing at 104°C;
 ●—● after annealing at 212°C

by annealing the films at 212°C an appreciable increase in reflectivity ($\sim 20\%$) is obtained. Hence the results of vacuum annealing that take place at 105°C occur only at 212°C .³⁰

3.5 Discussion

In the case of vacuum annealing it is quite clear that due to annealing at 105°C the film surface is smoothed as a result of which the reflectivity increases. But on increasing the annealing temperature, this phenomenon is almost stopped indicating the film surface becoming rough. The only thing which can take place on the surface of silver thin films due to heating is hillock growth and hence these results can be explained on that basis.

One knows that the film surface becomes irregular due to hillock growth and this occurs only when the condition in eqn.3.2 is satisfied. On heating the film to a temperature above deposition temperature, the thermal stress (σ_{thermal}) starts increasing and since this stress is opposite to the intrinsic stress ($\sigma_{\text{intrinsic}}$), this results in reduction of

resultant stress (σ) in the film. When the value of σ is reduced to such an extent that $\gamma > \frac{\sigma r_0}{2}$, no

hillock growth occurs and film surface is smooth. This results in the increase of reflectivity. Hence there is sharp increase in reflectivity for the films annealed in vacuum, upto 105°C .

But further increase in temperature results in the increase of thermal stress considerably so that it becomes the major component of the stress in the film (σ). Or in other words, the value of thermal stress goes much above that of the intrinsic stress and hence the stress in the film is steadily increasing along with the thermal stress. Therefore the condition for the hillock growth (eqn.3.2) is reestablished i.e., the film surface starts to become irregular thereby causing reduction in the increase of reflectivity.

In the case of films annealed in air these results occur only at a high temperature. The sharp increase in reflectivity occurs at 212°C . This can be explained by considering eqn.3.3 which gives the relation between surface energy γ and the pressure of oxygen. It is clear from the eqn. that γ is considerably

decreased in presence of oxygen. Hence for the films annealed in air, the value of γ will be much small. But to have the film surface smoothed, one should have,

$$\gamma > \frac{\sigma_r}{2} \quad (3.7)$$

Since γ is having a very low value in this case to satisfy the condition in eqn.3.7, the value of σ should also be lowered very much. For this, the value of thermal stress (σ_{thermal}) should be increased much. This can take place only at a higher temperature, compared to the case of vacuum annealing. Hence in this case the surface smoothing occurs only at a temperature of about 212°C.

3.6 Conclusion

In this work, mainly two things are studied optically. First one is the relation between surface roughness and the stress in the film while the second aspect is the variation of surface energy in the presence of oxygen.

In the former case, it has been found that, the stress in the film can be reduced to a minimum by

annealing it and the temperature at which the stress is minimised depends upon the value of intrinsic stress in the film, which in turn, depends on different parameters. Regarding the second aspect, it is found that the surface energy (of silver) is considerably reduced when the film surface is in contact with oxygen and hence the minimum value of stress can be achieved only at a very high temperature, when compared with vacuum annealing.

REFERENCES

1. K.L.Chopra in Thin film phenomena, McGraw Hill, New York (1969) p.777.
2. L.F.Drummer and G.Hass in G.Hass and R.E.Thun (eds.) Physics of thin films, Vol.2, Academic Press, New York (1964) p.305.
3. A.W.Czanderna in K.Behrndt (ed.), Vacuum Microbalance Technique, Vol.5, Plenum Press (1966) p.135.
4. O.Hunderi, Thin Solid Films, 57 15 (1979).
5. R.Zito, Thin Solid Films, 60 27 (1979).
6. A.E.B.Presland, G.L.Price and D.L.Trimm in Sydney G.Davison (ed.), Progress in Surface Science, Vol.3, Pergamon Press, Oxford (1973) p.63.
7. A.E.B.Presland, G.L.Price and D.L.Trimm, Surf. Sci., 29,424 (1972).
8. S.K.Sharma and J.Spitz, Thin Solid Films, 65,339 (1980).
9. S.K.Sharma and J.Spitz, Thin Solid Films, 56,L17 (1979).
10. S.K.Sharma and J.Spitz, Thin Solid Films, 66, L51 (1980).

11. S.K.Sharma and J.Spitz, Thin Solid Films, 67, 109 (1980).
12. S.K.Sharma and J.Spitz, Phil.Mag., A41, 209 (1980).
13. P.H.Smith and H.Gurev, Thin Solid Films, 45 159 (1977).
14. M.L.Gimpl, A.D.Mc Master and N.Fuschillo, J.Appl. Phys., 35, 3572 (1964).
15. W.B.Pennebaker, J.Appl.Phys. 40, 394 (1969).
16. W.M.Kane, J.P.Spratt and L.W.Hershinger, J.Appl. Phys., 37, 2085 (1966).
17. S.K.Lahiri and O.C.Wells, Appl.Phys.Lett., 15 234 (1969).
18. T.F.Swank and K.R.Lawless, J.Appl.Phys., 35, 3574 (1964).
19. P.Sharnhorst, Surf.Sci., 15, 380 (1969).
20. S.K.Lahiri, J.Appl.Phys., 41, 3172 (1970).
21. W.B.Pennebaker, I.B.M.Res.Rep. RC-2105 (1968).
22. A.Gangulee, Phil.Mag., 22, 865 (1970).
23. Maria Ronay and C.F.Aliotta, Phil.Mag., 42, 161 (1980).
24. F.H.Buttner, E.R.Funk and H.Udin, J.Phys.Chem., 56, 657 (1952).

25. W.W.Mullins, Phil.Mag., 6, 1313 (1961).
26. E.Klokholm, IBM Res.Rep.RC-1352 (1965).
27. David C.Campbell in Leon I.Maissel and Reinhard Glang (eds.), Hand Book of Thin Films Technology, McGraw Hill, New York (1970) p.12-3.
28. Robert W.Berry, Peter M.Hall and Murray T.Harris, Thin Film Technology, Van Nostrand Rheinhold, New York (1960) p.160.
29. S.Tolansky, Surface Microtopography, John Wiley and Sons, Inc., New York (1960).
30. K.P.Vijayakumar and C.Purushothaman, Thin Solid Films, 82, 225 (1981).

CHAPTER IV

STUDY OF THE SURFACE CHANGES ON COPPER FILMS DUE TO THERMAL TREATMENT

4.1 Introduction

Copper, like silver, is well-known for its high conductivity and good reflectivity. Hence this is used in different electronic devices as the conducting lead. Also copper thin films are used as mirrors in some lasers and solar reflectors. But in all these instances temperature variations cause drastic effects which are even detrimental in some cases. For example, an increase in temperature can cause interdiffusion between different layers (in the case of multilayer films), the formation of an oxide layer on the surface of the film, changes in the grain size of the film, or variations on the surface smoothness of the film depending upon the conditions and nature of heating. Hence active research is going on in the case of copper (both in thin film and bulk form) in order to understand the nature of changes due to heating and to find out the ways to minimise them. Some of the recent works in the most important aspects of copper are briefly reviewed below.

One of the active areas of research in the case of this material is the variations of particle (grain) size due to heating¹⁻⁷. Of these, Sen⁵ had reported that there can be a change of 800Å⁰ in the grain size due to annealing the copper films at 120°C for 2 hours. But Gangulee³ observed a two stage process in the phenomenon of grain growth as a result of heating. First stage is upto 200°C for which the activation energy is 0.3 - 0.4eV and in this stage only minor changes are taking place in grain size. The second stage occurs above 200°C and is having an activation energy of 0.65eV. In this stage major changes are taking place. Hofer et al^{1,2} also have some observations supporting the above results.

Studies on thermoelectric power⁸⁻¹³ can reveal a lot about transport mechanism and also distortions in Fermi surface. Research work in this direction is also very active in the case of copper. However, there is wide divergence among the experimentally obtained values by different workers¹³.

Another important area of research is perhaps the optical properties and the variations of the same under different conditions¹⁴⁻²⁶ (especially due to

heating). This broad topic includes the surface damages due to laser irradiation¹⁴⁻¹⁷, the variations in optical properties due to surface roughness^{25,26} and the studies on the film surface so as to know in detail about its use as a solar reflector²¹⁻²⁴. Of these, Harding et al²² have reported that copper surface will be stable upto 400°C in vacuum. In another reported work, Turley et al²³ have shown that the structure of copper surface, which is mechanically polished, is crystalline. Wu et al²⁶ reported that electrodeposited copper foils have two types of irregularities on their surfaces--one is cone shaped and the other, small nodules-like. Also Thomas et al¹⁴ have studied the variations in performance of the copper mirrors finished by different methods.

There has been not much published work on the study of variation of reflectivity with continuous variation of temperature. This may be of importance regarding the use of copper films as mirrors in different ambient conditions where temperature increase is expected to take place. Hence in this chapter the results of such a work is described in which the temperature is varied upto 200°C. This particular

temperature range has been selected because the stress minimisation is taking place in this range as described in chapter III.

4.2 Experimental set up

All the films used in this study were prepared by the vacuum evaporation technique as described elsewhere²⁷. The pressure during deposition was lower than 10^{-5} torr and the films were prepared both at room temperature and at higher temperature. The distance between the source and substrate was 15cm to ensure uniform coating. All the samples were prepared under identical conditions.

Films of thickness ranging from 500^oA to 3000^oA were prepared. The mass of the evaporant required for each thickness was calculated using the expression²⁸ given in the chapter III. After evaporation the thickness was again measured by using the method of multiple beam interferometry²⁹. In each case the film thickness was found to be accurate within the limit of ± 50 ^oA.

Heating of the films was done in a special type of glass cell described in chapter II, in which

both heating and reflectivity measurements could be done simultaneously. Films were always heated on the glass-side and temperature was measured by using an Iron-Constantan thermocouple. Heating rate was very low ($1^{\circ}\text{C}/\text{minute}$) for all the films to avoid any damage due to high heating rate. Also for all films, the pressure was below 10^{-2} torr during heating which helped to have identical ambient conditions in each case.

The measurement of reflectivity was done in the same way as described in chapter III and the set up is described in detail in chapter II. Here the only difference was that reflectivity was measured during heating at different temperature values. Before taking the reading the film was kept at the particular temperature for five minutes.

4.3 Results

Fig.4.1 gives the reflectivity variations with temperature for the films prepared at room temperature. Fig.4.2 shows the same for films prepared at higher temperature. In both the figures, readings from $\sim 100^{\circ}\text{C}$ is only shown since there is almost

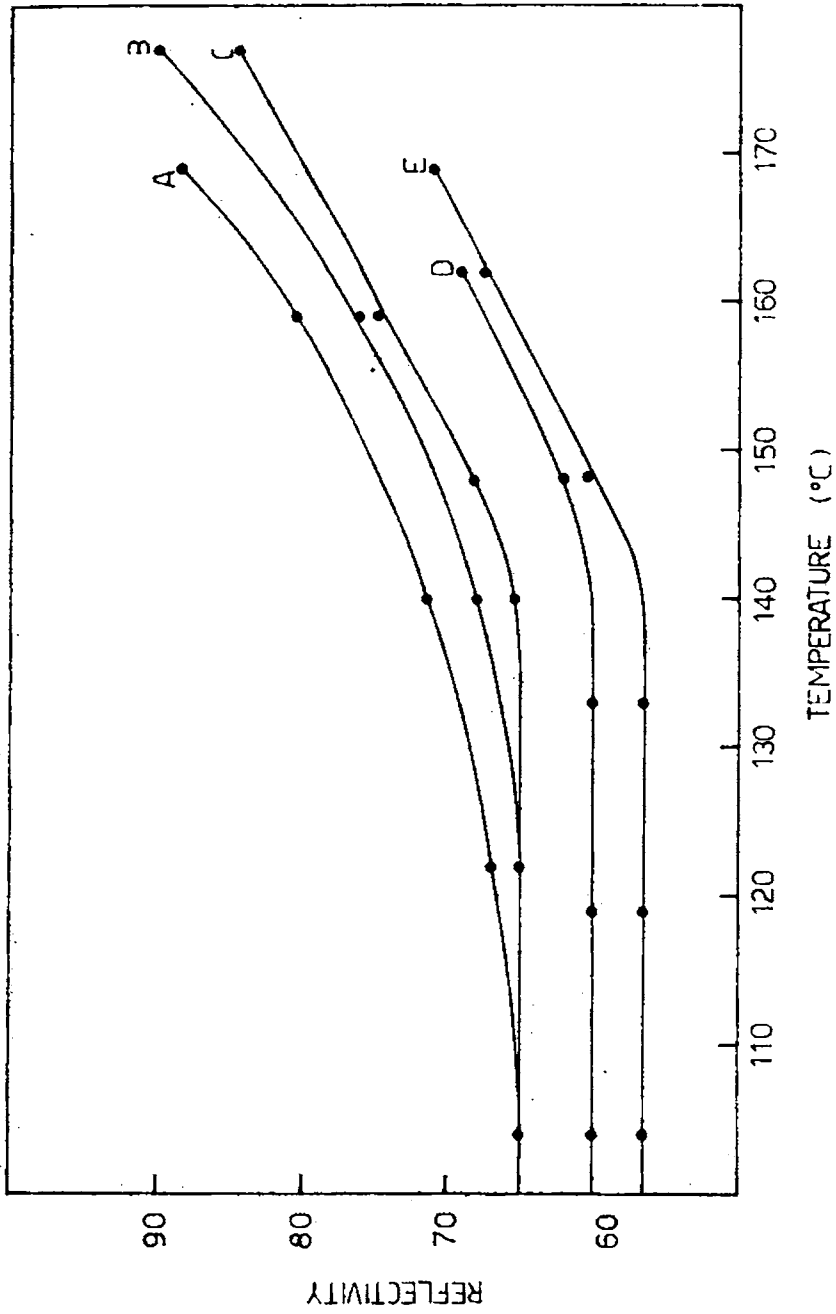


Fig.4.1 Variation in reflectivity with temperature for copper films of various thicknesses deposited at room temperature (wavelength - 4400Å). A - 3000Å, B - 2000Å, C - 1500Å, D - 1000Å, E - 500Å.

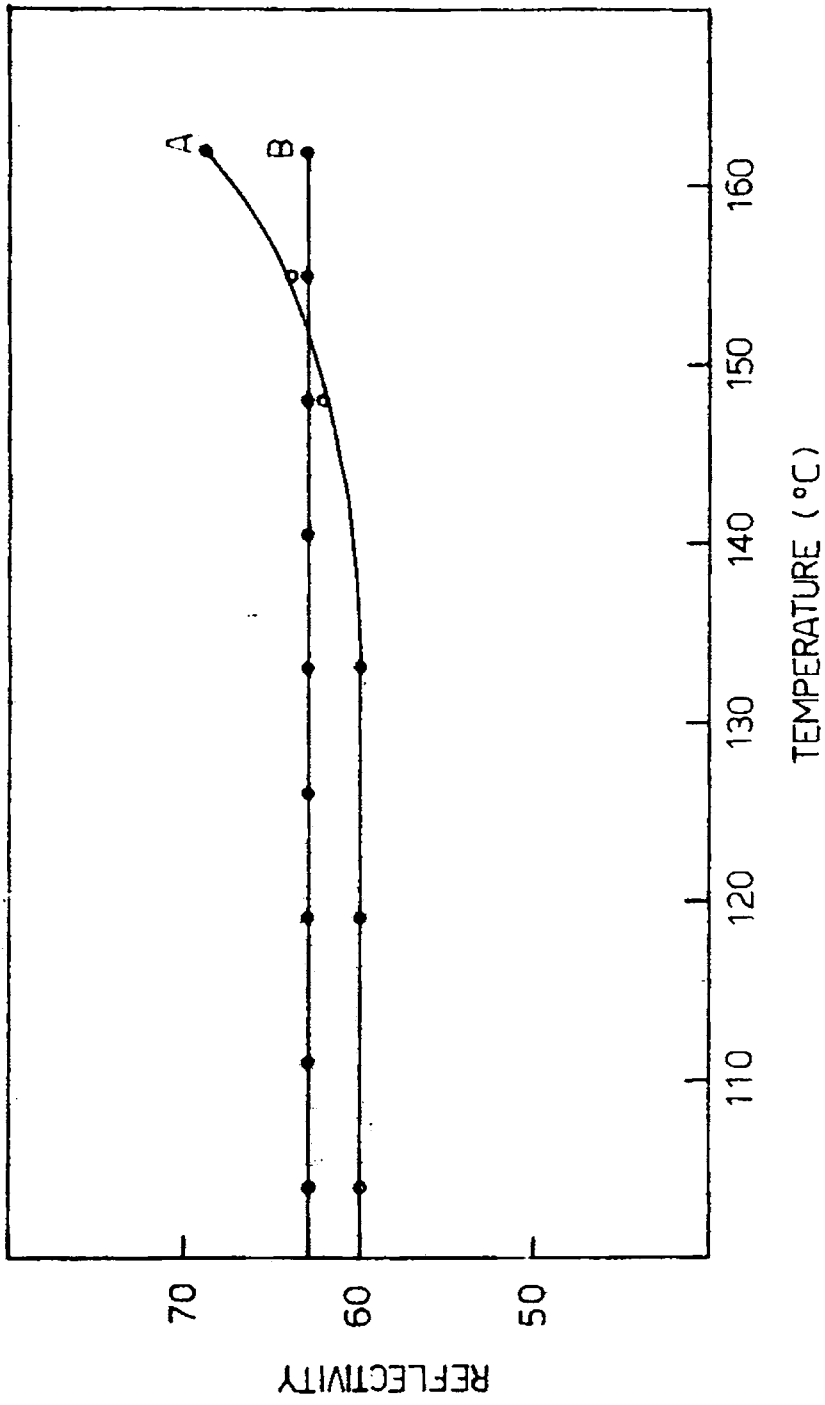


Fig.4.2 Variation in reflectivity of copper films with temperature (film thickness - 1000Å, wavelength - 4400Å).
 A - for film deposited at room temperature
 B - for film deposited at 200°C.

no variation in reflectivity before that temperature.

One can easily understand from the fig.4.1 that for all the films reflectivity increases after a particular temperature and the temperature at which this occurs is different for different thickness. In the case of films with thickness 500\AA and 1000\AA the increase starts at almost the same temperature i.e., $\sim 150^{\circ}\text{C}$ (see curves D and E). As the thickness increases the temperature value decreases. For 1500\AA the increase takes place at $\sim 140^{\circ}\text{C}$ while for 2000\AA and 3000\AA thick films the temperature values are 130°C and 120°C respectively.

In fig.4.2 curve A shows the variations in the reflectivity of a film of thickness 1000\AA deposited at room temperature (This is same as the curve D in fig.4.1). But the curve B in fig.4.2 is for a similar film of same thickness with the only difference that its deposition temperature was different (i.e., 200°C). Here the curve B does not show any increase in reflectivity.

Figures 4.3 and 4.4 are electron micrographs showing the structure of the surface of a film before



Fig. 4-3 SEM before annealing



Fig-4:4 SEM after annealing

and after heating. The thickness of the film was 500\AA and was deposited at room temperature. It is quite clear from fig. 4.3 that the surface of the film is rough before heating and becomes much smooth after the heat treatment (fig. 4.4). Since this is the case for all the other films (of different thicknesses) only one case is shown here as an example.

4.4 Discussion

As the reflectivity is also a measure of the surface smoothness and since it is found to be increasing, one can take it for granted that there is surface smoothing due to heating. Heating directly affects the stress in the film and hence the variation in the stress in the film may be the reason for the surface smoothing which in turn causes the reflectivity increase.

In order to understand clearly the reason for this phenomenon, one has to see fig. 4.2 also. In this case the reflectivity curve of the film deposited at a higher temperature (200°C) does not show any increase upto 170°C while the reflectivity of a similar film deposited at room temperature shows the usual

increase (curve A). If any variation in the thermal stress of a film is to occur, it has to be heated above its deposition temperature^{30,31}. Since in the case of curve B the film is heated only upto 170°C, which is well below its deposition temperature, there may not be any change in its thermal stress value and hence there is no smoothening process taking place. But in the case of the film deposited at room temperature, the thermal stress will be increasing due to heating. This results in the reduction of resultant stress in the film since the intrinsic stress is opposite to the thermal stress as explained in chapter III. When the resultant stress (σ) is reduced to such an extent that

$$\gamma > \frac{\sigma r_0}{2} \quad (4.1)$$

(where γ is surface energy of the film and r_0 is the radius of initial irregularities) the smoothening process starts.

It is also found that the temperature at which this happens varies with film thickness. This will be clear only after seeing fig.4.5 in which curve A gives the variations of intrinsic stress with

the film thickness^{32,33} (for copper films). It is obvious from the figure that for films upto a thickness of $1000\overset{\circ}{\text{A}}$ the intrinsic stress is very high ($\sim 1.5 \times 10^9$ dyne/cm²) and as the thickness increases further, the stress decreases. Hence for 'thinner films' (ie., with thickness upto $\sim 1000\overset{\circ}{\text{A}}$) the thermal stress has to go to a very high value in order to satisfy the condition in eqn 4.1 for the surface to become smooth. In the case of 'thicker films' (ie., with thickness greater than $1000\overset{\circ}{\text{A}}$) this can take place at a lower temperature since the intrinsic stress value is much smaller.

4.4a Calculation of the intrinsic stress

One can calculate the thermal stress in a film using the expression³⁴,

$$\sigma_{\text{thermal}} = \frac{\alpha_f - \alpha_s}{1 - \nu} E(\Delta T) \quad (4.2)$$

where α_f and α_s are linear thermal expansion coefficients of the film and substrate, E is the Young's modulus of the film material, ν is Poisson's ratio of the film and ΔT is temperature difference. If an approximation is made that the thermal stress is almost equal to

the intrinsic stress in the film at the temperature when reflectivity just starts increasing one can get the approximate value of intrinsic stress. Since these values for different thickness are calculated^{9,10} by other methods, they can be compared. This comparison with earlier intrinsic stress values is done in fig.4.5.

It is found that, except for very low thickness both values are in good agreement which is a strong support for the theory in the present work.

4.5 Conclusion

The variation in reflectivity of copper films due to heating is studied. It is found that the reflectivity increases after a particular temperature whose value depends on the film thickness. From the scanning electron micrographs it becomes clear that there is surface smoothening due to heating. Since there is a thickness dependence for this process, this can be related to the stress minimisation phenomenon due to heating. This is again verified by doing the same experiment on similar films prepared at higher temperature. There the increase in reflectivity does not occur indicating that the stress variation should be the reason for surface smoothening.

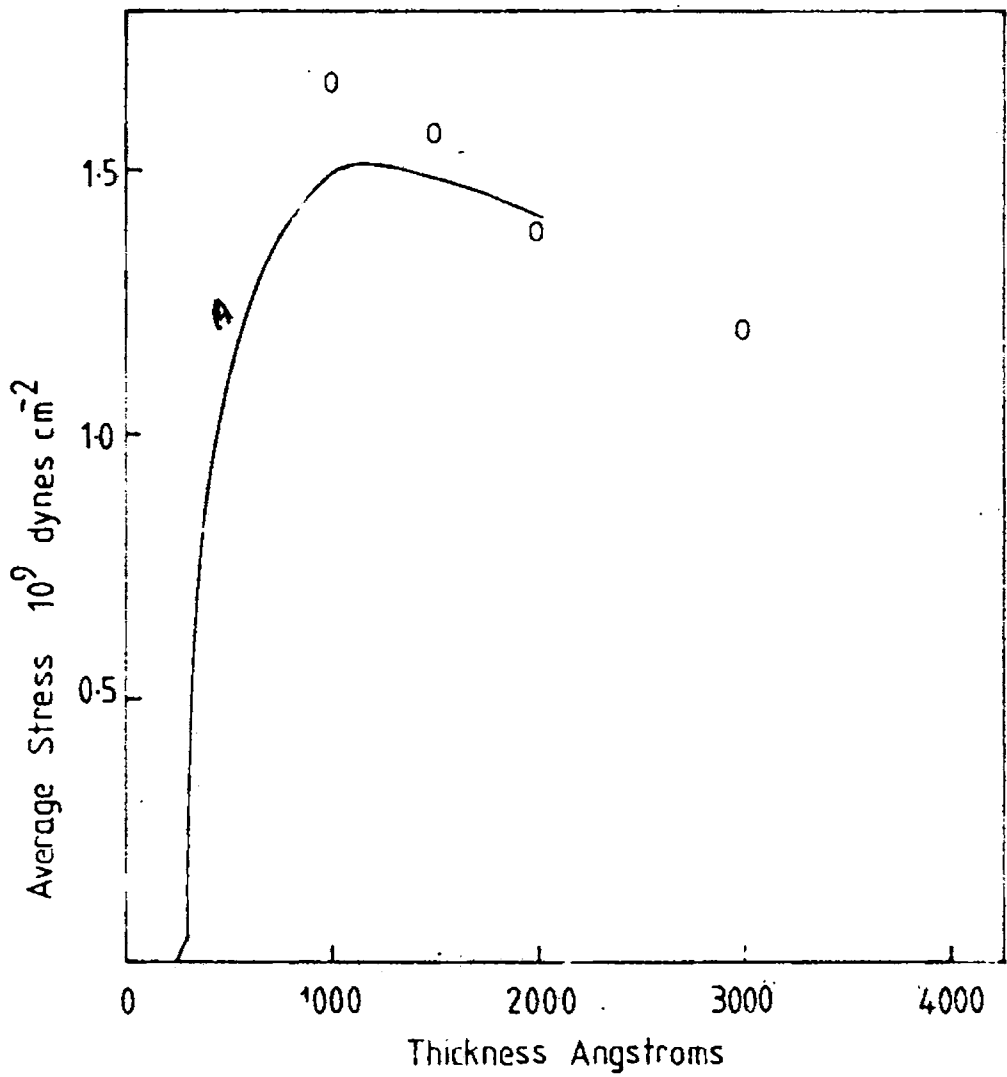


Fig.4.5 Variation of intrinsic stress in copper films with thickness.
 — obtained by earlier workers.,
 O, obtained in the present work.

REFERENCES

1. E.M.Hofer and P.Javet, *Helv.Phys.Acta*, 35, 369 (1962).
2. E.M.Hofer and H.E.Hintermann, *J.Electrochem.Soc.*, 112, 167 (1965).
3. A.Gangulee, *J.Appl.Phys.*, 43, 3943 (1972).
4. A.Gangulee, *J.Appl.Phys.*, 43, 867 (1972).
5. P.Sen, *Ind.J.Pure and Appl.Phys.* 16, 557 (1978).
6. F.Warkusz, *Prog.Surf.Sci.*, 10, 287 (1980).
7. M.Z.Butt and P.Feltham, *Fizika*, 14, 149 (1982).
8. L.Reimer, *Z.Naturforsch*, 12A, 525 (1957).
9. J.Gouault, *J.Physique*, 28, 931 (1967).
10. K.L.Chopra, S.K.Bahl and M.R.Randlett, *J.Appl.Phys.*, 39, 1525 (1968).
11. R.K.Angus and I.D.Dalgliesh, *Phys.Lett.*, 31A, 280 (1970).
12. H.Sugawara, T.Nagano, K.Uozumi and A.Kinbara, *Thin Solid Films*, 14, 349 (1972).
13. V.V.R.Narasimha Rao, S.Mohan and P.J.Reddy, *J.Phy.* D9, 89 (1976).
14. S.J.Thomas, C.R.Phipps Jr., and R.F.Harrison, *Proceedings of the symposium on 'Laser induced damages in optical materials'*, Boulder, CO, USA, 30 Sept-1 Oct (1980).

15. J.O.Porteus, D.L.Decker, S.C.Seitel and M.J.Soileau, Proceedings of the symposium on 'Laser induced damages in optical materials', Boulder, CO, USA, 30 Sept-1 Oct (1980).
16. S.C.Seitel, J.O.Porteus, D.L.Decker, W.N.Faith and D.J.Grandjean, IEEE J.Quantum Electron., QE-17, 2072 (1981)
17. J.F.Figueira and S.J.Thomas, IEEE J.Quantum Electron., QE-18, 1381 (1982).
18. L.J.Lisowski and G.A.Bootsma, Surf.Sci., 118, 1 (1982).
19. P.F.Robusto and R.Brawnstein, Phys.Status Solidi, B107, 443 (1981).
20. D.L.Decker and V.A.Hodgkin, Proceedings of the symposium on 'Laser induced damages on optical materials', Boulder, CO, USA, 30 Sept-1 Oct (1980).
21. F.K.Urban, R.E.Hummel and E.D.Vernik Jr., Corros. Sci., 22, 647 (1982).
22. G.L.Harding and M.R.Lake, Sol.Energy Mater., 5, 445 (1981).
23. D.M.Turley and L.E.Samuels, Metallography, 14, 275 (1981).
24. R.R.Zito, Thin Solid Films, 87, 87 (1982).

25. F.Varmer, M.Rasigni, G.Rasigni and J.P.Palmari, Appl.Opt., 21, 3681 (1982).
26. O.K.T.Wu and E.M.Butler, J.Vac.Sci. and Technol., 20, 453 (1982).
27. K.P.Vijayakumar and C.Purushothaman, Thin Solid Films, 112, 71 (1984).
28. Robert W.Berry, Peter M.Hall and Murray T.Harris, Thin film technology, D.Van Nostrand Company, New Jersey (1968) p.160.
29. S.Tolansky, Surface Microtopology, John Wiley and Sons, New York (1960).
30. K.L.Chopra in Thin film phenomena, McGraw Hill, New York (1969) p.183.
31. K.L.Chopra and L.C.Bobb, Acta Met., 12, 807 (1964).
32. R.W.Hoffman in Georg Hass and Rudolf E.Thun (eds.) Physics of Thin films, Vol.3, Academic Press, New York (1966) p.231.
33. H.Horikoshi, Y.Ozawa and H.Hasunuma, J.Appl.Phys. (Japan), 1, 304 (1962).
34. S.K.Sharma and J.Spitz, Thin Solid Films, 65, 339 (1980).

CHAPTER V

OPTICAL STUDY OF INTERDIFFUSION IN Al/Ag BILAYER FILMS

5.1 Introduction

Metal films of uniform thickness can easily be produced by vacuum deposition and when two such films of different metals are deposited one on top of the other and the resultant bimetallic film is annealed, diffusion generally takes place (unless the metals are completely immiscible). This leads to the formation of solid solutions or intermetallic compounds or both. As the films are having a columnar growth they have a fine meshed network of grain boundaries perpendicular to the film plane. The lattice periodicity is completely broken down in the grain boundaries resulting in looser atomic packing. As a result of this change the grain boundaries act as a highly diffusive channel system in which concentration gradients are rapidly smoothed out. Since the grain boundary area may much exceed the area of the interface, diffusion into and out of the lattice is to be expected preferably via grain boundaries. In fact, the grain boundaries are very effective short circuit path for diffusion at temperatures well below the melting point.

The study of interdiffusion in multilayer films is important since it can give information about the intermetallic compounds, the coefficient of diffusion of the materials etc. But it is still more important and relevant as far as technological aspects are concerned. Almost all the electronic devices now-a-days contain thin film integrated circuits and diffusion may take place between the layers of different materials of these devices due to their functioning at elevated temperatures or in an ambient which promotes diffusion. Hence, in the case of materials used in electronic devices, it becomes necessary to study in detail the problem due to interdiffusion, the compounds formed by that phenomenon and ways to minimise it. Thus metals like silver, platinum, copper, gold, aluminium, nickel and semi-conductors like silicon, germanium, gallium arsenide etc. become very important in this context.

A large number of workers have studied the interdiffusion of these materials using different experimental techniques. The main among them are X-ray interference, electron spectroscopy for chemical analysis (ESCA), and electron scanning microscopy. Optical methods like 'attenuated total reflection (ATR)

and spectroscopic ellipsometry are also used in this area of research. Since the interdiffusion in thin films is the basis of all the surface changes¹, surface analysis by optical methods can give a lot of information regarding the interdiffusion. For example, measurement of refractive indices or ellipsometric parameters² ψ and Δ or simple reflectivity measurement furnishes the required information. Another important aspect supporting the optical method is that it is nondestructive unless the materials are photosensitive (which will be the case most generally).

Considering the importance of the topic a brief review of the earlier works is also included in this chapter. These are selected on the basis of importance of materials studied or application of the result obtained in technological side or due to the speciality of experimental technique.

5.1a Brief review of earlier works

The number of review articles and books published in this area itself gives the idea of the amount of work done on this aspect. Of these only

very important reviews³⁻⁷ are considered here. Weaver³ gives review of interdiffusion in different bilayer metallic films with a stress on the optical study while Gupta⁷ gives an elaborate study of the matter considering experimental and theoretical aspects. There has been a large number of publications on interdiffusion taking place in different materials studied by using different experimental techniques from which very important and recent works are considered here⁸⁻²⁵. Saha et al¹⁸ have given a theoretical study on diffusion while Loisel et al¹⁹ report the diffusion in Al/Au system in the temperature range 64°C-80°C using ATR method. Another important work is that of Ilkka Suni et al²¹ in which the study of the interdiffusion in Cu/Ni system is presented. These materials are important due to their use in solar cells. Hwang et al¹⁴, using Auger sputter profile, studied the diffusion of aluminium into silicon in the temperature range 350°C-425°C. This is another important work since these two materials are much used in thin film integrated circuits. Also Wagendristel et al¹⁶ have reported the formation of Au₂Al in Au/Al system and they used X-ray diffraction technique for this study.

In order to understand the effect of different ambients on the interdiffusion of both bimetal and metal-semiconductor films one need go through the series of publications by Chin-An Chang²⁶⁻³⁴. Since his study includes materials like gallium arsenide, germanium, silicon, platinum, nickel, copper etc. this is very important from the point of view of applied science also. In one of his publications Chang has reported that, in presence of oxygen, diffusion of chromium and platinum in silicon is considerably reduced²⁶. Also in another work he showed that the interdiffusion in Au/Cr in presence of air can be completely suppressed by the presence of CO³¹. The presence of oxygen has been found to be capable of reducing the mixing between copper and chromium and platinum and copper in Cu/Cr and Pt/Cu/Cr film systems³⁴.

Coming to the case of Al/Ag thin film system there have been various studies on different aspects of interdiffusion by using different experimental methods³⁵⁻⁴². Of these, some³⁵⁻³⁷ provide the analysis of the properties of this bilayer system to find out the possibility of using it as a solar reflector. This is because, silver has good reflectivity and is inert to the ambient conditions⁴³ while

aluminium is having good adhesion also⁴⁴. If these two are combined, one can get a good solar reflector. Weaver et al³⁸ have studied this thin film system using optical techniques (ie., by reflectivity measurements) and to supplement these observations they used electron microscope also. Khan et al⁴¹ have obtained the activation energy from diffusion measurements. Wagendristel et al⁴² also calculated the activation energy from diffusion coefficient measurements. Here they used the X-ray interference method for the study and annealing temperature was within the range 80°C to 110°C.

In the present work also, Al/Ag system is selected because of two reasons. First one is that availability of experimental data both in thin film and bulk form. Second is that this system has larger application in electronic as well as energy conversion devices. Here the temperature of the film is continuously increased and reflectivity variations are recorded, which provide the data for the study of interdiffusion.

5.2 Experimental

The multilayer films for the experiment were prepared by the method of vacuum deposition as in other

cases (see chapter II). However in this case a double source evaporation technique was used since both silver and aluminium were to be evaporated one after the other. Silver was taken in a molybdenum boat while aluminium was in a coil made up of tungsten wire. Both sources were well separated using a mica sheet. For all the samples, silver formed outer layer and aluminium was the inner one. This was to avoid the oxidation of aluminium layer due to exposure to the atmosphere. Pressure during the evaporation of both the materials was well below 10^{-5} torr. The distance between heating sources and substrate was always 15 cms.

Two types of films were prepared which differed in the ratio of their thickness. The layer thickness is a very important factor for these materials. Since both these materials are having same atomic size and same structure their thickness ratio corresponds to the ratio of number of atoms of the materials^{38,42}. Here in the first type, the ratio of thickness between aluminium and silver was 1:2 and in the second type it was 1:1 (In both, aluminium was having a thickness of 500Å). The required thickness was obtained by taking the calculated mass of the evaporant using the expression⁴⁵ given in earlier chapters. Later the thickness was

measured by using the multiple beam interferometry⁴⁶. It was found that the thickness was having variation of the order of $\pm 50\overset{\circ}{\text{A}}$ from the calculated value which did not however affect the thickness ratio.

Heating of the films was done in the glass cell described in chapter II and IV. The pressure during heating was always 10^{-2} torr. The heating rate was $1^{\circ}\text{C}/\text{minute}$ when films were heated on the glass side (back side). But the rate was $0.5^{\circ}\text{C}/\text{minute}$ when heating was done on the film side (silver side). This was to avoid damages due to heating since it was directly applied on the film.

Here the reflectivity measurements were taken during heating. This was done using the set up described in chapter II ie., a PMT galvanometer arrangement. The wavelength of the light used was $4400\overset{\circ}{\text{A}}$. Always the reflectivity was measured at an angle of incidence equal to 45° .

5.3 Results

The reflectivity measurements were also done on both surfaces of the film ie., on silver side (front side of the film) and on glass side (back side of the film). All the observations are shown in figs.5.1,

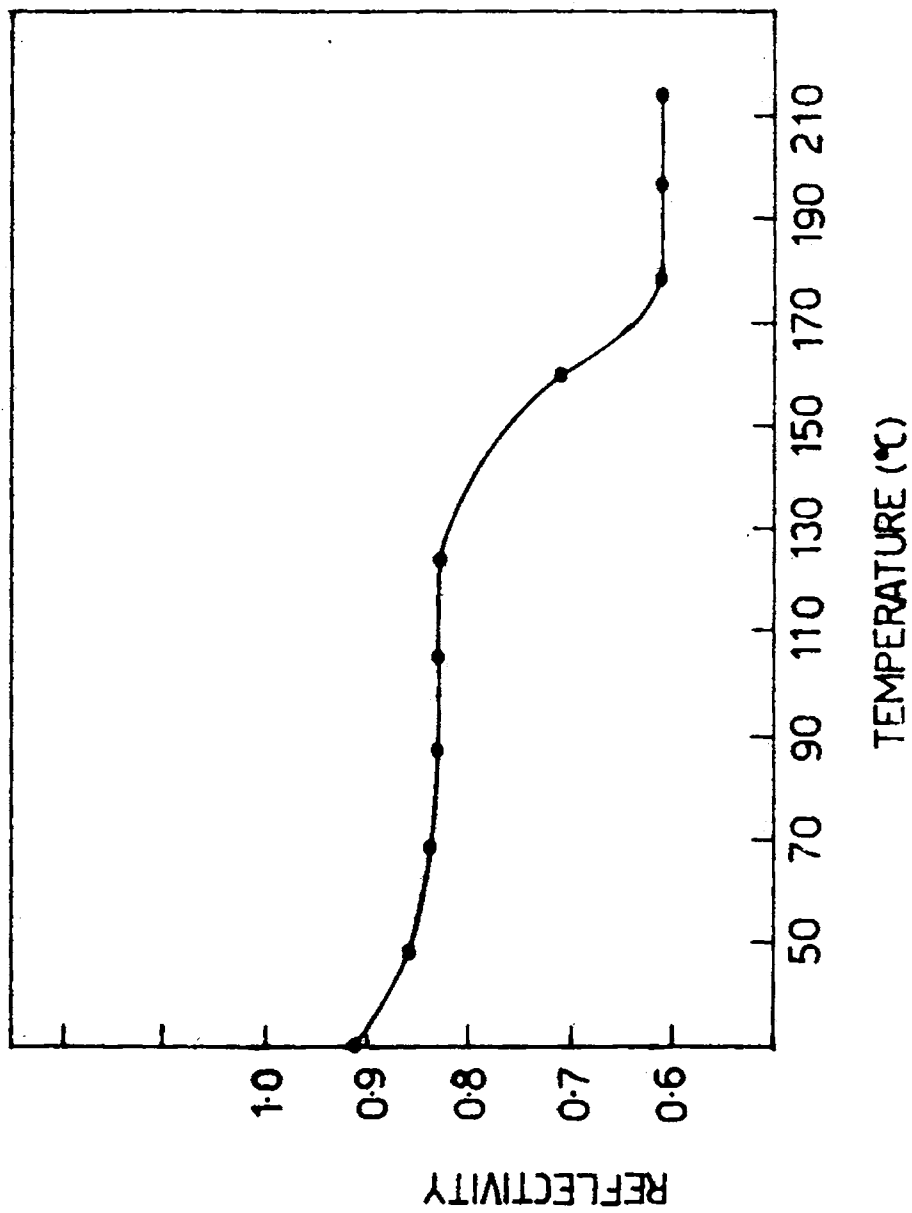


Fig.5.1 Variation in reflectivity with temperature of the Al-Ag bilayer film with thickness ratio 1:2 (wavelength 4400Å).

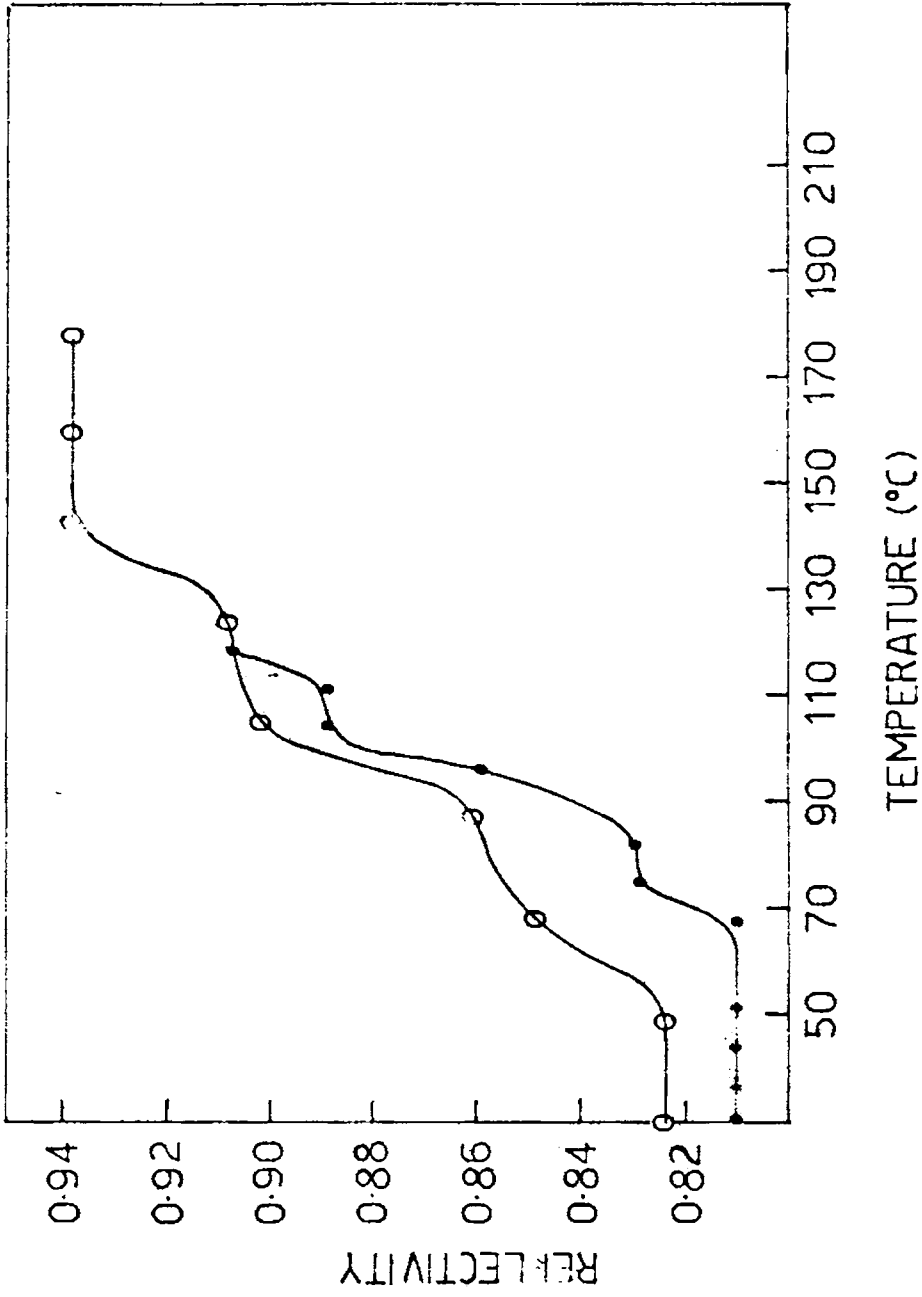


Fig. 5.2 (O-O) Variation in reflectivity of the Al-Ag bilayer film with thickness ratio 1:1 (measurement on the front surface of the film). The second curve for a similar film (●-●) gives the temperature value (at which the step formation takes place) more precisely.

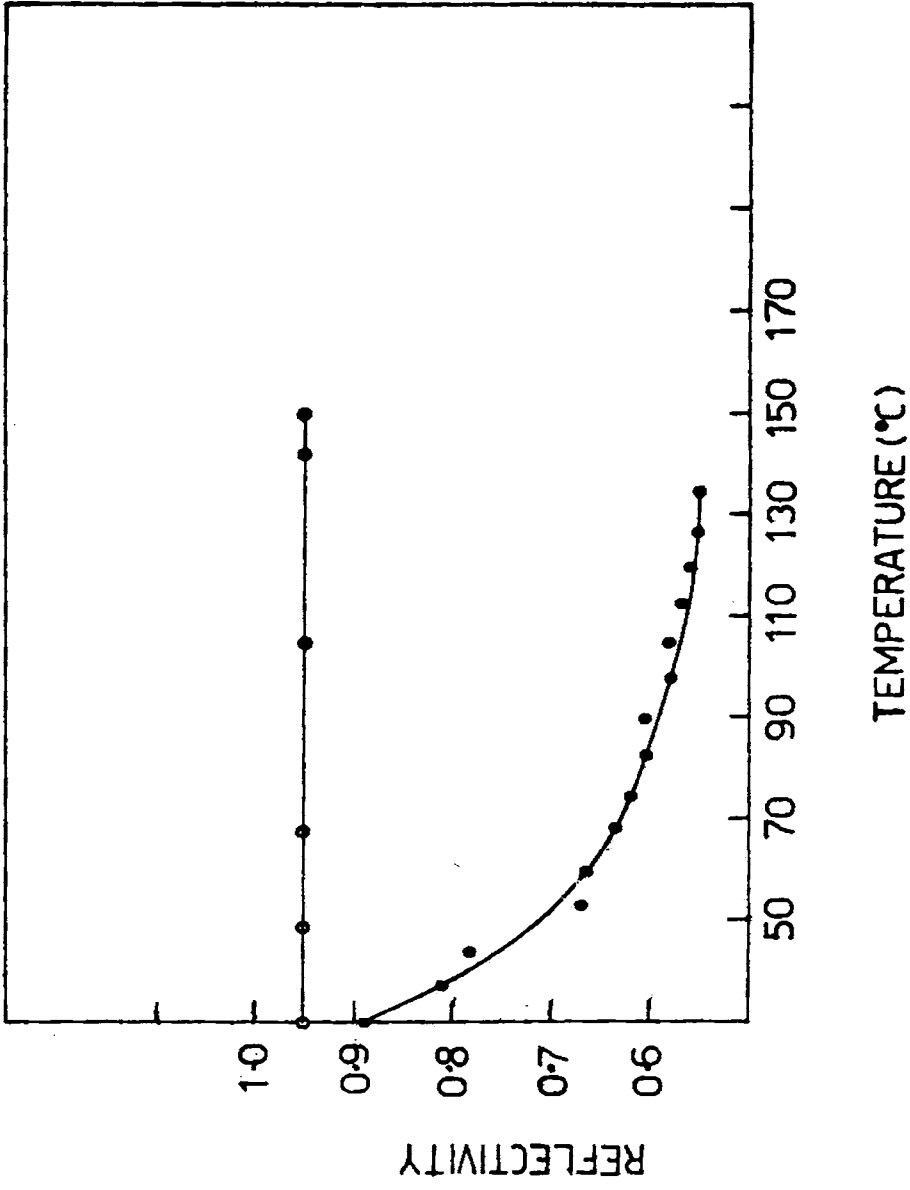


Fig.5.3 Variation in reflectivity (at glass side) of the Al-Ag layer film with temperature
 O—O for the thickness ratio 1:1
 ●—● for the thickness ratio 1:2

5.2 and 5.3. In this, the first one gives the reflectivity variations on the silver side of the films with thickness ratio 1:2 (first type) and the second one gives the same for the films of thickness ratio 1:1 (second type). The third figure shows the variations of reflectivity on the glass side for both types of films.

From fig.5.1 it can be seen that the reflectivity decreases to 0.83 at about 80°C. On increasing the temperature further decrease occurs in this value and it reaches 0.62 at about 175°C. It remains constant thereafter. But in fig.5.2, the reflectivity increases from 0.81 to 0.94. This curve also shows two steps--one between 70°C and 80°C the other between 110°C and 120°C. The fig.5.3 shows considerable difference from the other two. Here the reflectivity of first type of films steadily decreases to a value 0.55 as the temperature increases to 130°C. But for the second type of films, there is no change in reflectivity.

5.4 Discussion

5.4a The silver side

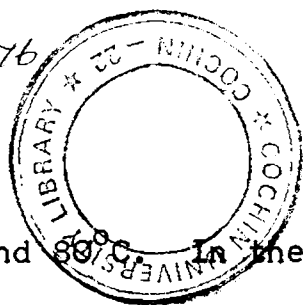
In the case of films having thickness ratio

1:2 the reflectivity, which was well above 0.9, is reduced to 0.83 (fig.5.1) and remains constant for a comparatively long range of temperature (ie., from 80°C to 125°C). But this value of reflectivity has been shown to be that of the compound Ag_3Al by different workers^{38,45,46}. This can happen as a result of diffusion of aluminium into silver due to heating. It can easily occur since silver film is aggregate in structure^{38,44} thus allowing grain boundary diffusion to take place. Due to this diffusion a small quantity of aluminium is coming into contact with large quantity of silver and Ag_3Al is the most probable compound to be formed⁴⁹. This compound seems to be unstable at high temperature and probably this may be the reason for the decrease in reflectivity from 125°C. As the temperature reaches 180°C the reflectivity value comes down to 0.63 and further increase in temperature makes no change in this value. This reflectivity value has been shown to be that of the compound Ag_2Al ^{38,47,48} in air. Hence it can be taken for granted that Ag_2Al is the final intermetallic compound, which is stable at higher temperature.

As the thickness ratio is changed to 1:1, the results are very much altered. From fig.5.2 it can be seen that the reflectivity is increasing with the temperature (ie., from 0.81 to 0.94). This clearly indicates that, in this case, no intermetallic compound like Ag_3Al or Ag_2Al is formed on the surface. The increase in reflectivity can be explained by considering certain other factors. Here, even if the whole silver present in the film is utilised for the formation of the stable compound Ag_2Al almost half of the aluminium present in the film will be left unreacted since the ratio of thickness in this case is 1:1. It has been pointed out earlier that the thickness ratio for these materials corresponds to the ratio of the number of atoms in them. Hence aluminium will be diffusing out through the grain boundaries to form a surface layer and then the reflectivity increases. A very similar result has been reported by Wood et al⁵⁰. This was a study of interdiffusion in Au/Ag thin film system and they found gold on the surface of silver film due to diffusion through grain boundaries. The analysis was done by using ESCA.

The steps found in the reflectivity curve in fig.5.2 also supports the above argument. The

G 34 76



99

first step occurs between 70°C and 80°C . In the fig.5.1, the formation of Ag_3Al also starts in this region. Hence due to this reaction, the quantity of pure aluminium available on the surface of the film is reduced, which results in the reduction of reflectivity and hence in the step formation. But this reduction in the quantity of aluminium on the surface does not last long due to two reasons. One is that the quantity of silver present in the film is small (since the thickness ratio is 1:1) and hence the reaction may not last long. A second reason is that the quantity of aluminium diffusing out increases as temperature is increased. These factors lead to the formation of a layer of aluminium over the phase layer and as a result the reflectivity again increases. The second step occurs in between 110°C and 120°C . This also exactly coincides with the temperature at which Ag_2Al formation starts. At about 140°C the curve reaches a constant value (ie., 0.94) indicating the formation of a comparatively thick layer of aluminium over the film surface.

5.4b Aluminium side

In the case of first type of films, the reflectivity is found to be decreasing steadily

until it reaches a value of 0.55 at about 125°C (fig.5.3). It has been shown by earlier workers that this is the reflectivity of the compound Ag_2Al through glass^{38,47,48}. Also at this temperature (ie., 125°C) the formation of Ag_2Al starts on the silver side of the film (in fig.5.1). Since the thickness ratio is 1:2, the whole material in the film will be utilised for the formation of Ag_2Al and hence the final compound observed on both surfaces of the film is Ag_2Al . No other phase formation is indicated on this side of the film.

When the thickness ratio is changed to 1:1 there is a marked variation in reflectivity on this face also. It can be seen that (fig.5.3) the reflectivity, in this case, is more or less constant. This happens because, the whole aluminium is not required for converting the whole quantity of silver present in the film into Ag_2Al when thickness ratio is 1:1. Only half of the total quantity of aluminium is required for this ie., half the thickness of the aluminium layer (ie., $250\overset{\circ}{\text{A}}$) is left unreacted. But aluminium films of thickness (approximately) $300\overset{\circ}{\text{A}}$ are found to be opaque for ordinary light³⁸. Hence even if a layer of Ag_2Al

is formed at a distance of $300\overset{\circ}{\text{A}}$ from the surface of the aluminium film, that cannot make any change in the reflectivity of the film. Due to this, the reflectivity of this film on aluminium side remains constant and it can be concluded that for the second type of films (on the aluminium side) there is a layer of unreacted aluminium.

5.5 Conclusion

The heat treatment of Al/Ag bilayer films produces very interesting results, which is found to be strongly dependent on the thickness ratio of the two layers. For films with ratio 1:2, it is found that the phase Ag_3Al is formed within the temperature range 80°C to 125°C , after which it decomposes. At about 180°C , the formation of Ag_2Al is complete and is found to be stable at high temperature ($> 200^\circ\text{C}$). For the same type of film, on the aluminium side, the only phase detected is Ag_2Al .

When the second type of films are heated, the reflectivity is found to be increasing on the silver side and this is considered to be due to the formation of a layer of aluminium which is left unreacted. On the aluminium side of the same type

of film, it is found that a layer of aluminium of thickness $250\overset{\circ}{\text{A}}$ is remaining unreacted even after the whole silver is converted into Ag_2Al . It may be this aluminium, which is diffusing out onto the silver side causing an increase in reflectivity.

Analysing these results, it is found that the diffusion of aluminium through silver is mainly through the grain boundaries of silver film and hence comparatively larger quantity of aluminium is diffusing out (note the formation of an aluminium layer on the surface of second type of films). On the other hand, the diffusion of silver through aluminium is mainly aided by the lattice diffusion and hence only small quantity of silver is diffusing into the aluminium layer (note that Ag_3Al is not formed on the aluminium side of first type of films).

REFERENCES

1. T.Nenadovic, Z.Fotiric, B.Djuric, O.Nesic, T.Dimitrijevic and R.Sofrenovic, *Thin Solid Films*, 12, 411 (1972).
2. Tennyson Smith and G.Lindberg, *Surface Technology*, 9, 1 (1979).
3. C.Weaver in Georg Hass, Maurice H.Francombe and Richard W.Hoffman (eds.), *Physics of thin films*, Vol.6, Academic Press, New York (1971) p.328.
4. N.A.Gjastein in 'Diffusion', American Society for Metals, Metals Park, Ohio (1973) p.241.
5. P.S.Ho, F.M.d'Heurle and A.Gangulee in R.E.Hummel and H.B.Huntington (eds.), *Electro- and Thermo-transport in metals and alloys*, American Institute of Mining, Metallurgical and Petroleum Engineers, New York (1977) p.108.
6. D.Gupta in J.M.Poate, K.N.Tu and J.W.Mayer (eds.), *Thin films : Interdiffusion and reactions*, Wiley, New York (1978) p.161.
7. D.Gupta and P.S.Ho, *Thin Solid Films*, 72, 399 (1980).
8. A.Gleiter, B.Chalmers, *Prog.Mater.Sci.*, 16, 77 (1972).

9. R.d'Heurle and R.Rosenberg in Georg Hass, Maurice H.Francombe and Richard W.Hoffman (eds.), Physics of thin films, Vol.7, Academic Press, New York (1973) p.251.
10. R.W.Balluffi and J.M.Blakely, Thin Solid Films, 25, 363 (1975).
11. F.Soria and J.L.Sacedon, Thin Solid Films, 57, 107 (1979).
12. S.Mokhlar and S.Abdel-Aziz, Pramāna, 14, 501 (1980).
13. Joy George and E.C.Joy, Thin Solid Films, 74, 153 (1980).
14. J.C.M.Hwang, P.S.Ho, J.E.Lewis and D.R.Campbell, J.Appl.Phys., 51, 1576 (1980).
15. S.U.Campisano, E.Costanzo and R.Cristofolini, J.Appl. Phys., 51, 3730 (1980).
16. A.Wagendristel, H.Schurz, E.Ehrmann-Falkenan and H.Bangert, J.Appl.Phys., 51, 4808 (1980).
17. S.Haridoss, F.Beniére, M.Gauneau and A.Rupert, J.Appl.Phys., 51, 5833 (1980).
18. H.Saha and K.Mukhopadhyaya, J.Appl.Phys., 51, 6165 (1980).
19. B.Loisel and E.T.Arakawa, Appl.Optics, 19, 1959 (1980).

20. S.Nakahara, R.J.McCoy, L.Buene and J.M.Vandenberg, Thin Solid Films, 84, 185 (1981).
21. Ilkka Suni, Marc-A.Nicolet and Marlti Maenpaa, Thin Solid Films, 79, 69 (1981).
22. N.M.Mayer, Thin Solid Films, 88, 225 (1982).
23. C.R.M.Grovenor, Thin Solid Films, 89, 367 (1982).
24. J.M.Vandenberg and R.A.Hamm, Thin Solid Films, 97, 313 (1982).
25. R.P.Volkova, L.S.Palatnik and A.T.Pugachev, Sov. Phys-Solid State 24, 655 (1982).
26. Chin-An Chang and W.K.Chu, Appl.Phys.Lett., 31, 161 (1980).
27. C.-A.Chang and N.J.Chou, J.Vac.Sci. & Technol., 17, 1358 (1980).
28. Chin-An Chang, J.Electrochem.Soc., 127, 1331 (1980).
29. Chin-An Chang, J.Appl.Phys., 52, 4620 (1981).
30. Chin-An Chang, and W.K.Chu, J.Appl.Phys., 52, 512 (1981).
31. Chin-An Chang, Appl.Phys.Lett., 38, 860 (1981).
32. Chin-An Chang, J.Vac.Sci. & Technol., 21, 639 (1982).
33. Chin-An Chang, J.Appl.Phys., 53, 7088 (1982).
34. Chin-An Chang, J.Appl.Phys., 53, 7092 (1982).

35. R.O.Adams, C.W.Nordin, F.J.Frankor and K.D.Masterson, Thin Solid Films, 63, 151 (1979).
36. R.O.Adams, C.W.Nordin and K.D.Masterson, Thin Solid Films, 72, 335 (1980).
37. R.E.Hummel, Sol.Energy, 27, 449 (1981).
38. C.Weaver and L.C.Brown, Phil.Mag., 17, 881 (1968).
39. S.T.Picraux, Proc. VI International Vac.Congress, Jap.J.Appl.Phys., Suppl., 2, 657 (1974).
40. J.E.Westmoreland and W.H.Weisenberger, Thin Solid Films, 19, 349 (1973).
41. S.S.Khan, J.P.Stark and S.Shih, Phy.Rev., B15, 5738 (1977).
42. A.Wagendristel, H.Bangert and W.Tonser, Surf.Sci., 86, 68 (1979).
43. Paul Schissel and A.W.Czanderna, Proceedings of Second Solar Reflective Materials Workshop, Sanfransisco, California, Feb.12-14 (1980), No.SERI/TP-334-571.
44. P.Benjamin and C.Weaver, Proc.Roy.Soc. A261, 516 (1961).
45. Robert W.Berry, Peter M.Hall and Murray T.Harris, Thin film technology, Van Nostrand, New York (1960) p.160.

46. S.Tolansky, Surface Microtopography, John Wiley and Sons, Inc., New York (1960).
47. L.Harris and B.M.Siegel, J.Appl.Phys., 19, 739 (1948).
48. J.Wulf, J.Opt.Soc.Am., 24, 223 (1934).
49. K.P.Vijayakumar and C.Purushothaman, Proceedings of Nuclear Physics and Solid State Physics Symposium, Banaras Hindu University Varanasi, Department of Atomic Energy, (1982) p.SJB5.
50. J.K.Wood, J.L.Alvarez and R.Y.Maughan, Thin Solid Films, 29, 359 (1975).

CHAPTER VI

ELLIPSOMETRY

6.1 Introduction

Ellipsometry is a non-destructive, sensitive and highly accurate optical method which is used for different purposes like, measurement of optical constants, testing of surface accuracy, study of corrosion etc. This technique though well known even a century ago¹ was not widely used mainly because the equations used to interpret the measured parameters involved tedious computations. In recent years these difficulties have been resolved by the introduction of automatic ellipsometers, high speed and rather cheap computers and development of better computer programmes for reducing the data. All these things resulted in the quick development of ellipsometry in the 1970's and now the technique is widely used in different areas including industries where the applications include the study of molecular contaminants on the performance of space born optical systems and the monitoring of dielectric layers deposited over silicon chips in semiconductor industry.

The basis of ellipsometry is the characterisation of changes in the state of polarisation of light reflected (transmitted) by an optical surface

(transparent material). The changes in polarisation is described by two angles Δ and ψ which correspond to the phase difference and amplitude attenuation of the electric field vectors perpendicular and parallel to the plane of incidence. Using these two parameters and the value of angle of incidence one can calculate the optical constants 'n' and 'k' of the material (ie., the real and imaginary parts of the refractive index). If the surface of the material is covered by a film its thickness can also be calculated, provided the refractive indices of both film and substrate (surface over which the film is formed) are known. An advantage of this method is that Δ and ψ are not dependent on the absolute light intensities but only on the ratio of intensities. Another important study using ellipsometry is on the nature of surfaces; the variation of ellipsometric parameters can characterise surface features. It is found that ψ is very sensitive to the surface roughness which is relatively insensitive to the thickness of dielectric (eg. oxide) films on the surface. But Δ is extremely sensitive to the film thickness and relatively insensitive to the surface roughness². The phase shift Δ can be used to detect as little as 0.1Å^o to as much as 5000Å^o of oxide or a film of contamination on the top of an oxide.

Another point supporting the ellipsometric technique is its capability to be used as a set up for in situ studies of different reactions which many other experimental techniques used in this direction (like electron microscopy) do not have. For example, ellipsometry can be used for the study of reaction taking place at a solid-liquid interface, which cannot be analysed by using an electron microscope since the surface to be analysed using it should be kept in high vacuum. The fact that the area of the surface to be studied can be very small, is another advantage over other methods of analysis. Along with these specialities it is also to be taken into account that this is a nondestructive technique.

6.1a Brief review of earlier works

The studies conducted by various investigators testify to the extent of applicability of this method. Meyer³ employed ellipsometry for the calculation of surface state densities of semiconductors for which he estimated the dielectric constants from the values of refractive indices. This technique was also adopted by different groups^{4,5} for studying the effect of doping

in different materials. For example, Tyagai et al⁴ studied the morphology of silicon surfaces after doping it with silver while Briska et al⁵ have analysed the effect of doping arsenic. They studied variations due to different arsenic concentrations at different temperatures in different ambient conditions. Hare et al⁶ have investigated the properties of F centres in KCl crystals using ellipsometry. These centres were formed as a result of bombardment by electrons with energy in the range 2-10KeV. It has been shown that, unlike earlier methods, this technique can give reproducible and consistent results. The study of oxide layer formation on different materials under different conditions is an important area in which this optical technique finds maximum application⁷⁻¹³. Among these, Allen⁷ developed an IR ellipsometer for studying the oxide layer formation by anodisation of aluminium and the instrument operated at 10.6 μ m. Boggio⁸ investigated ellipsometrically the oxidation of (111) face of copper single crystals at 21^oC for oxygen pressure from 0.03 to 760 torr and found that a monolayer of CuO forms on the top of Cu₂O film at high oxygen pressure. Habraken et al⁹ have also analysed

the oxidation of (111) face of copper for which they used Auger electron spectroscopy and LEED along with ellipsometry. The oxygen pressure in this investigation was very low (10^{-6} - 10^{-4} torr) while the temperature range was quite wide (23° - 400° C). Idozak et al¹⁰ have published an algorithm to determine the refractive index and thickness of oxide layers on absorbing substrate. The growth of very thin oxide layers (15-80Å) on polycrystalline silicon has been studied by Horiuchi¹² in low oxygen pressure (10^{-8} atm.) and high temperature range (850 - 1050° C). Another important study is performed by Belyaev¹⁴ in which this technique is used for noting the changes in ellipticity of light after passage through thin homogeneously oriented layers of liquid crystals. The use of this technique in the field of amorphous silicon is recently gaining prominence¹⁵⁻¹⁷. Theeten¹⁵ has given a good review regarding the use of ellipsometry in connection with vapour phase epitaxy or plasma processing of semiconductors. In this paper it is shown that this surface sensitive, nondestructive real time method can be used to monitor the kinetics of thin film deposition and also to analyse the interface regions between successive layers. Drevillon et al¹⁶ used fast real time ellipsometry

for studying the growth of amorphous hydrogenated silicon deposited in low pressure D.C. discharge of silane. Flamme¹⁷ developed a new method for measuring refractive index absorption index and thickness of thin films using ellipsometry and applied it on amorphous silicon films (with thickness less than 1050Å) prepared by low pressure chemical vapour deposition technique.

The use of ellipsometry in the area of corrosion is reviewed by Petit et al¹⁸. They show that this method is very much useful in the case of localised corrosion. Another good review in this direction is given by Kruger et al¹⁹ in which the necessary theory and experimental set up are described in an elaborate manner with due stress on materials like copper, aluminium, titanium iron and steel etc.

Analysis of surface roughness (of thin films and bulk materials) is a field where ellipsometry has a unique place. Works in this field, using this technique are reviewed in detail in chapter VII.

In order to get a clear idea about different types of ellisometers and their specified uses one

has to go through the concerned reviews. Aspenes²⁰, in his review, touches all aspects of spectroscopic ellipsometers. Muller²¹ gives the operating principles and capabilities of automatic ellipsometers. Also he **hints** about the possible developments. Kinoshita et al²² describe quick methods to evaluate the refractive index and thickness from the ellipsometric parameters using modern ellipsometers. They also consider the analysis of submonolayers. Hauge²³ in his recent review gives a good description of modern ellipsometers along with necessary theory. He describes the developments in different branches of ellipsometry.

6.2 Theory

For interpreting ellipsometric data, when polarised light is reflected from or transmitted through bare or filmed substrates, one should use the electromagnetic theory to derive expressions of complex amplitude reflection and transmission coefficients from macroscopic optical properties. A large amount of theoretical work has been done on this topic and detailed discussions can be found in a number of books²⁴⁻²⁶ and review articles²⁷⁻³⁰. Here a simple structure consisting

of a planar interface separating two homogeneous optically isotropic media (medium-0 and medium-1) is considered. On to this interface a plane polarised light beam is incident at an angle of incidence ϕ_0 . This is illustrated in fig.6.1. This model just enables one to get an idea about the relation between the ellipsometric parameters (ψ and Δ), Fresnel's reflection (transmission) coefficients and the refractive index. In the following treatment, the complex refractive index of an absorbing medium is always taken as

$$N = n - ik \quad (6.1)$$

where n is called index of refraction (or real part of N) and k the extinction coefficient (or imaginary part of N). Also the expression for the electric vector of an optical plane wave travelling in the positive direction of Z axis in an isotropic absorbing medium, with planes of constant phase and constant amplitude parallel, is given by

$$\begin{aligned} E &= E_0 e^{i(\omega t + \delta)} e^{-i\omega N z/c} \\ &= E_0 e^{i(\omega t + \delta)} e^{-i\omega n z/c} e^{-\omega k z/c} \end{aligned} \quad (6.2)$$

where δ is a constant phase angle, c is free space

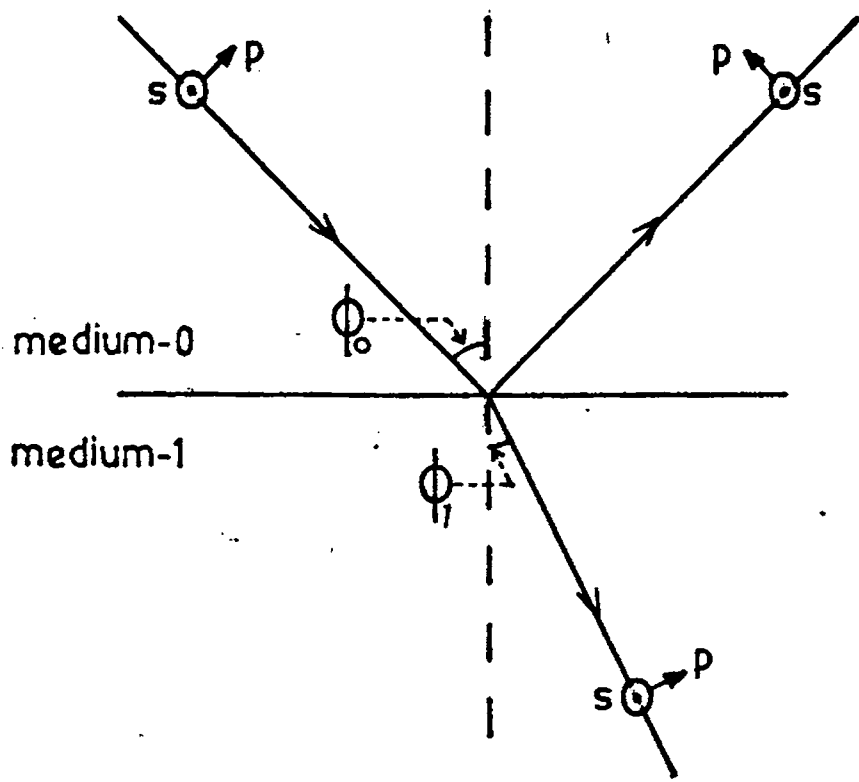


Fig.6.1 Oblique reflection and transmission of plane wave at planar interface between two semi-infinite media 0 and 1.

velocity and E_0 (which is in general complex) defines both amplitude and the polarisation of the wave. From eqn.(6.2) it is clear that the wave amplitude decays exponentially along the direction of propagation at the rate of $\omega k/c$.

From fig.6.1 it is quite clear that ϕ_1 is the angle of refraction in medium-1 and the plane of incidence is the plane of the paper. It is assumed that N_0 and N_1 are the complex refractive indices of medium-0 and medium-1 and the change of refractive index across the interface is abrupt. Now according to Snell's law we have,

$$N_0 \sin \phi_0 = N_1 \sin \phi_1 \quad (6.3)$$

If both media are transparent, N_0 and N_1 are real numbers, the angles ϕ_0 and ϕ_1 are also real and the case is very simple. However, when either one or both media is absorbing, the angles and refractive indices, in general, become complex and the physical picture becomes much complicated.

It is well-known that when incident wave is linearly polarised, with its electric vector vibrating

parallel (p) to the plane of incidence both reflected and transmitted waves will also be similarly polarised with their electric vectors vibrating parallel to the plane of incidence. Similarly, when the incident wave is linearly polarised perpendicular (s) to the plane of incidence, the reflected and transmitted waves are found to be linearly polarised perpendicular to the same plane. Hence the linear vibrations parallel (p) and perpendicular (s) to the plane of incidence are called the 'Eigenpolarisations' of reflection and refraction.

Now one can consider the amplitudes of reflected and transmitted waves in terms of those of the incident wave. For this, an arbitrarily polarised incident wave is considered and its electric vector is resolved into p and s components. Each component is treated separately and the results are combined later. Let E_{ip} and E_{is} represent the p and s components of the complex amplitudes of the electric vectors of the incident wave. Similarly (E_{rp}, E_{rs}) and (E_{tp}, E_{ts}) be the corresponding components of the electric vectors of the reflected and transmitted waves respectively.

Matching the tangential E and H fields across the interface one gets

$$\frac{E_{rp}}{E_{ip}} = r_p = \frac{N_1 \cos \phi_0 - N_0 \cos \phi_1}{N_1 \cos \phi_0 + N_0 \cos \phi_1} \quad (6.4)$$

$$\frac{E_{rs}}{E_{is}} = r_s = \frac{N_0 \cos \phi_0 - N_1 \cos \phi_1}{N_0 \cos \phi_0 + N_1 \cos \phi_1} \quad (6.5)$$

$$\frac{E_{tp}}{E_{ip}} = t_p = \frac{2N_0 \cos \phi_0}{N_1 \cos \phi_0 + N_0 \cos \phi_1} \quad (6.6)$$

$$\frac{E_{ts}}{E_{is}} = t_s = \frac{2N_0 \cos \phi_0}{N_0 \cos \phi_0 + N_1 \cos \phi_1} \quad (6.7)$$

These are called Fresnel's complex amplitude reflection (r) and transmission (t) coefficients for p and s polarisations. Snell's law (eqn (6.3)) can be used to change eqns.(6.4)-(6.7) such that these coefficients are dependent on ϕ_0 and ϕ_1 only.

In order to study the effect of reflection and transmission (refraction) on the amplitude and phase of

the waves separately one can write the complex Fresnel coefficients as

$$r_p = |r_p| e^{i\delta_{rp}} \quad (6.8)$$

$$r_s = |r_s| e^{i\delta_{rs}} \quad (6.9)$$

$$t_p = |t_p| e^{i\delta_{tp}} \quad (6.10)$$

$$t_s = |t_s| e^{i\delta_{ts}} \quad (6.11)$$

Here $|r_p|$ gives the ratio of amplitude of the vibrations of electric vectors of reflected wave to that of the incident wave when the latter is polarised parallel to the plane of incidence with similar meanings for $|r_s|$, $|t_p|$ and $|t_s|$. δ_{rp} represents the phase shift due to reflection experienced by the electric vector parallel to the plane of incidence with similar meanings for δ_{rs} , δ_{tp} and δ_{ts} .

It is obvious from eqns.(6.4)-(6.7) that the Fresnel complex amplitude reflection (r) and transmission coefficients have different values for

p- and s-polarisations. Hence due to reflection (or transmission) the relative amplitude and phase relationship between these two components will be changed. It is also clear that if the incident light wave is polarised in an arbitrary state (other than p or s states) the polarisation of the reflected and transmitted waves will be changed due to the difference in absolute values or the angles (or both) of the Fresnel coefficients of reflection and transmission.

In reflection ellipsometry one measures the states of polarisation of incident and reflected waves and determines the ratio (ρ) of complex Fresnel reflection coefficients for p and s polarisations as

$$\rho = \frac{r_p}{r_s} \quad (6.12)$$

Using eqns. (6.8) and (6.9) one can rewrite the above eqn. as

$$\begin{aligned} \rho &= \frac{|r_p|}{|r_s|} e^{i(\delta_{rp} - \delta_{rs})} \\ &= \tan \psi e^{i\Delta} \end{aligned} \quad (6.13)$$

Hence, ψ and Δ represent the differential changes in amplitude and phase respectively due to reflection by the component vibrations of the electric vector parallel and perpendicular to the plane of incidence.

Substituting values of r_p and r_s from eqns.(6.4) and (6.5) in eqn (6.12) one gets,

$$= \frac{N_1 \cos \phi_0 - N_0 \cos \phi_1}{N_1 \cos \phi_0 + N_1 \cos \phi_1} \times \frac{N_0 \cos \phi_0 + N_1 \cos \phi_1}{N_0 \cos \phi_0 - N_1 \cos \phi_1} \quad (6.14)$$

This on simplification using Snell's law (eqn.(6.3)) gives the following expression

$$\frac{N_1}{N_0} = \sin \phi_0 \left[1 + \left(\frac{1-e}{1+e} \right)^2 \tan \phi_0 \right] \quad (6.15)$$

Hence N_1 the refractive index of medium-1 can be computed provided one has e and ϕ_0 .

6.2a Ellipsometric evaluation of e

In this section, the theoretical aspects of the measurement of ellipsometric parameters ψ and Δ and the computation of e and the refractive index from

them are considered. For this, the most general ellipsometric set up consisting of Polariser, Compensator, System and Analyser (the PCSA arrangement) is taken into account and is shown in fig.6.2. The light waves (which is well collimated, unpolarised and monochromatic) from the source L is rendered plane polarised by the polariser P after which it passes through the compensator C. The emergent beam from C is reflected by the optical system, S which is under investigation and the reflected beam then comes to the detector D, after passing through the analyser A. Here the optical system S is assumed to be having its eigenpolarisations along the orthogonal coordinates X and Y (ie., in the case of a reflecting film, the p and s polarisations will be coinciding with X and Y coordinates). Also the orientations of polariser, compensator and analyser around the beam axis are specified by the azimuth angles P, C and A respectively in fig.6.2. For the polariser and analyser, azimuths P and A define the orientation of their transmission axes (ie., the directions of transmitted linear eigenpolarisations) while for the compensator the azimuth C defines orientation of its fast axis (ie., the direction of the

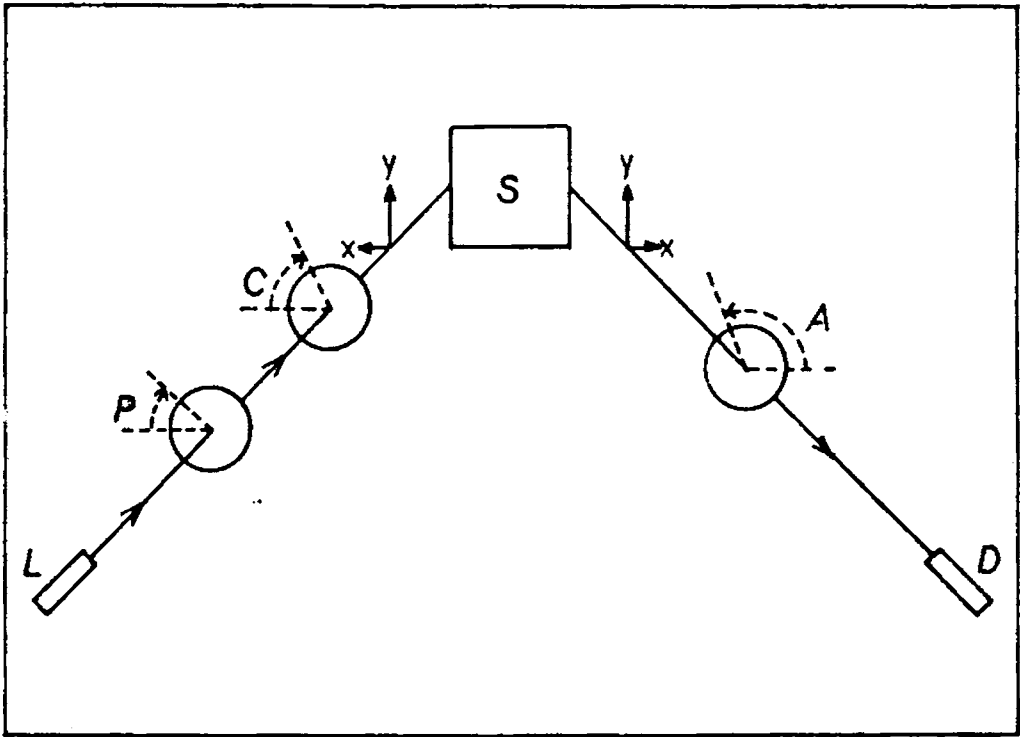


Fig.6.2 The Polariser-Compensator-System-Analyser (PCSA) arrangement.
 L - Light source; D - Detector.

fast linear eigenpolarisation). All these azimuths P , C and A are measured from the direction of the X linear eigenpolarisation of the optical system, S and the angles are taken to be positive in anticlockwise direction when looking against the direction of propagation of the beam. Here the light beam is described by its Jones vector and the optical elements by their Jones matrices³¹ since, by this method, one can easily follow the state of polarisation of the light beam as it progresses through the components of the ellipsometer.

The notation used in the following treatment can be explained in a simple way as follows. The superscripts denote the coordinate system with respect to which the Jones vector or matrix is referenced. In the subscript the first letter denotes the optical component while the second shows whether the beam is its input or output. For example E_{CO}^{fs} is the Jones vector (representing the electric field) of the light beam at the output of the compensator, in its fast slow principal frame of reference (The frame of reference is the coordinate system in which the Jones matrix of an optical component is diagonal). Another important

matter to be considered is the change of coordinate system, which becomes a necessary matter when the light beam after emerging from a system enters into a new one. This is accomplished by using the rotation matrix $R(\alpha)$ and the counter rotation matrix $R(-\alpha)$ and is written as

$$R(\alpha) = \begin{bmatrix} \cos \alpha & \sin \alpha \\ -\sin \alpha & \cos \alpha \end{bmatrix} \quad (6.16)$$

The effect of the polariser is to be considered first. The output of this system will be plane polarised light which can be denoted as,

$$E_{PO}^{te} = A_c \begin{bmatrix} 1 \\ 0 \end{bmatrix} \quad (6.17)$$

Here, A_c contains information regarding the intensity and absolute phase of the wave emergent from the polariser. The superscript 'te' denotes the 'transmission-extinction' principal frame of reference.

Before examining the effect of the compensator one has to change the reference coordinate system, from the transmission-extinction principal frame of the

polariser to the 'fast-slow' principal frame of the compensator. This is achieved by using the rotational matrix $R(P-C)$ as,

$$\begin{aligned}
 E_{CI}^{fs} &= R(P-C) E_{PO}^{te} \\
 &= A_C \begin{bmatrix} \cos(P-C) & -\sin(P-C) \\ \sin(P-C) & \cos(P-C) \end{bmatrix} \begin{bmatrix} 1 \\ 0 \end{bmatrix} \\
 &= A_C \begin{bmatrix} \cos(P-C) \\ \sin(P-C) \end{bmatrix} \quad (6.18)
 \end{aligned}$$

The compensator is having a slow-to-fast complex amplitude transmittance given by,

$$e_c = T_C e^{i\delta_c} \quad (6.19)$$

This equation shows that the component of the electric vector incident on the compensator parallel to its slow axis is retarded by $-\delta_c$ and is attenuated in amplitude by T_C relative to the component parallel to its fast axis. Its Jones matrix can be written as

$$T_C^{fs} = K_C \begin{bmatrix} 1 & 0 \\ 0 & e_c \end{bmatrix} \quad (6.20)$$

where K_C accounts for the equal attenuation and phase shift along the fast and slow axes. To get the Jones vector of the output beam, E_{CI}^{fs} should be multiplied by T_C^{fs} which gives,

$$\begin{aligned} E_{CO}^{fs} &= T_C^{fs} E_{CI}^{fs} \\ &= K_{C A} \begin{bmatrix} \cos(P-C) \\ e_c \sin(P-C) \end{bmatrix} \end{aligned} \quad (6.21)$$

In order to bring the Jones matrix to the X-Y principal frame of the optical system S, one has to perform a coordinate counter rotation by an angle C and can be performed as

$$\begin{aligned} E_{CO}^{xy} &= R(-C) E_{CO}^{fs} \\ &= K_{C A} \begin{bmatrix} \cos C \cos(P-C) - e_c \sin C \sin(P-C) \\ \sin C \cos(P-C) + e_c \cos C \sin(P-C) \end{bmatrix} \end{aligned} \quad (6.22)$$

Now one can note the modifications of the polarisation caused by the optical system, S. Since there is no other systems in between the compensator and the

system, S it can be taken that,

$$E_{CO}^{xy} = E_{SI}^{xy} \quad (6.23)$$

Hence the Jones vector of the beam at the output of S is given by the equation,

$$E_{SO}^{xy} = T_S^{xy} E_{SI}^{xy} \quad (6.24)$$

In the above equation the Jones matrix of the system, T_S^{xy} , is diagonal since it is assumed to have orthogonal linear eigenpolarisations, parallel to X-Y coordinate axes and the matrix can be written as

$$T_S^{xy} = \begin{bmatrix} V_{ex} & 0 \\ 0 & V_{ey} \end{bmatrix} \quad (6.25)$$

where V_{ex} and V_{ey} represent the eigenvalues of the X and Y linear eigenpolarisations. Substituting the values of E_{SI}^{xy} and T_S^{xy} in eqn.(6.24) we get,

$$E_{SO}^{xy} = K_{CC} A_C \begin{bmatrix} V_{ex} [\cos C \cos(P-C) - \rho_c \sin C \sin(P-C)] \\ V_{ey} [\sin C \cos(P-C) + \rho_c \cos C \sin(P-C)] \end{bmatrix} \quad (6.26)$$

This beam, coming from S has to pass through the analyser A which can be rotated around the beam axis. To study the effect of the analyser on the polarisation of the beam, one has to make a coordinate rotation from the optical system's X-Y principal frame to the analyser's t-e principal frame as

$$E_{AI}^{te} = R(A) E_{AI}^{XY} \quad (6.27)$$

Taking that $E_{AI}^{XY} = E_{SO}^{XY}$ and substituting for R(A) the above equation becomes,

$$\begin{bmatrix} E_{AI,t} \\ E_{AI,e} \end{bmatrix} = \begin{bmatrix} (\cos A E_{AI,x} + \sin A E_{AI,y}) \\ (-\sin A E_{AI,x} + \cos A E_{AI,y}) \end{bmatrix} \quad (6.28)$$

(In eqn.(6.28) the third term in the subscripts denote the corresponding coordinate axis). The Jones matrix of the analyser is given by the expression

$$T_A = K_A \begin{bmatrix} 1 & 0 \\ 0 & 0 \end{bmatrix} \quad (6.29)$$

where K_A represents the amplitude and phase changes experienced by the transmitted linear eigenpolarisation.

Then the electric vector at the output of the analyser is obtained as,

$$E_{AO}^{te} = T_A^{te} E_{AI}^{te} \quad (6.30)$$

Substituting for the value of T_A from eqn.(6.29),

$$E_{AO}^{te} = K_A \begin{bmatrix} E_{AI,t} \\ 0 \end{bmatrix} \quad (6.31)$$

Now the intensity of the detected signal I_D is given by the expression,

$$\begin{aligned} I_D &= K_D (E_{AO}^\dagger E_{AO}) \\ &= K_D K_A K_A^* (E_{AI,t} E_{AI,t}^*) \\ &= K_D |K_A|^2 |E_{AI,t}|^2 \end{aligned} \quad (6.32)$$

where K_D is a real factor which depends on the intensity profile of the light beam and nature of the photodetector. From eqn.(6.28) it can be easily be

written as,

$$E_{AI,t} = \text{Cos}A E_{AI,x} + \text{Sin}A E_{AI,y} \quad (6.33)$$

But the values of $E_{AI,x}$ and $E_{AI,y}$ are given by eqn.6.26. Substituting these values in eqn.(6.33) one gets

$$E_{AI,t} = K_{C A} \left\{ V_{ex} \text{Cos}A [\text{Cos}C \text{Cos}(P-C) - \rho_c \text{Sin}C \text{Sin}(P-C)] \right. \\ \left. + V_{ey} \text{Sin}A [\text{Sin}C \text{Cos}(P-C) + \rho_c \text{Cos}C \text{Sin}(P-C)] \right\} \quad (6.34)$$

Now eqn.(6.32) can be written in a more convenient form as

$$I_D = G L L^* = G |L|^2 \quad (6.35)$$

$$\text{where } G = |A|^2 |K|^2 |K_A|^2 K_D \quad (6.36)$$

$$\text{and } L = V_{ex} \text{Cos}A [\text{Cos}C \text{Cos}(P-C) - \rho_c \text{Sin}C \text{Sin}(P-C)] \\ + V_{ey} \text{Sin}A [\text{Sin}C \text{Cos}(P-C) + \rho_c \text{Cos}C \text{Sin}(P-C)] \quad (6.37)$$

The above result has been obtained by analysing the state of polarisation at different points along the

path of the beam. The same result can be achieved by using the fact that the effect of a large number of devices placed in the path of the light beam is given by the resultant Jones matrix which is obtained by multiplying the Jones matrices of different devices taking into account of their arrangement and coordinate transformation. Applying this, the Jones vector of the output of the analyser is given by the expression

$$E_{AO} = T_A^{te} R(A) T_S^{xy} R(-C) T_C^{fs} R(P-C) E_{PO}^t \quad (6.38)$$

The eqns.(6.35) and (6.37) show that

$$I_D = f(P, C, A, \rho_c, V_{ex}, V_{ey}) \quad (6.39)$$

which means that the detected signal intensity is a function of (i) the azimuth angles of polarizer compensator and analyser (ii) the slow-to-fast relative complex amplitude transmittance of the compensator and (iii) the complex eigenvalues V_{ex} and V_{ey} of the optical system to be analysed. In both photometric and null ellipsometric systems, one tries to gather information about V_{ex} and V_{ey} by proper use of eqn.(6.39).

6.3a Null ellipsometry

This is based on finding a set of azimuth angles for the polariser, compensator and analyser (P,C,A) to make the intensity of light falling on the detector to be zero. This condition can be represented as

$$I_D = 0 \quad (6.40)$$

for which the necessary condition is

$$L = 0 \quad (6.41)$$

Substituting this condition in eqn.(6.37) one gets

$$\begin{aligned} 0 = & V_{ex} \cos A [\cos C \cos(P-C) - e_c \sin C \sin(P-C)] \\ & + V_{ey} \sin A [\sin C \cos(P-C) + e_c \cos C \sin(P-C)] \end{aligned}$$

Or

$$\frac{V_{ex}}{V_{ey}} = - \frac{\sin A [\sin C \cos(P-C) + e_c \cos C \sin(P-C)]}{\cos A [\cos C \cos(P-C) - e_c \sin C \sin(P-C)]} \quad (6.42)$$

Or

$$e = - \frac{\tan A [\tan C + e_c \tan(P-C)]}{1 - e_c \tan C \tan(P-C)} \quad (6.43)$$

$$\text{where } e = \frac{V_{ex}}{V_{ey}} \quad (6.44)$$

which is the same constant defined in eqns.(6.12) and (6.13). If one gets the values of one set of 'nulling angles' P,C and A and also the value of slow-to-fast relative complex amplitude transmittance e_c , the value of e can be easily calculated. Using e and the angle of incidence ϕ_0 , the refractive index of the material (which forms the optical system S) can be computed for which the expression in eqn.(6.15) may be used.

6.3b Photometric ellipsometers

In this type of ellipsometers, as the name indicates, the detected intensity is never zero. Actually here the variation of the detected light flux as a function of the azimuth angles, phase retardation or angle of incidence is noted. For different intensity values, different equations (of the type given in eqn.(6.45)) can be formed and by solving them the value of e and hence the refractive index can be calculated.

$$I_D = G \left| V_{ey} \right|^2 \left| e \cos A [\cos C \cos(P-C) - e_c \sin C \sin(P-C)] + \sin A [\sin C \cos(P-C) + e_c \cos C \sin(P-C)] \right|^2$$

(6.45)

Eqn.(6.45) is directly obtained from eqn.(6.35) when $V_{ex} = \rho V_{ey}$ is substituted.

There are two types of photometric ellipsometers; one is dynamic and the other is static. Both differ in the way by which the parameters P, C, A and ρ_c are varied. In dynamic photometric ellipsometers, some of these parameters are periodically varied with time and the detected signal intensity is analysed using Fourier analysis. But in the static photometric ellipsometers the intensity of the signal is measured at predetermined fixed values of P, C, A and ρ_c .

6.3b.1 Dynamic photometric ellipsometers

A very brief note on this type of ellipsometers is included here merely to complete the description of methods of evaluation of ρ and hence the refractive index. In this type, as stated earlier, one or more optical parameters is modulated and the detected signal is Fourier analysed. Depending upon the parameter or combination of parameters selected for modulation there are large number of possibilities and here the most important and recent systems are considered.

The first one is the Rotating Analyser Ellipsometer (RAE). This has either polariser-compensator-system-analyser or polariser-system-compensator-analyser arrangement. Keeping other elements (P,C) set at fixed azimuths, the analyser is rotated at a constant angular velocity ω and the intensity of the detected signal is Fourier analysed. The detailed description regarding its working, theory, method of computation and accuracy are given in several recent publications³²⁻³⁷.

The next one is the Polarisation Modulated Ellipsometer (PME). In this, the state of polarisation of the light beam at a suitable point in its path is modulated in a prescribed fashion so that information on the optical system under investigation is retrievable from harmonic analysis of the resulting time-varying detected intensity. Here also, there are several possibilities, depending upon the position and method of modulation. A convenient arrangement is the one proposed by Jaspersen^{38,39} in which the sequence of the optical components is polariser (P), modulator (M), the optical system under investigation (S) and analyser (A). This PMSA arrangement can be considered to be the same as the conventional PCSA

arrangement in which the compensator's relative retardation δ_c is periodically modulated as a function of time. The main advantages of this ellipsometer are that all optical components remain stationary and it allows very high speed of measurement.

6.3b.2 Static photometric ellipsometers

The theory of this type of ellipsometers will be dealt in detail here since it is this type which is constructed and used for the present work. Since no compensator is required one can consider the polariser-system-analyser (PSA) arrangement. The detected signal is a function of azimuth angles P and A only and this is directly obtained by setting $C = 0$ and $\ell_c = 1$ in eqn.(6.45) and it becomes,

$$\begin{aligned} I_D &= G |V_{ey}|^2 |e \cos A \cos P + \sin A \sin P|^2 \\ &= G |V_{ey}|^2 |\tan \psi e^{i\Delta} \cos A \cos P + \sin A \sin P|^2 \end{aligned} \quad (6.46)$$

On further simplification eqn.(6.46) becomes,

$$\begin{aligned} I_D &= F' [1 - \cos 2\psi (\cos 2A + \cos 2P) + \cos 2A \cos 2P \\ &\quad + \sin 2\psi \cos \Delta \sin 2A \sin 2P] \end{aligned} \quad (6.47)$$

(where F' is a constant).

If I_{D1} , I_{D2} and I_{D3} represent the detected intensities for three different settings (P_1A_1) , (P_2A_2) and (P_3A_3) of the polariser and the analyser, three equations of the type in eqn.(6.47) can be formed. F' can be avoided by dividing any two of the equations by the third one. Using the remaining two equations the two unknown quantities ψ and Δ can be obtained.

In the above method, nothing is stated regarding the choice of the settings of the polariser and analyser and is left arbitrary. However, to make the computations still easier, one can select $\pi/4$ as the azimuth of the polariser and $+\pi/4, 0$ and $-\pi/4$ to be the three analyser settings for which the corresponding intensity values are I_{D1} , I_{D2} and I_{D3} . From eqn.(6.47) one gets,

$$I_{D1} = I_D(\pi/4, -\pi/4) = F'(1 - \sin 2\psi \cos \Delta) \quad (6.48a)$$

$$I_{D2} = I_D(\pi/4, 0) = F'(1 - \cos 2\psi) \quad (6.48b)$$

$$I_{D3} = I_D(\pi/4, \pi/4) = F'(1 + \sin 2\psi \cos \Delta) \quad (6.48c)$$

From these three equations two simpler equations

can be formed as

$$I_{D1} + I_{D3} = 2F' \quad (6.49a)$$

$$I_{D3} - I_{D1} = 2F' \sin 2\psi \cos \Delta \quad (6.49b)$$

Using eqns.(6.48b), (6.49a) and (6.49b) one gets

$$\psi = \frac{1}{2} \cos^{-1} [(I_{D1} - 2I_{D2} + I_{D3}) / (I_{D1} + I_{D3})] \quad (6.50)$$

$$\Delta = \cos^{-1} [(\frac{1}{2} \sin 2\psi)(I_{D3} - I_{D1}) / (I_{D1} + I_{D3})] \quad (6.51)$$

Knowing ψ and Δ , the value of e and hence the value of the refractive index can be computed.

An ellipsometer working on this principle has been constructed and its details are given in chapter II. Using this set up the nature of the surface changes due to heating on silver films has been studied. The experimental details along with the relevant theory are given in chapter VII.

REFERENCES

1. P.Drude, Ann.d.Phys.n.Chem., N.F.36 532, 865 (1889).
2. Tennyson Smith and G.Lindberg, Surface Technology, 9, 1 (1979).
3. F.Meyer, Phy. Rev., B9, 3622 (1974).
4. V.A.Tyagai, O.V.Snitko, N.A.Rastrenenko, V.U.Milenin, V.I.Poludin and V.E.Primachenko, Sov.Phys-Semicond., 11, 608 (1977).
5. M.Briská, G.Metzger and K.P.Thiel, IBM.Tech.Disclosure Bull., 23, 224 (1980).
6. J.T.Hare and O.S.Heavens, J.Phys.C, 10, 4211 (1977).
7. T.H.Allen, Thin Solid Films, 45, 169 (1977).
8. J.E.Boggio, J.Chem.Phys. 70, 5054 (1979).
9. F.H.P.M.Habraken, E.Ph.Kieffer and G.A.Bootsma, Surf.Sci., 83, 45 (1979).
10. E.Idczak, E.Oleszkiewicz and K.Zukowska, Opt.Appl. 9, 47 (1979).
11. T.N.Krylova, I.F.Bokhonskaya and G.A.Karapetyan, Opt. & Spectrosc., 49, 437 (1980).
12. M.Horiuchi, J.Appl.Phys., 53, 4943 (1982).

13. L.J.Hanekamp, W.Lisowski and G.A.Bootsma, Surf.Sci., 118, 1 (1982).
14. V.V.Belyaev, Sov.Phys.Crystallogr., 24, 627 (1979).
15. J.B.Theeten, Surf.Sci., 96, 275 (1980).
16. D.Drevillon, J.Huc, A.Lloret, J.Perrin, G.de Rosng and J.P.M.Schmitt, A.I.P.Conf.Proc. No.73, 31 (1981).
17. B.Flamme, Siemens Firsch & Entwicklungsber, 10, 48 (1981).
18. J.A.Petit and F.Dabosi, Corros.Sci., 20, 745 (1980).
19. J.Kruger and P.C.S.Hayfield in William H.Ailor (ed.), Handbook on corrosion testing and evaluation, John Wiley and Sons Inc., New York (1971) p.783.
20. D.E.Aspnes in B.O.Seraphin (ed.), Optical properties of solids, North Holland, Amsterdam (1975) p.799.
21. R.H.Muller, Surf.Sci., 56, 19 (1976).
22. K.Kinosita and M.Yamamoto, Thin Solid Films, 34, 283 (1976).
23. P.S.Hauge, Surf.Sci., 96 108 (1980).
24. O.S.Heavens, Optical properties of thin films, Dover, New York (1965).

25. O.S.Heavens, Thin Film Physics, Methuen, London (1970) ch.6.
26. A.Vašiček, Optics of thin films, North Holland, Amsterdam (1960).
27. F.Abelés in E.Wolf (ed.), Progress in Optics, Vol.12, North Holland, Amsterdam (1963).
28. O.S.Heavens in G.Hass and R.E.Thun (eds.), Physics of thin films, Vol.2, Academic Press, New York (1964).
29. H.E.Bennett and J.M.Bennett in G.Hass and R.E.Thun (eds.), Physics of thin films, Vol.4, Academic Press, New York (1967).
30. F.Abeles in G.Hass and R.E.Thun (eds.), Physics of thin films, Vol.6, Academic Press, New York (1971).
31. R.C.Jones, J.Opt.Soc.Am., 31 488 (1941).
32. B.D.Cahan and R.F.Spanier, Surf.Sci., 16 166 (1969).
33. R.Greef, Rev.Sci.Instr. 41, 532 (1970).
34. J.C.Suits, Rev.Sci.Instr. 42, 19 (1971).
35. D.E.Aspnes, J.Opt.Soc.Am., 64, 639 (1974).
36. D.E.Aspnes, J.Opt.Soc.Am., 64, 812 (1974).
37. R.M.A.Azzam and N.M.Bashara, J.Opt.Soc.Am., 64, 1459 (1974).

38. S.N.Jasperson and S.E.Schnatterly, Rev.Sci.Instr.,
 40, 761 (1969).
39. S.N.Jasperson, D.K.Burge and R.C.O'Handley, Surf.
 Sci., 37, 548 (1973).

CHAPTER VII

ELLIPSOMETRIC STUDY OF THERMAL EFFECTS ON SILVER THIN FILM SURFACES

7.1 Introduction

In the study of the optical properties of thin films it is generally assumed that the boundaries between the media are perfectly flat planes. However, in practice, it is difficult to prepare perfectly smooth flat surfaces. Hence the interpretations of the experimental results, based on the above assumption, may be seriously affected (especially in the short wavelength region). It is therefore necessary to consider the influence of the surface roughness on the optical studies of thin films.

As stated in the earlier chapter, ellipsometry finds a unique place in this field. Of the two parameters ψ and Δ in ellipsometry, the first one is directly affected by the surface roughness and the second one by the thickness factor in the case of films with thickness $< 100\overset{\circ}{\text{A}}$ and for films of larger thickness, both these parameters are equally affected by the factors^{1,7}. Probably this may be the reason due to which this technique is widely used for this type of investigations. A brief review of earlier works gives an idea about the importance of this technique.

7.1a Brief review of earlier works

Mainly the works in this field can be divided under two subheadings; one based on the Maxwell Garnett theory²⁻⁴ and the other on Kirchhoff's theory of diffraction. The work by Fenstermaker et al⁵ can be taken to be the pioneering one in this field. In that they calculated the effects on the optical constants (mainly the refractive index) produced by the surface irregularities of known shapes like square ridges, triangular ridges and pyramidal shaped irregularity. They found large errors in the refractive index values even for a small value of roughness ($\sim 50\text{\AA}$). Smith also used the same theory for the study of the surface of aluminium in different conditions^{1,6,7}. In the study of aluminium surface during fatigue cycling⁶, he had described ellipsometry as a unique means of following the developments of submicroscopic cracks. In another work he studied the variations in ellipsometric parameters by using controlled surface roughness experiments on aluminium. In this work, he also used the scanning electron microscope, light scattering technique, photoelectron emission, surface potential difference and water

contact angle measurement along with ellipsometry. In another very elaborate study on aluminium surface¹ itself he analysed the effect of 32 contaminants comprising of different types like, processing errors (like anodisation voltage or anodisation time) handling damages, human contamination (like finger prints or cigarette smoke) and constituents of smog (like stearic acid, Eruic acid, Brassidic acid, Benzoic acid, Amino-Benzoic acid etc.). In this ellipsometric technique alone was found to be capable of detecting the effect of 26 contaminants. The surface potential difference method was capable of detecting the effects of 17 contaminants while the water contact angle measurement could detect the effects of only 14.

Ohlidal et al⁸⁻¹² through a series of publications developed a theory to deal with the variations of ψ and Δ due to surface roughness and is based on the Kirchhoff's theory of diffraction. In their earlier works^{8,9} they developed the theory by which they analysed the variations in ψ and Δ caused by rough surfaces of isotropic materials. Later in another publication¹⁰ the effect of randomly rough surface was studied which was based on Stratton-Chu-Silver integral and compared it with earlier results

obtained using Kirchhoff's theory. They also showed that the theoretically calculated value of the ellipsometric parameters for a randomly rough surface correspond to the experimental values measured with ideal ellipsometers. Brudzewski¹³ used this technique to measure the variations in polarisation of He-Ne laser light reflected from silicon and germanium surfaces. In this a rough surface is taken to be equivalent to a thin rough layer over a smooth surface and the theoretically calculated values of polarisation are compared with those measured in experiment for different samples of rms roughness in the range 2-20nm. The author used the same theory for the study of tungsten-tungsten oxide system¹⁴ also to calculate the variation of ellipsometric parameters due to surface roughness. Here the rough surface is considered as a transitional layer between the bulk substrate and the surrounding medium. Maris et al¹⁵ studied the surface of gold film on glass substrate and showed that ψ and Δ depend not only on surface roughness, but also on the root mean slope of the irregular height. Chan¹⁶ analysed the free surface as well as the metal-glass interface of rough metallic films sputtered onto smooth pyrex

substrate. The work was based on Maxwell Garnett theory²⁻⁴ and the study was performed on platinum, molybdenum and vacuum annealed molybdenum. Scanning electron microscopy was also used along with ellipsometry. Marten¹⁷ also elucidated the capability of Maxwell Garnett theory for the study of roughness of silicon surfaces. Svilashov et al¹⁸ studied the surface of silicon and germanium at different stages of etching. They considered the roughness as a transition layer with optical constants that change continuously from those of the bulk material (which forms the lower layer) to those corresponding to air. They pointed out that the changes in the values of the optical constants are due to the variations in the polarisation angles caused by the roughness. Vorburger et al¹⁹ also noted the effect of roughness on ellipsometric parameters. They found that, due to roughness, the values of Ψ and Δ varied much rapidly with the angle of incidence.

In the present work, the surface roughness created by heating on silver films is analysed by using ellipsometry. It has been stated (in chapter III) that heating (annealing) of silver films results in the hillock growth on the surface of the films. This

growth is found to be strongly dependent on the stress in the film. Hence the low temperature annealing (ie., upto $\sim 250^{\circ}\text{C}$) produces very interesting result of minimisation of hillock growth at a particular temperature.²⁰ In order to get a clear picture of this phenomenon (for example, to have an idea regarding the relation between the temperature and thickness of the film or the variation of the temperature in different ambient conditions) ellipsometric technique was selected for the elaborate investigation. A two layer model consisting of rough upper layer and a smooth lower layer, is considered for this study. The theory for this investigation is given briefly in the next section.

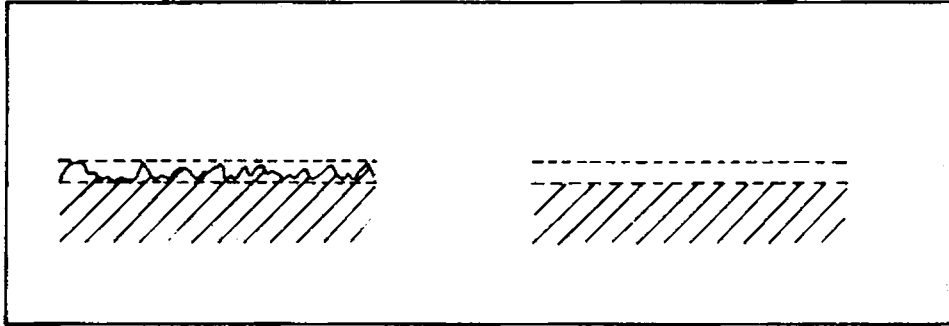
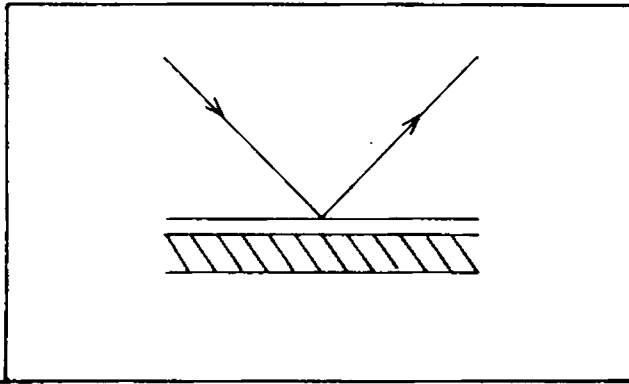
7.2 Theory of roughness measurement

In the last chapter, it was shown that for any plane polarised light, there can have two components; one in the plane of incidence (p-component). Due to reflection from a surface, in general, there is a relative phase change Δ and a relative amplitude reduction Ψ of these two components. These are the parameters directly measured in ellipsometric technique and used for the calculation of the refractive index

of the material. But in the derivation of the equations connecting the refractive index and ellipsometric parameters the most important assumption is that the surface is perfectly smooth (see fig.7.1a). Hence, when the surface is rough, the calculated value of refractive index may not be correct and can have large deviations from the actual value.

Representing the rough surface as equivalent to a homogeneous film for reflection may not appear to be correct. In terms of ray optics, reflection occurs from the sides and top of the 'irregularity'. Then the multiple reflected beam can be combined together to get the total reflected light beam. However, in almost all the cases, the dimensions of the roughness will be always much smaller than the wavelength of the visible light and hence the ray optics cannot be used here⁵. On the other hand, the light 'sees' an average effective refractive index (N_e) for the rough surface. Optically this has the effect of replacing the 'roughened surface layer' by an equivalent film with refractive index N_e and having plane parallel boundaries (see fig.7.1b). The thickness

7.1a



7.1b(i)

7.1b(ii)

Fig.7.1a Smooth surface of an ideal film as conceived in the theory.

Fig.7.1b(i) Actual film surface with irregularities.

Fig.7.1b(ii) Replacement of the roughened surface by an equivalent film with parallel boundaries.

of the 'equivalent film' is equal to the characteristic roughness height parameter (eg. the rms value). The relation between the effective refractive index (N_e) and the actual refractive index of the material of the film (N_f) is given by the relation (according to Maxwell Garnett theory²⁻⁴)

$$\frac{N_e^2 - N_a^2}{N_e^2 + 2N_a^2} = Q \frac{N_f^2 - N_a^2}{N_f^2 + 2N_a^2} \quad (7.1)$$

where N_a is the refractive index of the ambient and Q is the volume factor occupied by the irregularities. Hence any change in the size of the irregularities will be represented by a corresponding change in the Q -factor value. In the present work the ambient is air so that $N_a = 1$. Using ellipsometry one can calculate the value of N_e and for silver N_f is easily obtained. Thus Q becomes the only unknown which can be calculated from eqn.(7.1).

7.3 Experimental

Silver films for the present work, were prepared by using the vacuum evaporation technique which is described elsewhere²⁰. All the thin films

were prepared under identical conditions. The samples were of two types which differed in thickness only; the first type was having a thickness of 1500Å while the second type was 3000Å thick. The wide difference in thickness was kept in order to have the variations due to thickness difference more pronounced (Here also the required thickness for the films was obtained by evaporating calculated mass of the evaporant which was obtained using the relation²¹ given in chapter III. Later the thickness was verified by using the multiple beam interferometric technique²² and the difference from the calculated value was not greater than $\pm 50\text{Å}$).

Heating of the films was done in a glass cell both in air and vacuum (the pressure being maintained at 10^{-2} torr for the latter case) and the set up is described in chapter II. The films were kept pressed against an aluminium block which was electrically heated and temperature was measured by using a thermocouple. The heating rate for all the films was $1^{\circ}\text{C}/\text{minute}$.

The ellipsometric set up used for the measurements was a static photometric type and consisted of polarised-system-analyser arrangement.

Its detailed description is given in chapter II and the theoretical aspects are included in chapter VI. Using this set up ψ and Δ values were measured at different values of angle of incidence (in the range 60° - 75°). The Q-factor value was computed from the values of the ellipsometric parameters at the angle of incidence 60° for all the films. A mini computer (Micro-78) was used for this purpose.

7.4 Results

Figs.7.2 and 7.3 represent the variations of the Q-factor with temperature for the films of thickness 1500Å and 3000Å respectively. Figs.7.4a and 7.4b give the Δ values at different temperatures for the films of thickness 1500Å when annealed in vacuum and air respectively while Figs.7.5a and 7.5b give the corresponding values for the other type of films with thickness 3000Å.

7.4a For films with thickness 1500Å

In the case of this film, the Q-factor shows a steady increase with temperature when annealed in air. But when the films are annealed in vacuum, the Q-factor value at first shows a very slight decrease

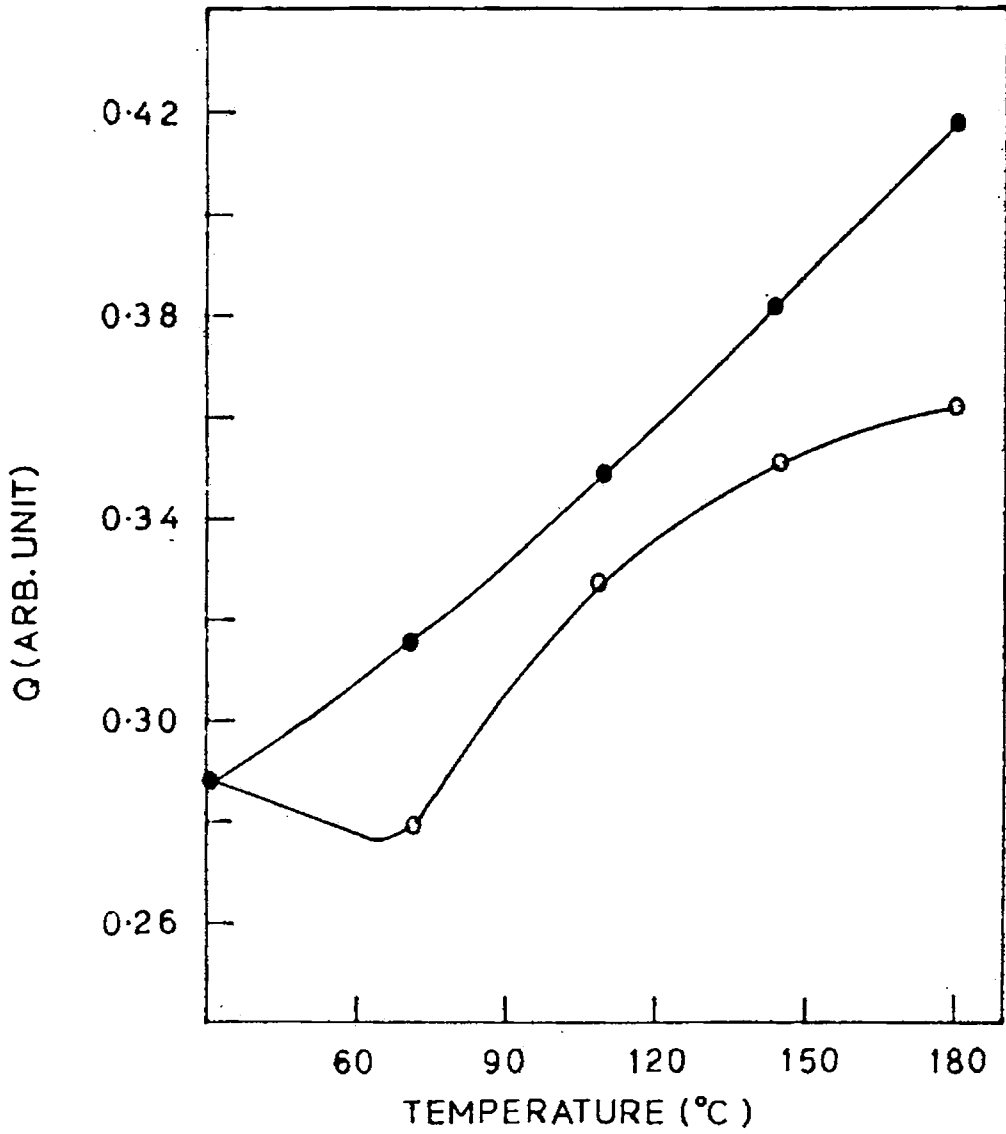


Fig.7.2 Variation in Q-factor with annealing temperature for silver films of thickness 1500A.
 o—o when annealed in vacuum;
 ●—● when annealed in air.

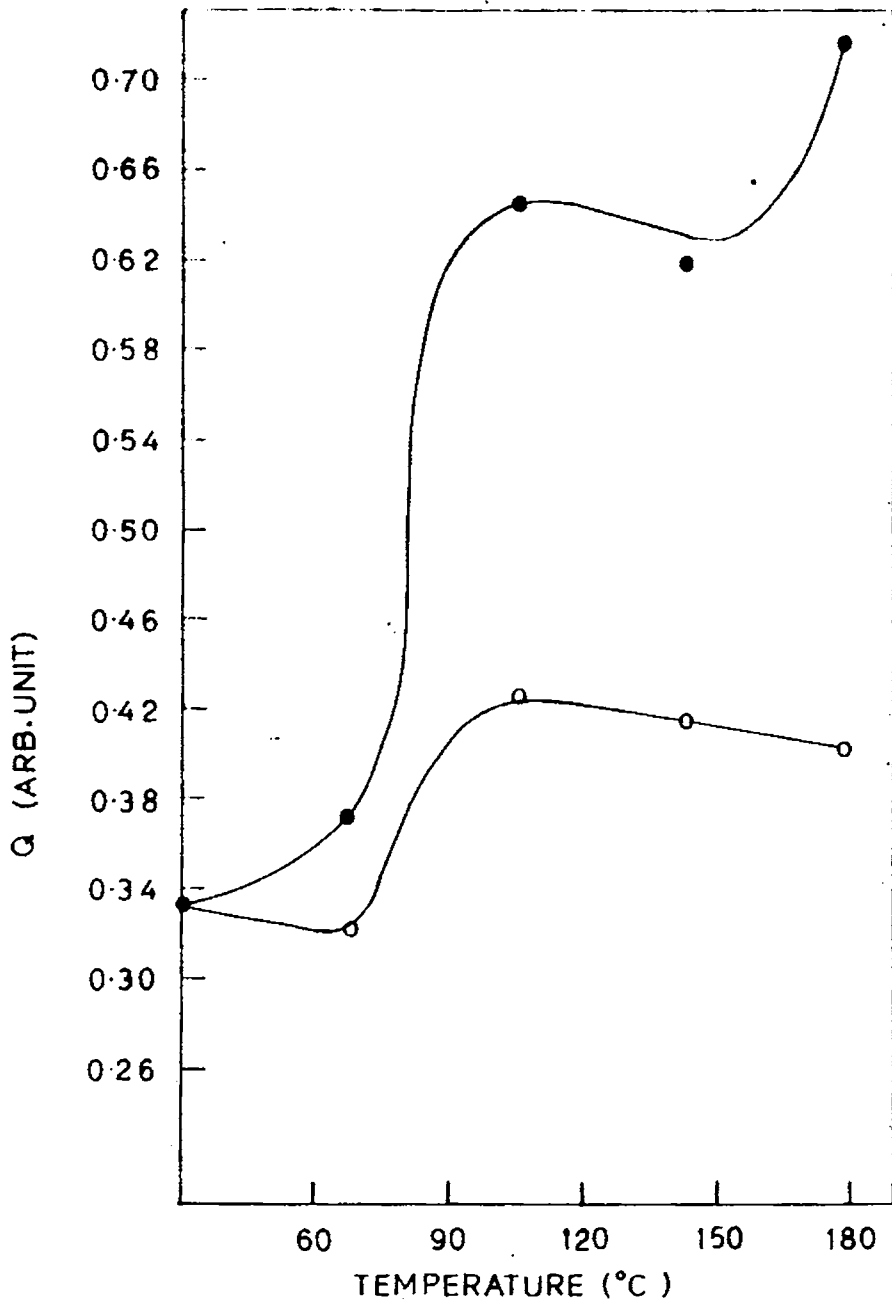


Fig.7.3 Variation in Q-factor with annealing temperature for silver films of thickness 3000 Å.
 o—o when annealed in vacuum,
 ●—● when annealed in air.

upto $\sim 70^{\circ}\text{C}$ and then increases. As the temperature value reaches $\sim 160^{\circ}\text{C}$ the increase in Q-value is almost stopped and it tends to remain a constant.

The variations in Δ values are also of the same nature (Figs.7.4a and 7.4b). Due to annealing in air, Δ value is reduced and this reduction is more or less uniform. On the other hand, when the films are annealed in vacuum, there is a very sharp decrease in Δ value upto 109°C . But as the annealing temperature increases, the reduction is rather retarded showing a tendency to remain constant.

The variations of the Q-factor and Δ values with annealing temperature lead to the same conclusion. When these are annealed in vacuum, upto $\sim 70^{\circ}\text{C}$ there is no hillock growth and thereafter the growth takes place upto $\sim 160^{\circ}\text{C}$. As the temperature increases above 160°C the growth is stopped. But when annealing is done in air, the hillock growth starts from the beginning of heating and continues with no retardation.

7.4b For films with thickness $3000\overset{\circ}{\text{A}}$

As the thickness is doubled, there is marked variations in the nature of the changes of the film surface. Here also, annealing in air causes increase

Fig. 7.4a

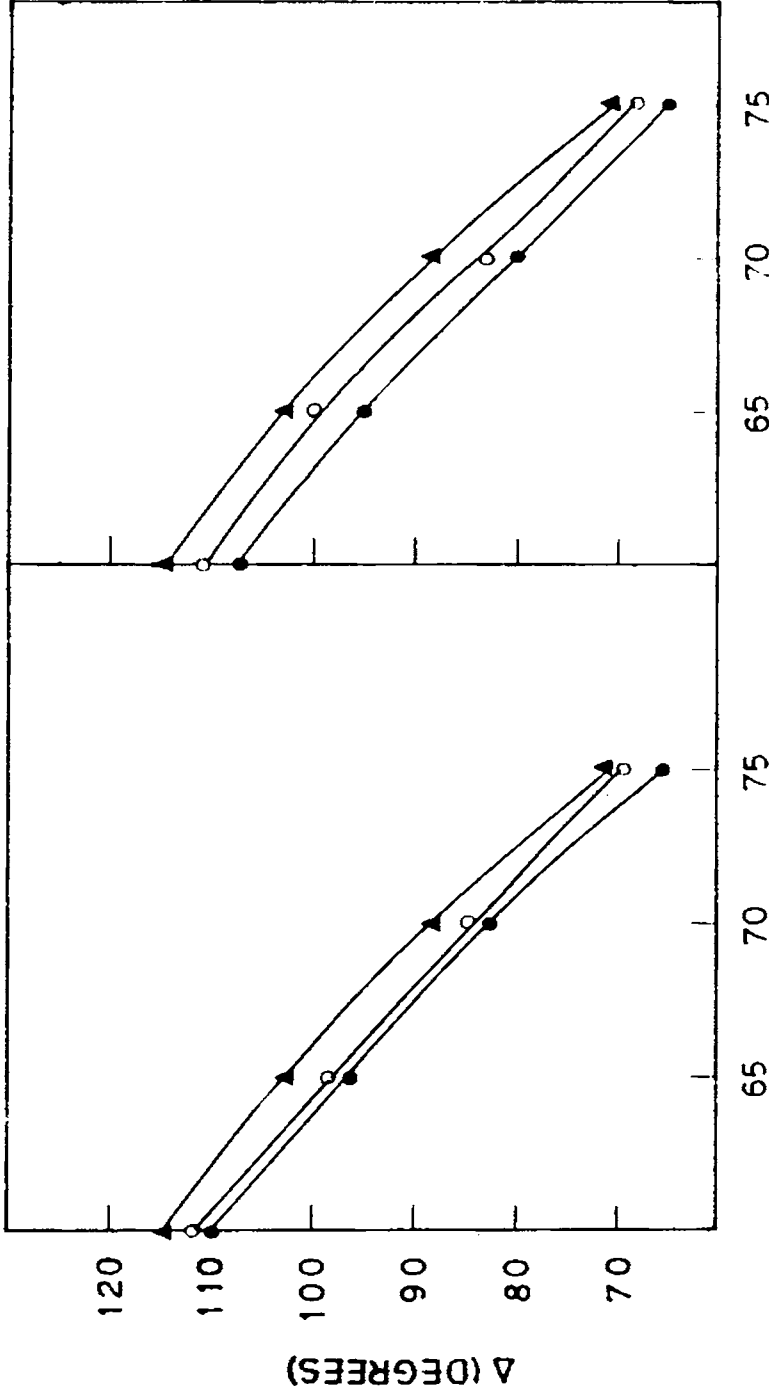


Fig. 7.4b

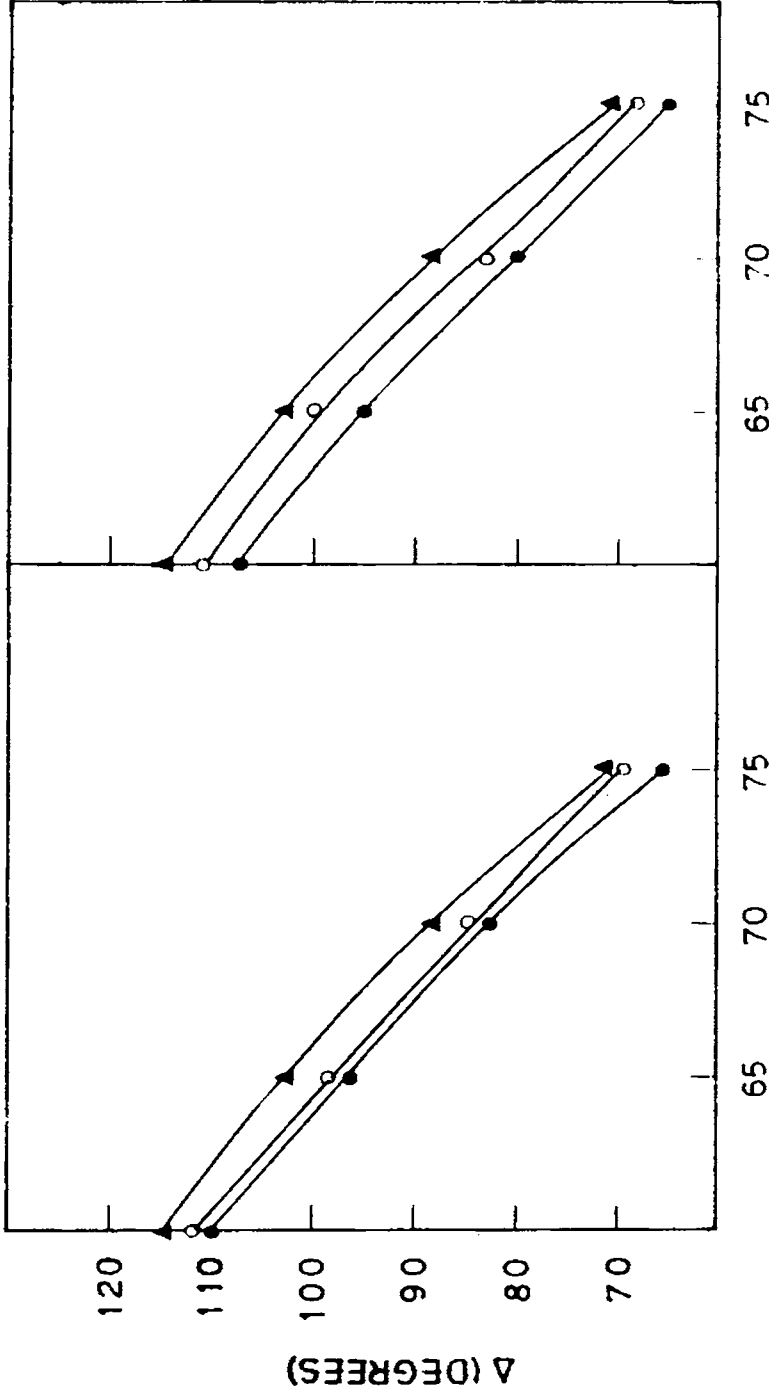


Fig. 7.4a

Variation in Δ values with angle of incidence for silver films (of thickness 1500Å) at different annealing temperatures (annealing in vacuum): ▲—▲, before annealing; ○—○ after annealing at 109°C, ●—●, after annealing at 180°C.

Fig. 7.4b

Variation in Δ values with angle of incidence for silver films of same thickness at different annealing temperatures (annealing in air): ▲—▲, before annealing; ○—○, after annealing at 109°C, ●—●, after annealing at 180°C.

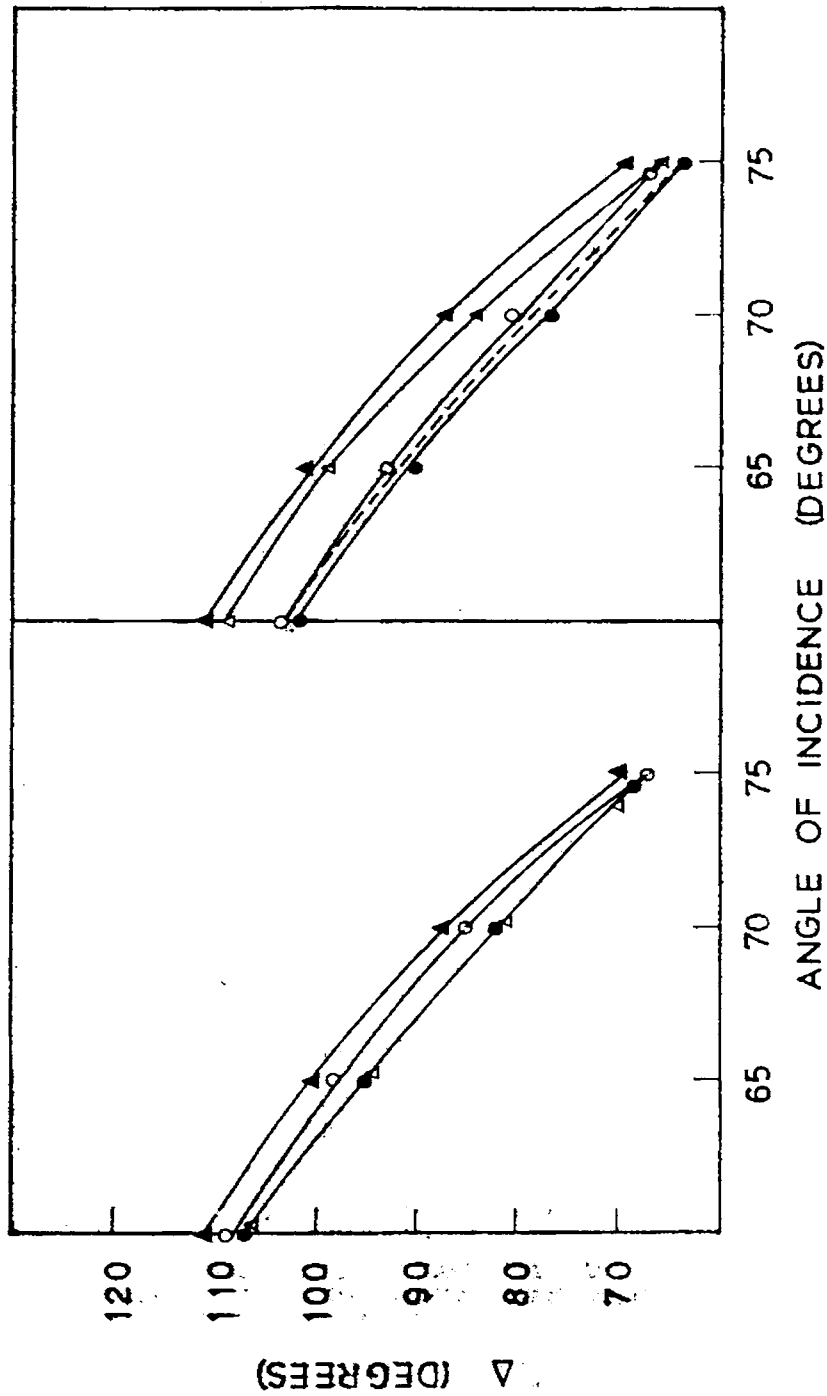


Fig. 7.5a

Variation in Δ values with angle of incidence for silver films (thickness - 3000 Å) at different temperatures (annealing in vacuum) \blacktriangle - \blacktriangle , before annealing; \triangle - \triangle , after annealing at 105°C, \circ - \circ , after annealing at 143°C; \bullet - \bullet , after annealing at 180°C, \bullet - \bullet , after annealing at 180°C.

Fig. 7.5b

Variation in Δ values with angle of incidence for silver films of same thickness at different temperatures (annealing in air) \blacktriangle - \blacktriangle , before annealing; \triangle - \triangle , after annealing at 67°C; \circ - \circ , after annealing at 105°C; ----, after annealing at 143°C; \bullet - \bullet , after annealing at 180°C.

in Q-factor value. But this happens upto $\sim 120^{\circ}\text{C}$ only. Beyond that temperature the Q-factor is constant upto $\sim 150^{\circ}\text{C}$. As the temperature increases further, there is a sharp increase in its value also. But when annealing is performed in vacuum there is slight reduction at first (upto $\sim 70^{\circ}\text{C}$) after which it increases till about 100°C . Beyond that temperature, the Q-factor value shows a slight decrease.

The variations of Δ values are also indicating the same result. In the fig.7.5a (which gives the variations due to vacuum annealing) it can be seen that the Δ values at 105°C and 143°C are the same for all angles of incidence, which indicates that the size of the irregularities is remaining constant in this temperature range. But at 180°C , the values show an increase hinting that the size of the irregularities is slightly reduced which is also clear from the Q-factor values in fig.7.3. In the case of the films annealed in air also, the Δ value variations support the Q-value variations. Here, the Δ values show a slight decrease at 67°C while at 105°C the decrease is considerably large and steep. (Compare this with the sharp increase in Q-value at 105°C in fig.7.3). At the angle

of incidence 60° , there is no change in its value for 105°C and 143°C , (which can be compared with the constant value of Q in the same range of temperature in fig.7.2). On further increasing the temperature, Δ is found to be decreasing again.

Thus here the observations lead one to the following conclusions. When thickness of the film is increased, the vacuum annealing results in the retardation of hillock growth at a lower temperature. Annealing in air also has a no-hillock growth region (or a constant Q -value region) between 120°C and 150°C which is not observed in the case of films with thickness 1500\AA .

7.5 Discussion

In this case also, the relationship between the hillock growth and the stress in the film should be considered for the explanation and this theory has been described in detail in chapter III. The most important point in the theory, put forward by Presland et al²³, is the condition for hillock growth to take place and that can be written as

$$\gamma \leq \frac{\sigma r_0}{2} \quad (7.2)$$

where γ , σ and r_0 represent the same parameters as stated in chapter III. For convenience, the discussion part may be divided into two; one part deals with the results of annealing in vacuum while the other deals with those of annealing in air.

7.5a Annealing in vacuum

On heating a metallic film coated over glass substrate, beyond its deposition temperature, thermal stress develops in the film which will be compressive in nature. The intrinsic stress formed in the film during deposition itself is tensile in nature. Hence due to heating, the net effect will be to reduce the resultant stress in the film because these components of stress are opposite to each other. When the stress in the film is reduced to such a low value that the condition in eqn.(7.2) is not satisfied the hillock growth stops. When this happens the Q-factor in eqn.(7.1) remains constant. This is exactly taking place here. Due to vacuum annealing, for the films with thickness 1500Å this happens at $\sim 160^\circ\text{C}$ (fig.7.2) and for the other type of films (3000Å thick) it occurs at $\sim 100^\circ\text{C}$ (fig.7.3). These observations are again supported by Δ values in figs.7.4a and 7.5a.

But there is a striking difference between the temperature values at which the hillock growth stops (at which Q-value becomes constant) for the two types of films. It can be very easily seen from the figs.7.2 and 7.3 that for the thinner films this takes place at a higher temperature while in the case of thicker films this happens at a lower temperature. In order to understand its reason one has to see fig.7.6 which shows the variation of intrinsic stress with thickness^{24,25} (of silver films). It is quite clear from the figure that silver films, with thickness $\sim 1500\text{\AA}$, have maximum intrinsic stress and as the thickness increases further, the intrinsic stress decreases. Hence for the films with thickness 1500\AA , the thermal stress has to be increased to a very high value in order to reduce the resultant stress in the film to such a low value that eqn.(7.2) is not satisfied and thereby the hillock growth is retarded. On the other hand for the thicker film, this phenomenon can take place at a low temperature because of the low intrinsic stress.

For both types of films, no appreciable change in Q-value is noted upto $\sim 70^{\circ}\text{C}$. This may be due to the 'induction time effect' observed by

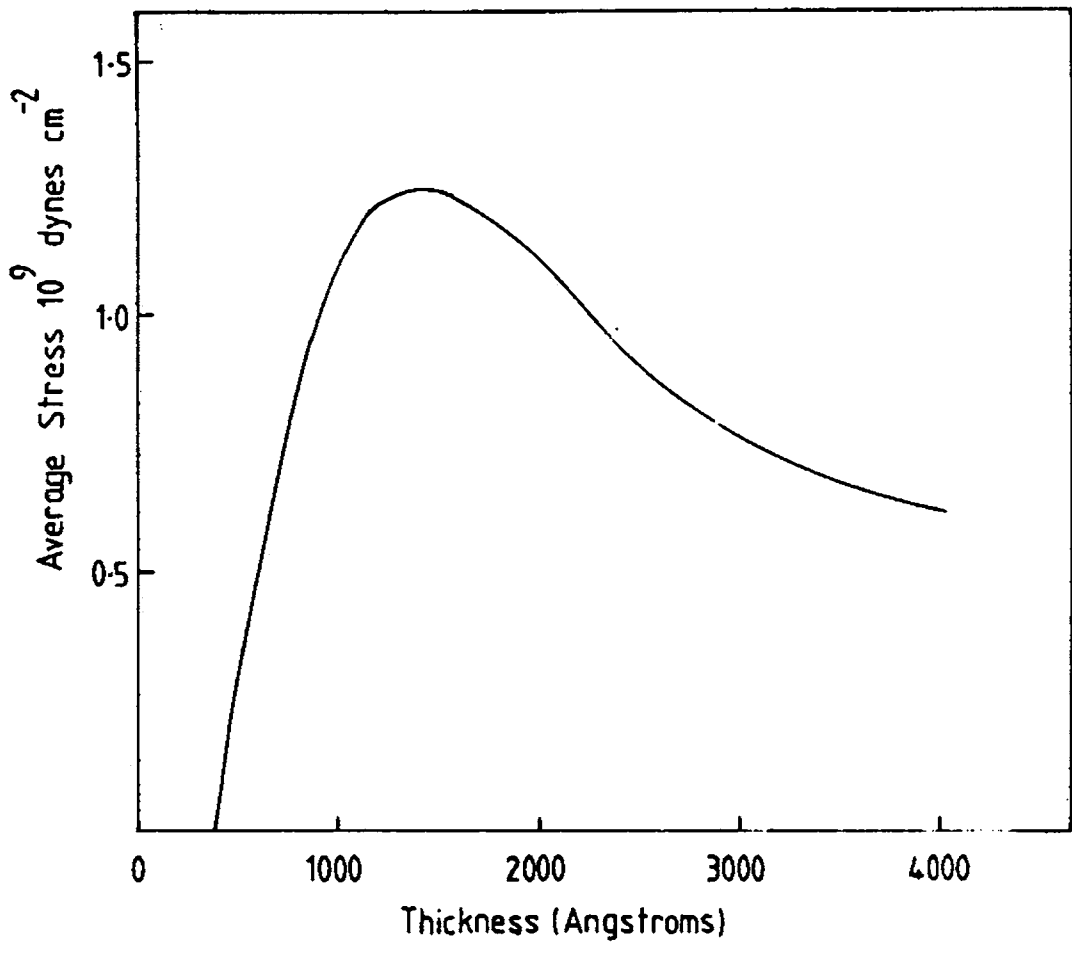


Fig.7.6 Variation of intrinsic stress in silver films with thickness.

Presland et al²³ on silver films annealed in vacuum. During the annealing process of silver film they observed that there was no appreciable change for the film for a particular period of time in the initial stage of annealing and this period of time was called the 'induction time' (t_i). They also found that t_i is very much reduced in presence of oxygen and the variation is governed by the relation

$$t_i = 11.5 - 3.8 \log_{10} P_{O_2} \quad (7.3)$$

where P_{O_2} is the pressure of oxygen. In the present work also no such variation in Q-factor is observed for annealing in air. Hence it is concluded that this effect may be due to induction time.

7.5b Calculation of intrinsic stress

As a support to the above argument, the intrinsic stress in the silver films (for the two thickness) has been calculated. For this calculation, the value of the thermal stress, at the temperature at which the Q-factor becomes a constant, is assumed to be (approximately) equal to the intrinsic stress. But the thermal stress can be easily calculated using

the expression²⁶,

$$\sigma_{\text{thermal}} = \frac{\alpha_t - \alpha_s}{1 - \nu} E(\Delta T) \quad (7.4)$$

where α_f and α_s are linear thermal expansion coefficients of film and substrate, E is the Young's modulus of the film material, ν is Poisson's ratio of the film and ΔT is the temperature difference. The values obtained in the present work and those obtained by earlier workers²⁴ are given in table 7.1.

Table 7.1

The intrinsic stress ($\sigma_{\text{intrinsic}}$) values for silver films

Thickness Å	$\sigma_{\text{intrinsic}}$ (from earlier works) $\times 10^9$ dynes cm^{-2}	$\sigma_{\text{intrinsic}}$ (present work) $\times 10^9$ dynes cm^{-2}
1500	1.25	1.5
3000	0.75	0.82

It can be seen that they are in good agreement in spite of the approximation that both the intrinsic and thermal stresses are taken to be equal at the temperature for which Q-factors becomes constant.

7.5c Annealing in air

When silver films are kept in air, the only change to be taken into account is that of the surface energy (γ). It will be considerably reduced in presence of oxygen in air and the variation is given by the relation (ref.24 of chapter III)

$$\gamma = 228 - 188 \log_{10} P_{O_2} \quad (7.5)$$

where P_{O_2} is the pressure of oxygen. Hence, when the annealing is in air, γ will have a very low value. But to stop the hillock growth one should have,

$$\gamma > \frac{\sigma r_o}{2} \quad (7.6)$$

When annealing is in air, to satisfy the above condition σ (the resultant stress in the film) must be reduced to a very low value for which the thermal stress must be increased very much (ie., the temperature at which the difference between the thermal stress and intrinsic stress becomes less than γ , is very high when compared with the corresponding temperature value in the case of vacuum annealing). This is clearly indicated by the Q-factor variations with temperature in figs.7.2 and 7.3.

In the case of films with thickness $1500\overset{\circ}{\text{A}}$, due to vacuum annealing, the Q-values become constant at $\sim 160\overset{\circ}{\text{C}}$. But when similar films are annealed in air, no such variations are taking place even upto $180\overset{\circ}{\text{C}}$. Similarly for the other type of films ($3000\overset{\circ}{\text{A}}$ thick) the vacuum annealing results in a constant Q value at $\sim 100\overset{\circ}{\text{C}}$ while due to annealing in air the Q-factor becomes constant at about $120\overset{\circ}{\text{C}}$. Here also for the thinner films, this phenomenon occurs at higher temperature due to reasons stated in section 7.5a while discussing the results of vacuum annealing.

The second increase in Q-factor after $150\overset{\circ}{\text{C}}$ (in fig.7.3) is due to the action of the thermal stress alone. Even after making the resultant stress in the film a minimum, the thermal stress is increasing along with the temperature. Now as the intrinsic stress is completely overcome, the resultant stress starts increasing along with the thermal stress component. Hence the condition in eqn.(7.2) is again satisfied whereby the hillock growth resumes. This is the reason behind the second increase of the Q-factor.

7.6 Conclusion

The relation between hillock growth and the stress distribution in silver films is studied in the

present work using ellipsometry. Here the conclusions are drawn from the variations of two factors viz., the Q-factor and Δ . It has been found that due to annealing in low temperature range (ie., $< 200^{\circ}\text{C}$) the stress in the films can be minimised. The temperature at which this occurs depends upon the thickness of the film and the ambient in which annealing is performed. As stress is minimised the hillock growth (surface roughness due to thermal effects) on the film surface is also stopped.

REFERENCES

1. Tennyson Smith and G.Lindberg, Surface technology, 9, 1 (1979).
2. M.Garnett, Phil.Trans.Roy.Soc. 203, 385 (1904).
3. M.Garnett, Phil.Trans.Roy.Soc. 205, 237 (1906).
4. O.S.Heavens, Optical properties of thin solid films, Butterworths, London (1955) p.177.
5. Carl A.Fenstermaker and Frank L.McCrackin, Surf.Sci., 16, 85 (1969).
6. Tennyson Smith, Surf.Sci., 45, 117 (1974).
7. Tennyson Smith, Surf.Sci., 56, 252 (1976).
8. I.Ohlidal and F.Lukes, Opt.Acta., 19, 817 (1972).
9. I.Ohlidal and F.Lukes, Opt.Comm., 5, 323 (1972).
10. I.Ohlidal and F.Lukes, Opt.Comm., 7, 76 (1973).
11. I.Ohlidal and F.Lukes, Proceedings of 6th Czechoslovakia Conference on 'Electronics and vacuum physics', Czechoslovakia Acad.Sci., 16-19 Oct.(1972).
12. I.Ohlidal and E.Schmidt, Scr.Fac.Sci.Nat.Unuv. Purkynianae, Brunensis Phys., 5 65 (1975).
13. K.Brudzewski, Appl.Opt., 5, 115 (1976).

14. K.Brudzewski, Thin Solid Films, 61, 183 (1979).
15. Z.Maris and E.Zamfir, An.Univ. 24, 30 (1975).
16. E.C.Chan, J.Vac.Sci. & Technol., 13, 981 (1976).
17. J.P.Marten, Proceedings of Society of Photo-Optical Instrumentation Engineers, Vol.112, Soc. Photo-Optical Instrumentation Engineers, Bellingham, WA, USA (1977) p.82.
18. K.K.Svilashov, A.I.Semenenkov, L.V.Semenenko and N.L.Shvarts, Opt. & Spectrosc., 43, 88 (1977).
19. T.V.Vorburger and K.C.Ludema, Appl.Opt., 19, 561 (1980).
20. K.P.Vijayakumar and C.Purushothaman, Thin Solid Films, 82, 225 (1981).
21. Robert W.Berry, Peter M.Hall and Murray T.Harris, Thin film technology, D.Van Nostrand Company, New Jersey (1968) p.160.
22. S.Tolansky, Surface Microtopography, John Wiley and Sons, New York (1960).
23. A.E.B.Presland, G.L.Price and D.L.Trimm in Sydney G.Davison (ed.) Progress in Surface Science, Vol.3, Pergamon Press, Oxford (1973) p.63.

24. H.Kato, K.Nagasima and H.Hasunuma, Oyo Butsuri, 30, 700 (1961).
25. R.W.Hoffman in Georg Hass and Rudolf E.Thun (eds.), Physics of thin films, Vol.3, Academic Press, New York (1966) p.231.
26. S.K.Sharma and J.Spitz, Thin Solid Films, 65, 339 (1980).

CHAPTER VIII

LIGHT SCATTERING MEASUREMENTS ON SILVER FILM SURFACE

8.1 Introduction

This is another optical method by which the material surface nature can be analysed. Comparing with other techniques this is much simple. Here, the variation of intensity of the reflected light with the angle of incidence (most generally) is noted. Another important factor, supporting this method is that this is also a non-destructive technique. The general theory which describes the scattering of the electromagnetic radiation by rough surfaces is based on Kirchhoff method in diffraction theory. This theory can be used for different purposes depending upon the wavelength of the radiation used. For example, in the smaller wavelength region, this can be used to explain the characteristics of reflection of elementary particles from metal surfaces as scattering of De Broglie waves from rough metal surfaces¹, while in the longer wavelength side, the scattering of radio waves by terrain, sea or atmospheric layers can be studied.

Usually, in the visible range, this is used as a supplementary method along with some other major experimental technique. Here also this technique has been used to analyse the film surfaces which are already studied by using the ellipsometric technique (in chapter VII) to serve as an additional verification of the results obtained there. It should also be noted here that the analysis by using the light scattering measurements is performed after the final annealing described in the last chapter (ie., after annealing at 180°C). Thus in the present work the surface roughness of silver films due to annealing is studied by using this method. The variation of the roughness with film thickness and due to the annealing in vacuum and air are also studied. The detailed theory of the technique is given in the next section.

8.2 Theory

The theory of light scattering by rough surfaces has been developed by several workers²⁻¹² over the last 30 years for the application to both periodic and random rough surfaces. Probably the most comprehensive development of the theory has been given by Beckmann^{9,10}. Houchens and Hering¹³,

in their review of Kirchhoff theory, have concluded that Beckmann model is applicable over a wide range of roughness parameters. The Kirchhoff theory has been applied to the study of rough metal surfaces by several authors¹⁴⁻¹⁸. Almost all of them describe the theory in some detail and compare the results obtained from measurement of intensity of the specular component with determinations of the roughness using a mechanical stylus. In this work also the Beckmann model is used and hence that is described in this section.

Let the surface irregularity be denoted by a function $Z(x,y)$ where Z is the deviation from the mean x - y plane. When the surface is statistically rough the function is a random process depending on the space coordinates x and y only (Here the roughness having some periodic nature, like that of a grating, is not considered. As the most general case one can consider the surface irregularities fluctuating in time as the surface of the sea. In that case, the function will depend on time also as $Z(x,y,t)$. But that is also avoided in the present discussion).

Let a plane electromagnetic wave be incident on this surface and the coordinates be so considered that the wave vector \bar{k}_1 of the incident wave be in the x-z plane and the angle of incidence, θ_1 be between \bar{k}_1 and the z-axis (See fig.8.1). One can represent the electric vector of the wave as,

$$E_1 = E_0 e^{i(k_1 \cdot r - \omega t)} \quad (8.1)$$

where ω is the angular velocity and \bar{r} is the position vector,

$$\bar{r} = x\bar{x}_0 + y\bar{y}_0 + z\bar{z}_0 \quad (8.2)$$

with \bar{x}_0 , \bar{y}_0 and \bar{z}_0 as the unit vectors of the coordinate system. In this work, the aim is to find out the field scattered into the arbitrary direction defined by θ_2 , θ_3 (from fig.8.1). If it is assumed that the radius of curvature of the surface is much larger than the wave length of the light incident on it and the surface to be locally perfectly reflecting, one can apply the Kirchhoff method. If \bar{k}_2 is the wave vector along the direction of scattering (defined by θ_2 , θ_3) the scattered field E_2 at a point P is

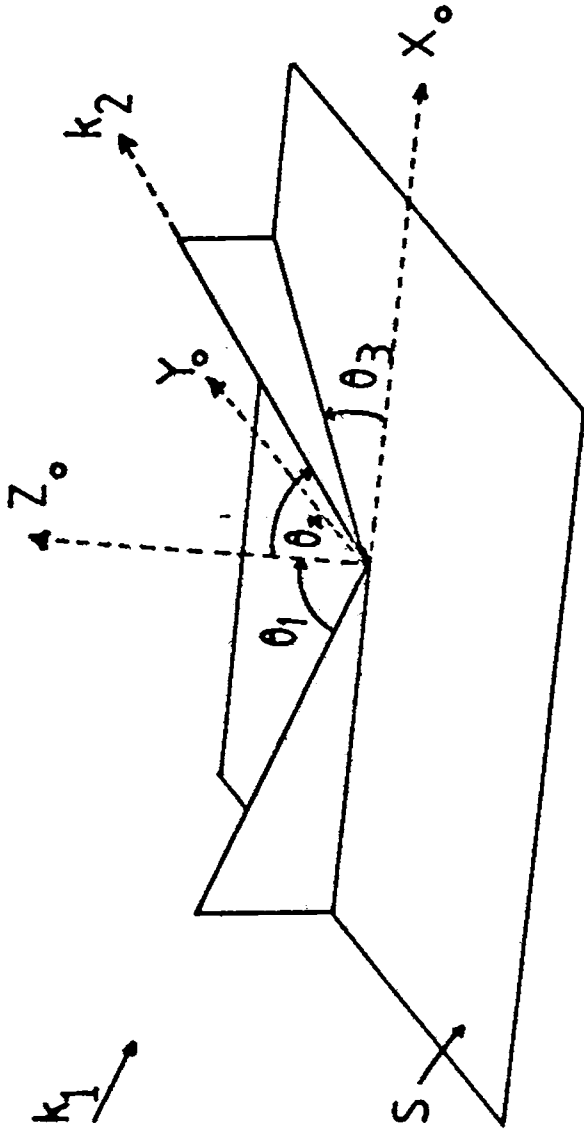


Fig.8.1 Orientation of coordinate system and scattering geometry $\theta_1, \theta_2, \theta_3$. The incident wave propagates in the direction of the propagation vector K_1 and the scattered wave in the direction K_2 .

given by the Helmholtz integral,

$$E_2(P) = \frac{1}{4\pi} \iint (E \frac{\partial \psi}{\partial n} - \frac{\partial E}{\partial n}) ds \quad (8.3)$$

$$\text{where } \psi = \frac{e^{i\bar{k}_2 \cdot R_2}}{R_2} \quad (8.4)$$

where \bar{R}_2 is the distance of P from a variable point on the rough surface S, E is the field on the surface and $\frac{\partial}{\partial n}$ is the derivative along the normal to the surface. Since it is assumed that the radii of curvature of the surface are much larger than the wavelength, one can consider each point on the surface S to make the same contribution to the scattered field as if it were a part of the tangent plane to the rough surface S at that point i.e., one can consider the surface S as 'locally flat'. Using these conditions, the field and its normal derivative on the surface S can be obtained, with the help of the boundary conditions, as

$$(E)_S = (1+R)E_1 \quad (8.5)$$

$$\left(\frac{\partial E}{\partial n}\right)_S = (1-R)E_1 \bar{k} \cdot \bar{n} \quad (8.6)$$

where \bar{n} is the normal to the surface and R is the local reflection coefficient.

The dimensionless 'scattering coefficient' is defined as

$$e = E_2/E_{20} \quad (8.7)$$

where E_2 is the scattered field and E_{20} the field that would be reflected in the specular reflection (ie., when $\theta_2 = \theta_1$ and $\theta_3 = 0$) by a smooth reflecting plane of same dimensions under same angle of incidence at the same distance. Adopting the method of Beckmann⁹ it can be obtained from the eqns.(8.2)-(8.7) as,

$$e = \frac{F(\theta_1, \theta_2, \theta_3)}{A} \iint_A e^{i\bar{v} \cdot \mathbf{r}} dx dy \quad (8.8)$$

where

$$F(\theta_1, \theta_2, \theta_3) = \frac{1 + \cos \theta_1 \cos \theta_2 - \sin \theta_1 \sin \theta_2 \cos \theta_3}{\cos \theta_1 (\cos \theta_1 + \cos \theta_2)} \quad (8.9)$$

A is the area subtending the surface in x - y plane

$$\begin{aligned} \bar{v} &= \bar{k}_1 - \bar{k}_2 \\ &= k[(\sin \theta_1 - \sin \theta_2 \cos \theta_3)\bar{x}_0 - \sin \theta_2 \sin \theta_3 \bar{y}_0 \\ &\quad - (\cos \theta_1 + \cos \theta_2)\bar{z}_0] \end{aligned} \quad (8.10)$$

$$\text{and } \bar{r} = x\bar{x}_0 + y\bar{y}_0 + Z(x,y)\bar{z}_0 \quad (8.11)$$

is the position vector describing the rough surface. The factor k in eqn.(8.10) represents the magnitude of the wave vector and is equal to $2\pi/\lambda$.

The integral in eqn.(8.8) is the general Kirchhoff solution of the problem and one can apply it to either periodic or random rough surfaces.

8.2a Random rough surfaces

In most of the applications the scattering surface is statistically rough ie., $Z(x,y)$ is a random function of position and Z is a random variable assuming values z with probability density $p(z)$. Now one should know the joint probability density $p_2(z_1, z_2)$ where z_1 and z_2 are the values of Z at points (x_1, y_1) and (x_2, y_2) respectively. In almost all the cases, it can be assumed that the two dimensional probability density $p_2(z_1, z_2)$ depends only on the distance between the points (x_1, y_1) and (x_2, y_2) and not on these points. Hence, one can get the two dimensional characteristic

function (the Fourier transform) associated with the distribution $p_2(z_1, z_2)$ as,

$$\chi(t_1, t_2) = \int_{-\infty}^{\infty} \int_{-\infty}^{\infty} p_2(z_1, z_2) e^{it_1 z_1 + it_2 z_2} dz_1 dz_2 \quad (8.12)$$

and the one dimensional characteristic function as

$$\chi(t) = \int_{-\infty}^{\infty} p(z) e^{itz} dz \quad (8.13)$$

Hence the mean scattered field in any direction may be obtained from eqns(8.8) and (8.13) as

$$\langle e \rangle = \frac{F \chi(v_z)}{A} \int_{-x}^x \int_{-y}^y e^{iv_x x + iv_y y} dx dy \quad (8.14)$$

which on integration gives,

$$\langle e \rangle = \frac{F}{A} \chi(v_z) e_0 \quad (8.15)$$

$$\text{where, } e_0 = \frac{\sin v_x X}{v_x X} \frac{\sin v_y Y}{v_y Y} \quad (8.16)$$

is the scattering coefficient of a plane sheet of equal area $A = 4XY$.

The mean square of eqn.(8.8), which is proportional to the mean scattered power, is given by $\langle ee^* \rangle$ and it can be obtained from eqns.(8.8) and (8.12) as

$$\langle ee^* \rangle = \frac{2\pi F^2}{A} \int_0^\infty J_0(v_{xy}\tau) \chi_2(v_z - v_z\tau)\tau d\tau \quad (8.17)$$

$$\text{where } v_{xy} = \sqrt{(v_x^2 + v_y^2)} \quad (8.18)$$

$$\text{and, } \tau = \sqrt{(x_2 - x_1)^2 + (y_2 - y_1)^2} \quad (8.19)$$

which is the distance between (x_1, y_1) and (x_2, y_2) and J_0 is the Bessel function of first kind of order zero.

The integral in eqn.(8.17) is the basis for the calculation of the scattered field from the random rough surfaces and for computational purpose, one can assume particular type of the random process $Z(x, y)$. If $Z(x, y)$ is a normal process with mean, zero standard deviation σ and the autocovariance $C(\tau)$ to be Gaussian as

$$C(\tau) = e^{-\tau/T^2} \quad (8.20)$$

(where T is the correlation distance) one gets the general solution to be⁹

$$\langle ee^* \rangle = e^{-g} \left(e_0^2 + \frac{\pi T^2 F}{A} \sum_{m=1}^{\infty} \frac{g^m e^{-v_{xy}^2 T^2 / 4m}}{m! m} \right) \quad (8.21)$$

$$\text{where } \sqrt{g} = v_x \sigma = \frac{2\pi\sigma}{\lambda} (\cos \theta_1 + \cos \theta_2) \quad (8.22)$$

The first term, which forms eqn.(8.16) vanishes everywhere except in the neighbourhood of the specular direction and is the coherent (specular) component.

The scattered field consists of both specular and diffusely scattered components. When $g \rightarrow 0$ the specular component will be dominant and for $g \gg 1$ the diffusely scattered field is the only important component. For the specular direction one has

$v_x = v_y = 0$ and hence from eqn.(8.16) $e_0 = 1$ and the specular term in eqn.(8.21) becomes

$$\langle ee^* \rangle_{\text{spe}} = \exp\left[-\left(\frac{4\pi\sigma \cos \theta_2}{\lambda}\right)^2\right] \quad (8.23)$$

If one has I_s to be the intensity of the specularly reflected light from the rough surface and I_{s0} that from an ideally smooth surface (under the same conditions)

then,

$$R_s = I_s/I_{s0} = \langle ee^* \rangle = \exp\left[-\left(\frac{4\pi\sigma \cos \theta_i}{\lambda}\right)^2\right] \quad (8.24)$$

Here, if the incident beam is plane polarised with electric vector in the plane parallel to the plane of incidence (p-plane) the intensity of the reflected wave from the smooth surface (I_{s0}) can be easily calculated using Fresnel's coefficients (chapter VI sec. 2). Hence if a graph is plotted with $\cos^2 \theta$ on the X-axis and $\ln R_s$ on the Y-axis, it will have a slope $m = -(4\pi\sigma/\lambda)^2$. From this, the value of σ , which is the rms value of the height of the irregularities, can be obtained.

8.3 Experimental

The silver films used for the ellipsometric study were used in this experiment also. Hence, the two types of films with thickness $1500\overset{\circ}{\text{Å}}$ and $3000\overset{\circ}{\text{Å}}$ were analysed by using the light scattering technique. But, here the experiment was performed after the final annealing (ie., after the annealing at 180°C). The film preparation method and the annealing techniques are the same as described in chapter VII. For this

study also annealing in vacuum and air were separately done on two sets of films.

The optical system consisted of the light source, filter, collimator, polariser, the film PMT and galvanometer. It is same as that described in chapter III (See fig.2.6) with the difference that here polariser was also used. Its detailed description is included in chapter II. The calculations were done using a mini-computer (Micro-78).

8.4 Results

The graphs ($\ln R_s$ vs. $\cos^2 \theta$) for all the films are shown in fig.8.2. Here the curves before annealing for the two types of films are found to be almost coinciding and hence only one curve is given with average values of both films. From the slope of the graphs, the value of σ for each film is calculated and is given in table 8.1 along with the percentage of increase, in σ value. It can be seen that the σ value increases with thickness of the film. Also, for the same thickness annealing in air results in larger σ value. The largest σ value is obtained for

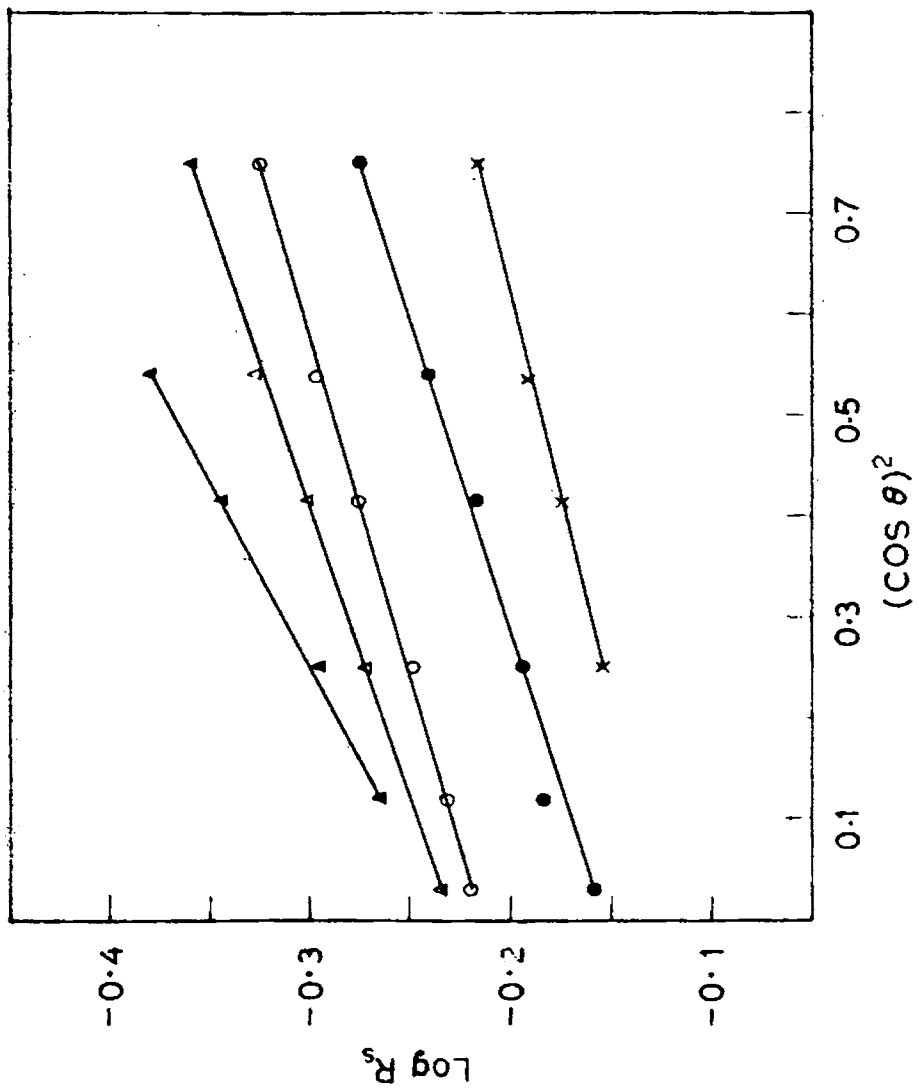


Fig.8.2 Log R_s vs. $\text{Cos}^2\theta$ curves for films of thicknesses 3000A (▲ - annealed in air; ● - annealed in vacuum) and 1500A (△ - annealed in air; ○ - annealed in vacuum) x - unannealed film averaged for both types of films.

Table 8.1

The values of σ and its percentage of increase

Thickness $\overset{\circ}{\text{A}}$	Nature of annealing	$\overset{\circ}{\sigma}$ $\overset{\circ}{\text{A}}$	Percentage of increase
1500 and 3000	Unannealed	171	--
1500	In vacuum	189	10.3
1500	In air	206	20.3
3000	In vacuum	198	15.4
3000	In air	259	51.1

the film with thickness $3000\overset{\circ}{\text{A}}$ annealed in air ($\overset{\circ}{\sigma} = 259\overset{\circ}{\text{A}}$). The most important point to be noted here is that these results are in close agreement with those obtained using ellipsometry.

8.5 Discussion

It has been clearly stated earlier (in chapters III and VI) that the important variation occurring on the silver film surface while it is kept in air (in presence of oxygen) is that its surface energy is much decreased and hence there can be increased surface

diffusion on heating. This results in larger surface irregularities or hillock growth. This is exactly shown by the larger σ values (rms value of hillock height) for films annealed in air¹⁹.

In chapter VII it is stated that for silver films, the intrinsic stress is maximum when thickness is $\sim 1500\text{\AA}$ and as the thickness increases the intrinsic stress is decreasing. Hence a minimisation of stress occurs, due to annealing and this happens at a temperature below 180°C in the case of thicker films (3000\AA thick) and above or near 180°C in the case of thinner films (1500\AA thick). This is reflected in the hillock growth also and due to this reason, σ value is smaller for the films with thickness 1500\AA and larger for the 3000\AA thick films.

8.6 Conclusion

The important conclusion is that these observations lend support to ellipsometric results. It is also seen, (in agreement with results mentioned earlier) that, annealing in air results in larger hillocks. Also, with thickness of the film, the rms value of

hillock height increases which clearly shows the relationship between the stress in the film and the surface diffusion.

REFERENCES

1. J.H.Healey, The scattering of particles from rough surfaces, Dissertation, Elect.Engg., University of Colarado.
2. L.M.Brekhovskikh, Dokl.Akad.Nauk. SSR., 81, 1023 (1951).
3. L.M.Brekhovskikh, Zh.Eksp.Teor.Fiz., 23, 275 (1952).
4. L.M.Brekhovskikh, Zh.Eksp.Teor.Fiz., 23, 289 (1952).
5. Yu.P.Lysanov, Dokl.Akad.Nauk. SSR., 87, 719 (1952).
6. H.Davies, Inst.Elect.Eng., 101 209 (1954).
7. M.A.Isakovich, Zh.Eksp.Teor.Fiz., 23, 305 (1952).
8. W.C.Meecham, J.Appl.Phys., 27, 361 (1956).
9. P.Beckmann, The scattering of electromagnetic waves from rough surfaces, Part I, Macmillan, New York (1963).
10. P.Beckman in E.Wolf (ed.), Progress in Optics, Vol.6, North Holland, Amsterdam (1967) p.53.
11. J.M.Elson and J.M.Bennett, J.Opt.Soc.Am., 69, 31 (1979).
12. F.U.Hillebrecht, J.Phys.D.13, 1625 (1980).

13. A.F.Houchens and R.G.Hering, Progr.Astronaut.
Aeronaut., 20, 65 (1967).
14. H.E.Bennett and J.O.Porteus, J.Opt.Soc.Am.,
51, 123 (1961).
15. R.C.Birkebak and E.R.G.Eckert, Trans.ASME.,
C87, 85 (1965).
16. R.C.Birkebak, Appl.Opt., 10, 1970 (1971).
17. T.J.Love and R.E.Francis, Progr.Astronaut.
Aeronaut., 20, 115 (1967).
18. C.A.Depew and R.D.Weir, Appl.Opt., 10, 969 (1971).
19. K.P.Vijayakumar and C.Purushothaman, Proc.of
Nuclear Physics and Solid State Physics Symposium,
University of Mysore, Mysore (1983) p.SAB8.

CHAPTER IX

SUMMARY OF CONCLUSIONS

The studies presented in this thesis are centred around the variations of the nature of surface of some metallic thin films due to heating (annealing) and interdiffusion. The results and conclusions in the different chapters are summarised here.

In chapter III, the changes on the surface of silver thin films due to annealing are presented. The study is based on reflectivity measurements. From the results one can arrive at the conclusion that there is a minimisation of surface roughness created by heating (annealing). The value of temperature, at which it happens, strongly depends on the ambient condition in which the film is annealed. In this case, due to vacuum annealing, the surface smoothening takes place at 100°C while the annealing in air results in this phenomenon at 212°C . This can be due to the difference in the surface energy of the film and hence, the relation between the surface roughness due to annealing (hillock growth) and the stress in the film is revealed. It has been shown that the surface smoothening takes place as a result of the stress minimisation in the film.

Similar work on copper films (with thickness varying from $500\overset{\circ}{\text{A}}$ to $3000\overset{\circ}{\text{A}}$) is presented in chapter IV, with the difference that in this case the reflectivity measurements were taken during heating keeping the sample in vacuum. Here also surface smoothening is taking place which is indicated by the sharp increase in the reflectivity. The electron micrographs of the films before and after heating also indicate this very clearly. The temperature value at which the smoothening takes place shows a strong dependence on thickness of the films. This again points out the relationship between stress in the film and surface smoothening. It has been shown by earlier workers that copper films with thickness in the range $500\overset{\circ}{\text{A}}$ to $1000\overset{\circ}{\text{A}}$ have maximum intrinsic stress and as the thickness further increases, the stress decreases. This is clearly indicated by the temperature values also. The intrinsic stress values calculated from optical results also agree well with those obtained by earlier workers.

The relationship between the surface smoothening and thickness of film (and hence the stress in the film) was studied in the case of silver films also. For this a more sensitive and precise method viz., ellipsometry, has been employed. These results are

given in chapter VII. It is again found that, for silver films with a thickness of $1500\overset{\circ}{\text{Å}}$, the surface smoothening occurs at a higher temperature while for the $3000\overset{\circ}{\text{Å}}$ thick films, it takes place at a lower temperature. Also it has been shown that the intrinsic stress is maximum when thickness is $1500\overset{\circ}{\text{Å}}$ and for further increase in thickness there is corresponding decrease in the stress. The relation between stress and surface smoothening is thus elucidated. The dependence of ambient condition (described in chapter III) is verified again in this chapter. Intrinsic stress in silver thin films (for thickness $1500\overset{\circ}{\text{Å}}$ and $3000\overset{\circ}{\text{Å}}$) has been calculated and these values show good agreement with values obtained by earlier workers by different methods.

The films used for ellipsometric investigations are also analysed using light scattering technique. This is included in chapter VIII. Here, by measuring the actual size of the surface irregularities the thickness dependence and ambient dependence are once again verified.

The variations of the surface nature of a bi-layer film (Al-Ag) are also studied optically. These

results are given in chapter V. From the results obtained it can be concluded that

i) the diffusion of aluminium through silver is much easier due to the predominance of grain boundary diffusion and the reverse case is not so easy as aluminium film, which is more continuous in nature, does not promote the grain boundary diffusion,

ii) when the thickness ratio between aluminium and silver layers is 1:2, due to diffusion of aluminium into silver, the intermetallic compound Ag_3Al is formed first, which decomposes to give Ag_2Al at higher temperature,

iii) due to diffusion of silver into aluminium, only Ag_2Al is formed for the same thickness ratio, and

iv) a layer of aluminium is formed over the film surface when the thickness ratio is changed to 1:1.

APPENDIX - I

LATTICE DYNAMICS AND EIGENVECTOR MAGNITUDES IN ZnS CRYSTAL

A.1 Introduction

In any solid the atoms are continuously oscillating about their equilibrium positions with an energy governed by the temperature of the solid. These oscillations are responsible for a large number of characteristic properties like specific heat, optical and dielectric properties and electrical resistance. In crystals these oscillations are called Lattice vibrations. At the limit of long wavelength the vibrations of the lattice are described by the classical theory of elasticity. In this, the solid is considered as a continuum having macroscopic elastic constants. As the wavelength becomes shorter and approaches the inter-atomic distance the microscopic crystal structure and the forces between individual pairs of atoms become the dominant features in determining the nature of modes of vibration. The theoretical and experimental studies on these vibrations yield information about the interatomic force and frequencies of the vibrations which in turn can be

directly used to predict the temperature dependence of some incoherent scattering properties of crystals.

In the present work, the phonon frequencies along [100], [111] and [110] directions of the wavevector are determined for ZnS by employing the Rigid ion model (which will be described later). Also the eigenvector values are obtained by using the method of isotopic substitution i.e., by replacing ^{32}S with ^{34}S in the ZnS crystal.

A.1a Brief review of earlier works

The lattice dynamics of ZnS crystal (and more generally crystals of Zinc blende structure) has been a topic of interest for the solid state physicists and a large number of works have been published regarding different aspects in this field and using different models. The work by Smith¹, using the central force model, can be considered to be the pioneering one on this type of crystals. Rajagopal et al² modified it using the rigid ion model in which the Coulomb interaction between ions is also taken into account. Vetelino et al³ had also used the rigid ion model for their calculation of phonon frequencies of ZnS. Almost at

the same time, Feldkamp et al⁴ obtained the dispersion curves by neutron scattering along all the three directions of the wave vector. Another notable development in this direction was the calculation of effective charges in crystals of zinc blende structure by Mani et al^{5,6}. In this work they performed the calculation for crystals like GaAs, CdTe, AlSb, InSb and ZnS. They also obtained the dispersion curves using rigid ion model. The development of the deformable bond model by Kunc et al⁷ is another important point to be noted here. They used this model to determine the dispersion relation of fifteen crystals (including ZnS) with zinc blende structure⁸. Later the deformable ion model was employed by Jaswal⁹ in the case of ZnS and obtained good agreement with experimental results. Soma¹⁰ theoretically calculated the thermal expansion against temperature for ZnS, ZnTe and ZnSe. He also obtained dispersion relations of the crystals at metallic transition pressure. Kushwaha¹¹ employed the newly developed Bond bending force model (BBFM) for phonon dispersion in ZnS, GaAs and GaSb. Using the Deformation dipole model (DDM), Yadav¹² obtained lattice specific heat and Debye-Waller factor for ZnS. Very recently Soma et al¹³ calculated the

the phonon dispersion relations in crystals with zinc blende structure with the help of the pseudo-potential method.

A.2 Theory

The pioneering work in this field i.e., lattice dynamics was by Born and Von Kārmān^{14,15}. From then onwards different lattice models have been developed to describe the interatomic forces responsible for a stable structure of the crystal depending on the empirical data available and the physical nature of the problem. The model put forward by Born and Von Kārmān, which is the basis for all the later models, considers the atoms as point masses arranged in some effective potential provided by their mutual interaction which determines their motion. The difficulty of this model is to reconcile this simple picture with the crystal seen as an assemblage of nuclei and electrons.

Here a brief summary of the theory leading to the rigid ion model is included. Detailed description and review of investigations are given in book by Born and Huang¹⁶ and in review articles by de Launay¹⁷,

Blackman¹⁸, Leibfried¹⁹, Cochran²⁰ and Cochran and Cowley²¹. Another book by Maradudin et al²² contains all the basic theories of lattice dynamics and also the modern developments like neutron scattering, effect of defects and disorder and surface effects on lattice dynamics.

A.2a Approximations in the theory

It will be extremely difficult if one attempts to solve the many particle Schrodinger equation for a complicated system like a crystal and to obtain its properties. Hence the easiest method is to approach the problem with some approximations in the beginning and at a later stage to remove the same to the possible extent especially when they hinder in the prediction and explanation of some of the properties of the solid.

The most important and basic ingredients in the theory of lattice vibrations are crystal symmetry, Adiabatic approximation and Harmonic approximation. The crystal symmetry is the one simplifying the initial many body problem. By invoking the symmetry arguments one can calculate the properties of entire crystal from a knowledge of the behaviour of a very small region.

However this is applicable only to perfect ideal crystals without defects. In the adiabatic approximation or Born-Oppenheimer approximation²³ the essential idea is that the atomic nuclei being much heavier, moves much more slowly than the electrons. Therefore at any instant the electrons 'see' the nuclei fixed in some configuration. When the nuclei move the electrons follow the nuclear motion adiabatically in the sense that electronic state follows a smooth variation merely keeping in step with no abrupt transitions. Hence the electronic energy becomes a function of nuclear coordinates and appears as potential energy in the Shrodinger equation. Essentially this approximation neglects any interaction between the valence electrons and lattice vibrations. Deviation from this approximation gives rise to electron-phonon interaction. In the harmonic approximation, it is assumed that the force on an atom is proportional to the first power of its displacement. Hence neglecting the electronic excitations, the Hamiltonian of the crystal consists of the kinetic energy (T) of the nuclei and the potential energy (ϕ) which is a

function of nuclear coordinates and which is a minimum for certain configuration. Thus the Hamiltonian (H) can be written as

$$H = T + \phi \quad (\text{A.1})$$

In this the potential energy ϕ can be expanded in Taylor series in powers of nuclear displacements from the equilibrium configuration as,

$$\begin{aligned} \phi = \phi_0 + \sum_{1k\alpha} \phi_{\alpha}(1k)U_{\alpha}(1k) \\ + \frac{1}{2} \sum_{\substack{1k\alpha \\ 1'k'\beta}} \phi_{\alpha\beta}(1k;1'k')U_{\alpha}(1k)U_{\beta}(1'k') + \dots \end{aligned} \quad (\text{A.2})$$

where ϕ_0 is the potential energy of the non-vibrating crystal and

$$\phi_{\alpha}(1k) = \left. \frac{\partial \phi}{\partial U_{\alpha}(1k)} \right|_0 \quad (\text{A.3})$$

$$\phi_{\alpha\beta}(1k;1'k') = \left. \frac{\partial^2 \phi}{\partial U_{\alpha}(1k) \partial U_{\beta}(1'k')} \right|_0 \quad (\text{A.4})$$

Here the subscript '0' in the eqns.(A.3) and (A.4)

denote that the derivatives are evaluated in the equilibrium configuration. The subscript l denotes the unit cell and k distinguishes the different atoms in that cell. Also $U_\alpha(lk)$ is the α -Cartesian component of $U(lk)$ with $\alpha = x, y, z$. If the terms upto the second power in eqn.(A.2) are retained one is said to be within the harmonic approximation. Thus one can restrict oneself to two body forces under this approximation and deviation from this leads to phonon-phonon interaction.

From eqn.(A.3) one can easily see that $\phi_\alpha(lk)$ denotes the negative of the force acting in the α -direction on the atom at (lk) in the equilibrium configuration. However in the equilibrium configuration the force on any particle must vanish and hence one has

$$\phi_\alpha(lk) = 0 \quad (\text{A.5})$$

Now the kinetic energy can be written as,

$$T = \frac{1}{2} \sum_{lk\alpha} M_k \dot{U}_\alpha^2(lk) \quad (\text{A.6})$$

The expression for the Hamiltonian becomes (in harmonic approximation)

$$H = \frac{1}{2} \sum_{1k\alpha} M_k \dot{U}_\alpha^2(1k) + \phi_0 + \sum_{\substack{1k\alpha \\ 1'k'\beta}} \phi_{\alpha\beta}(1k;1'k') U_\alpha(1k) U_\beta(1'k') \quad (\text{A.7})$$

Hence the equations of motion of the lattice follow immediately.

$$M_k \ddot{U}_\alpha(1k) = - \frac{\partial \phi}{\partial U_\alpha(1k)} = - \sum_{1'k'\beta} \phi_{\alpha\beta}(1k;1'k') U_\beta(1'k') \quad (\text{A.8})$$

Here the coefficients $\phi_{\alpha\beta}(1k;1'k')$ are called the atomic force constants. (They are the second derivatives of the potential energy with respect to atomic displacements). The coefficient represent the negative of the force exerted in the α -direction on the atom (1k) when the atom (1'k') is displaced a unit distance in the β -direction, all the other atoms being kept at their equilibrium positions. If one chooses as the solution to the eqn.(A.8) a function of the form,

$$U_\alpha(1k) = \bar{M}_k^{-1/2} U_\alpha(k) \exp[-i\omega t + iK \cdot x(1)] \quad (\text{A.9})$$

the eqn.(A.8) becomes

$$\omega^2 U_\alpha(k) = \sum_{k'\beta} D_{\alpha\beta}(kk'|K) U_\alpha(k') \quad (\text{A.10})$$

where the elements of the matrix $D(k)$ (called the Fourier transformed dynamical matrix) are given by

$$D_{\alpha\beta}(kk'|K) = (M_k M_{k'})^{-1/2} \sum_{l'} \phi_{\alpha\beta}(lk; l'k') \exp[-i\bar{K} \{x(l) - x(l')\}] \quad (\text{A.11})$$

Here $x(l)$ and $x(l')$ denote the position vectors of l and l' unit cells respectively and the vector K is called the Wavevector. Also M_k and $M_{k'}$ are the masses of k^{th} and k'^{th} atoms. The condition that the sets of eqns.(A.10) have a nontrivial solution is that the determinant of the coefficients vanish.

$$\left| D_{\alpha\beta}(kk'|\bar{K}) - \omega^2 \delta_{\alpha\beta} \delta_{kk'} \right| = 0 \quad (\text{A.12})$$

The number of solutions of eqn.(A.12) is equal to thrice the number of atoms in a unit cell (ie., thrice the number of values of k). If there are ' r ' atoms in the unit cell, the number of solutions is $3r$. Thus for each value of \bar{K} there can be $3r$ values of $\omega^2(\bar{K})$

and the $3r$ functions of $\omega_j^2(\bar{K})$ (where $j=1,2,\dots,3r$) can be regarded as the branches of a multivalued function $\omega^2(\bar{K})$. This relation can be written as,

$$\omega = \omega_j(\bar{K})$$

which is called the 'dispersion relation'.

For each of the $3r$ values of $\omega_j^2(\bar{K})$ corresponding to a given value of \bar{K} , there exists a vector $e(k|\bar{K}j)$ whose components are the solutions to the set of eqns.(A.10) and this can be denoted as

$$\omega_j^2(\bar{K})e_\alpha(k|\bar{K}j) = \sum_{k'\beta} D_{\alpha\beta}(kk'|\bar{K})e_\beta(k'|\bar{K}j) \quad (\text{A.14})$$

The squared frequencies $\omega_j^2(\bar{K})$ are called the eigenvalues and the vectors $e(k|\bar{K}j)$ are called the eigenvectors.

In rigid ion model the elements of the dynamical matrix $D_{\alpha\beta}(kk'|\bar{K})$ are considered to be constituted by two parts; one representing the Coulomb interaction and the other representing the non-Coulomb interaction part. Hence the force constants $\phi_{\alpha\beta}(1k;1'k')$ are taken as a sum of two terms $\phi_{\alpha\beta}^C(1k;1'k')$ and $\phi_{\alpha\beta}^N(1k;1'k')$ representing Coulomb and non-Coulomb parts respectively. Considering these things the

dynamical matrix can be written as,

$$D_{\alpha\beta}(kk';|\bar{K}) = T_{\alpha\beta}(kk'|K) + R_{\alpha\beta}(kk'|K) \quad (\text{A.15})$$

where

$$T_{\alpha\beta}(kk'|K) = (M_k M_{k'})^{-1/2} \sum_{l'} \phi_{\alpha\beta}^C(lk;l'k') \exp[-iK \cdot x(lk) - x(l'k')] \quad (\text{A.16})$$

$$R_{\alpha\beta}(kk'|K) = (M_k M_{k'})^{-1/2} \sum_{l'} \phi_{\alpha\beta}^N(lk;l'k') \exp[-iK \{ x(lk) - x(l'k') \}] \quad (\text{A.17})$$

In order to get the dynamical matrix the two parts $T_{\alpha\beta}(kk'|K)$ and $R_{\alpha\beta}(kk'|K)$ are to be evaluated separately and added together from which one gets the eigenvalues.

It is quite well-known that the replacement of an atom in the crystal by its isotope gives rise to shifts in the normal mode frequencies of the crystal. Since the potential and hence the interatomic force depend only on the position coordinates of the substituted atom the frequency (or eigenvalue) is inversely proportional to the square root of the mass of the atom (see eqns.(A.10) and(A.11)) i.e., there is no

change in the dynamical matrix of the crystal when one of the atoms is substituted with its isotope except for the term involving the mass. Margaret²⁴ has shown that the frequency shift due to isotopic substitution can be used for the calculation of eigenvectors and the expression can be written as

$$\frac{\omega_j^{*2}(\bar{K}) - \omega_j^2(\bar{K})}{\omega_j^2(\bar{K})} = \sum_{k=1}^r \frac{M_k - M_k^*}{M_k^*} e^{\dagger}(k|\bar{K}j) \cdot e(k|\bar{K}j) \quad (\text{A.18})$$

Here * denotes the quantity for substituted material and † denotes the complex conjugate.

In the present work two crystals, Zn³²S and Zn³⁴S, are considered and the phonon frequencies of both are calculated using the rigid ion model for the [100], [111] and [110] wavevector directions. Here the part of the dynamical matrix representing Coulomb interaction (eqn.(A.16)) is calculated by using the method of Kellerman²⁵ and the part for non-Coulomb interaction (eqn.(A.17)) the expressions given by Smith¹ and Rajagopal² are employed, Using the expression given by Margaret²⁴ (in eqn.A.18) the eigenvector magnitudes are also determined²⁶. Fig.A.1 gives the dispersion curves of normal crystal (Zn³²S)

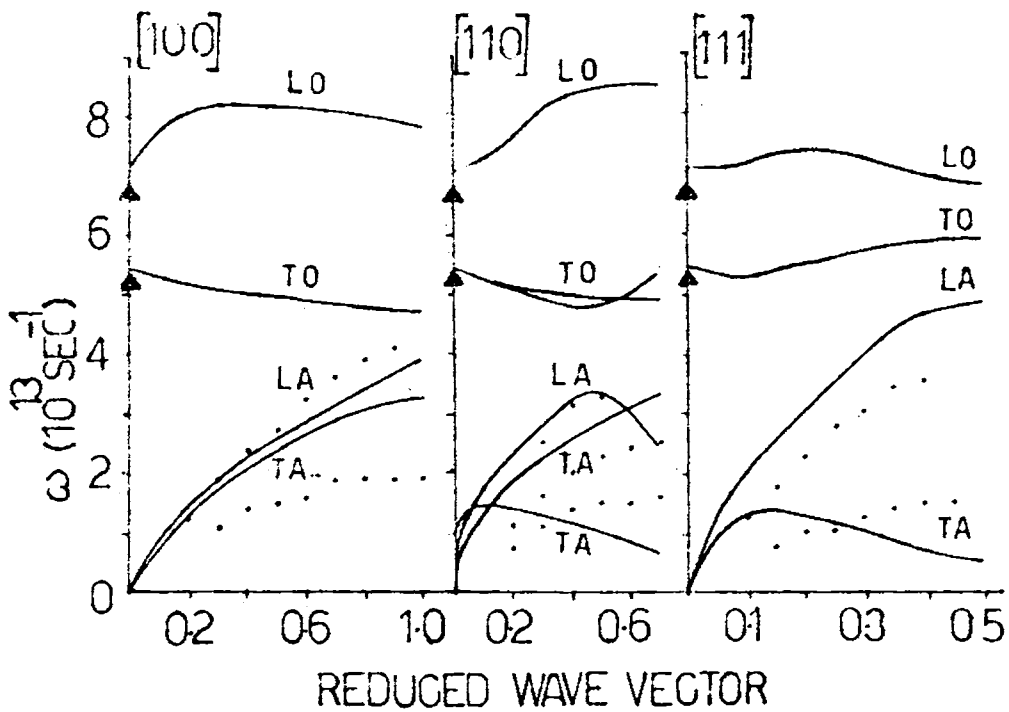


Fig.A.1 Phonon dispersion relations for Zn³²S in [100], [110] and [111] directions.
 —, present theoretical study;
 ▲, experimental Raman frequency (Ref.27);
 ●, inelastic neutron scattering data (Ref.4).

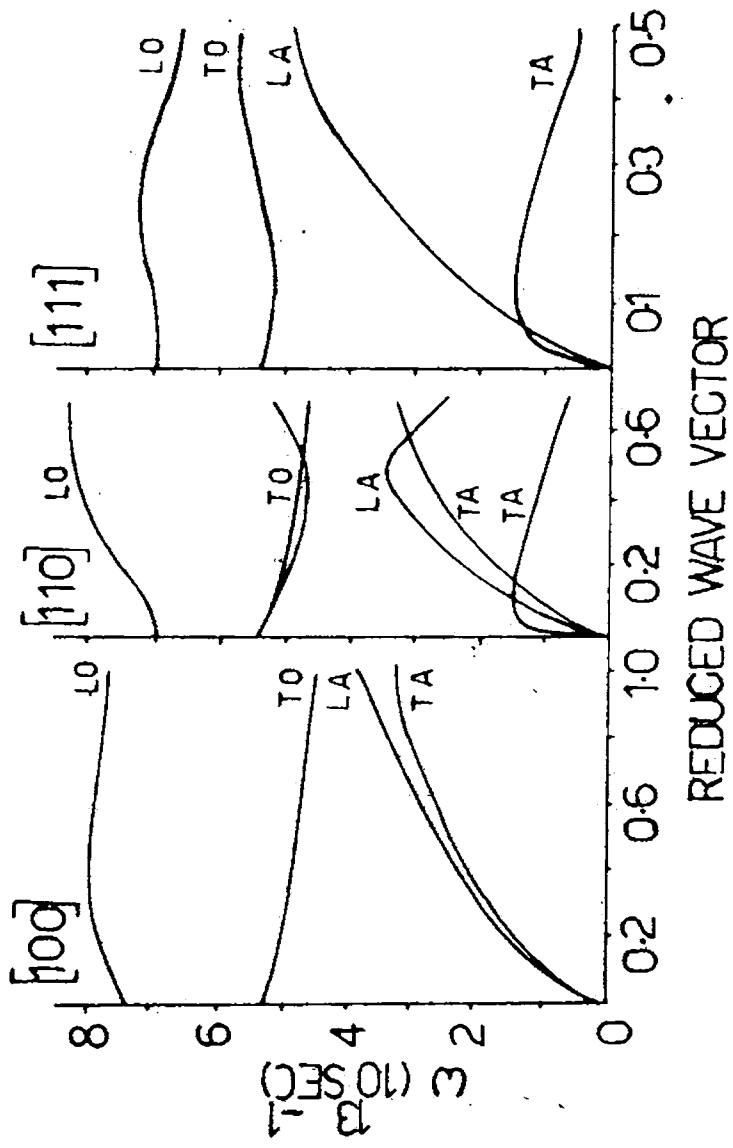


Fig.A.2 Phonon dispersion relations for $Zn^{34}S$.

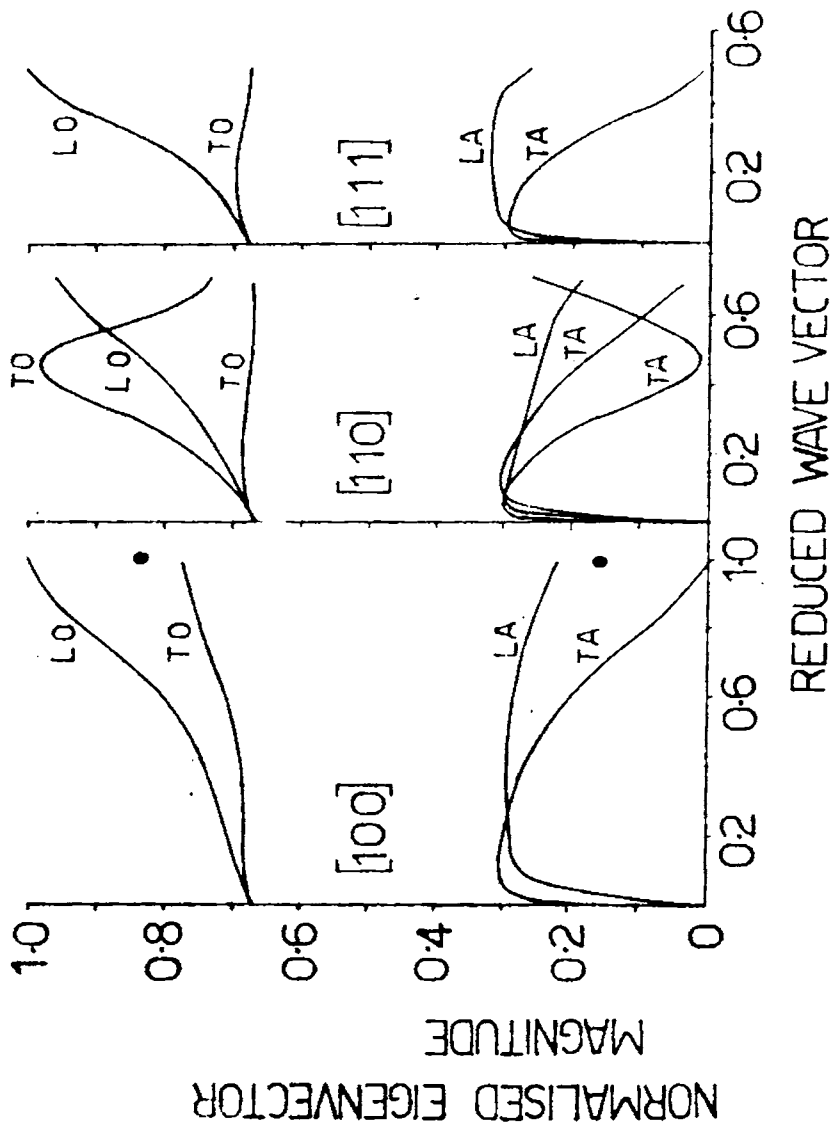


Fig.A.3 Normalised eigenvector along [100], [110] and [111] directions. —, present theoretical study; ●, calculated values from literature (Ref.24).

and fig.A.2 shows that of the substituted crystal (Zn^{34}S). Fig.A.3 shows the eigenvector magnitudes.

In fig.A.3 it can be seen that, as the wavevector value approaches the Brillouin zone boundary, the eigenvector values corresponding to the transverse acoustic modes are decreasing while those corresponding to longitudinal optical modes are increasing. But in $[110]$ direction, at the reduced wavevector value of 0.4 (approximately) the eigenvalues for transverse acoustic mode have a minimum and those for transverse optical mode have a maximum. At the Brillouin zone boundary, in $[100]$ direction the eigenvector values agree very well with those given by Margaret²⁴.

REFERENCES

1. Helen Smith, Philos.Trans.R.Soc.(London), A241, 105 (1948).
2. A.K.Rajagopal and R.Srinivasan, Z.Phys., 158, 471 (1960).
3. J.F.Vetelino, S.S.Mitra, O.Brafman and T.D.Damen, Solid State Commun., 7, 1809 (1969).
4. L.A.Feldkamp, G.Venkataraman and J.S.King, Solid State Commun., 7, 1571 (1969).
5. K.K.Mani and R.P.Singh, Phys.Status Solidi, B56, 723 (1973).
6. K.K.Mani and R.P.Singh, Phys.Status Solidi, B57, 289 (1973).
7. K.Kunc, M.Balkanski and M.A.Nusimovici, Phys.Status Solidi, B71, 341 (1975).
8. K.Kunc, M.Balkanski and M.A.Nusimovici, Phys.Status Solidi, B72, 229 (1975).
9. S.S.Jaswal, J.Phys.C 11, 3559 (1978).
10. T.Soma, Solid State Commun., 34, 927 (1980).
11. M.S.Kushwaha, Phys.Status Solidi, B 98, 623 (1980).
12. R.B.Yadav, Indian J.Phys.A56, 254 (1982).

13. T.Soma, H.Matsuo Kagaya, Solid State Commun., 46, 885 (1983).
14. M.Born and Von Kārmān, Z.Phys., 13, 297 (1912).
15. M.Born and Von Kārmān, Z.Phys., 14, 15 (1913).
16. M.Born and K.Huang, Dynamical theory of crystal lattices, Oxford University Press, London (1954).
17. J.de Launay in Henry Ehrenreich, Frederick Seitz and David Turnbull (eds.), Solid State Physics, Vol.2, Academic Press, New York (1956) p.219.
18. M.Blackman in S.Flügge (ed.), Handbuch der Physik, Vol.VII Pt.1, Springer, Berlin (1955) p.325.
19. G.Leibfried in S.Flügge (ed.), Handbuch der Physik, Vol.VII Pt.1, Springer, Berlin (1955) p.104.
20. W.Coehran, Rep.Progr.Phys., 26, 1 (1963).
21. W.Cochran and R.A.Cowley in S.Flugge (ed.), Handbuch der Physik, Vol.XXV Pt.2a, Springer, Berlin (1967) p.59.
22. A.A.Maradudin, E.W.Montroll, G.H.Weiss and I.P.Ipatova in Henry Ehrenreich, Frederick Seitz and David Turnbull (eds.), Theory of lattice dynamics in the harmonic approximation, Academic Press, New York (1971).

23. M.Born and J.R.Oppenheimer, Ann.Physik., 84, 457 (1927).
24. Margaret M.Elcombe, J.Phys., C,7,L202 (1974).
25. E.W.Kellermann, Philos.Trans.R.Soc.(London), A238, 513 (1940).
26. K.P.Vijayakumar and C.Purushothaman, Indian J. Pure & Applied Phys., 19, 749 (1981).
27. O.Brafman and S.S.Mitra, Phys.Rev., 171, 931 (1968).